

AD-A155 452

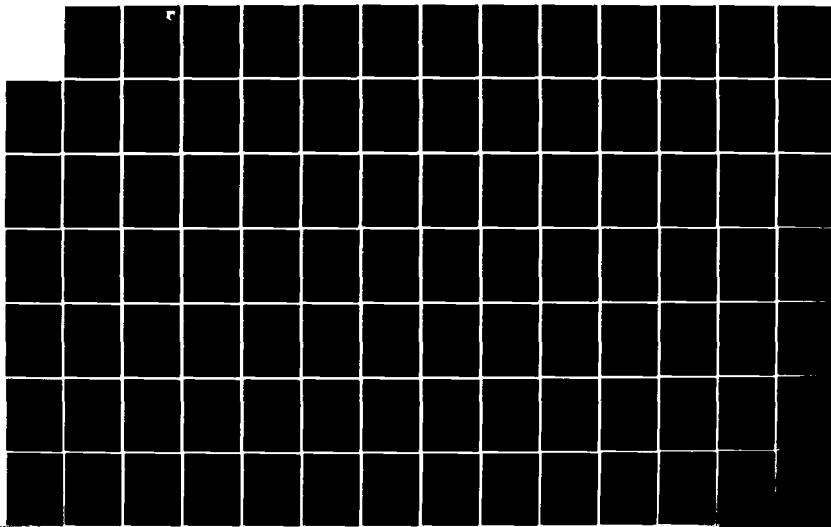
A THEORY OF EXCITON PHOTOLUMINESCENCE FOR TWO TYPES OF
NEUTRAL ACCEPTORS I. (U) DAYTON UNIV OH RESEARCH INST
D S MOROI ET AL. FEB 85 UDR-TR-85-10 AFWAL-TR-85-4031
F33615-81-C-5095

1/2

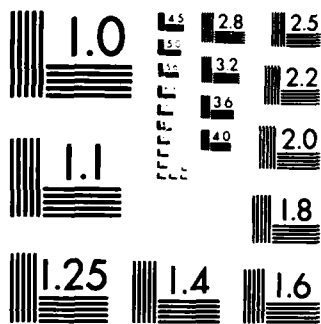
UNCLASSIFIED

F/G 20/12

NL







MICROCOPY RESOLUTION TEST CHART
NATIONAL BUREAU OF STANDARDS-1963-A

AFWAL-TR-85-4031



A THEORY OF EXCITON PHOTOLUMINESCENCE FOR
TWO TYPES OF NEUTRAL ACCEPTORS IN SILICON -
A STUDY OF THE SYSTEMS Si:(B,In), Si:(Al,In),
Si:(Ga,In), Si:(B,Al), Si:(B,Ga), and Si:(Al,Ga)

DAVID S. MOROI
Kent State University
Kent, Ohio 442

MELVIN C. OHMER
Laser and Optical Materials Branch
Electromagnetic Materials Division

DAVID H. BROWN
University of Dayton
Research Institute
Dayton, Ohio

FEBRUARY 1985

INTERIM REPORT FOR PERIOD JUNE 1983 - AUGUST 1984

APPROVED FOR PUBLIC RELEASE; DISTRIBUTION UNLIMITED

DTIC FILE COPY

MATERIALS LABORATORY
AIR FORCE WRIGHT AERONAUTICAL LABORATORIES
AIR FORCE SYSTEMS COMMAND
WRIGHT-PATTERSON AIR FORCE BASE, OHIO 45433

85 5 31 0 31

AD-A155 452

NOTICE

When Government drawings, specifications, or other data are used for any purpose other than in connection with a definitely related Government procurement operation, the United States Government thereby incurs no responsibility nor any obligation whatsoever; and the fact that the government may have formulated, furnished, or in any way supplied the said drawings, specifications, or other data, is not to be regarded by implication or otherwise as in any manner licensing the holder or any other person or corporation, or conveying any rights or permission to manufacture use, or sell any patented invention that may in any way be related thereto.

This report has been reviewed by the Office of Public Affairs (ASD/PA) and is releasable to the National Technical Information Service (NTIS). At NTIS, it will be available to the general public, including foreign nations.

This technical report has been reviewed and is approved for publication.

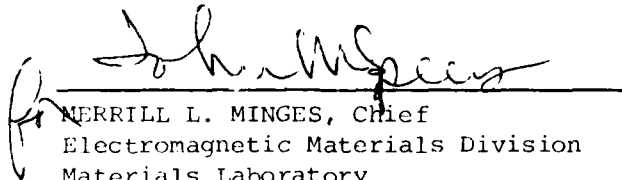


DAVID W. FISCHER
Project Monitor
Laser & Optical Materials Branch



G. EDWARD KUHL, Chief
Laser & Optical Materials Branch
Electromagnetic Materials Division

FOR THE COMMANDER



MERRILL L. MINGES, Chief
Electromagnetic Materials Division
Materials Laboratory
Air Force Wright Aeronautical Laboratories

"If your address has changed, if you wish to be removed from our mailing list, or if the addressee is no longer employed by your organization please notify AFWAL/MLPO, W-PAFB, OH 45433 to help us maintain a current mailing list".

Copies of this report should not be returned unless return is required by security considerations, contractual obligations, or notice on a specific document.

REPORT DOCUMENTATION PAGE

1a. REPORT SECURITY CLASSIFICATION Unclassified		1b. RESTRICTIVE MARKINGS	
2a. SECURITY CLASSIFICATION AUTHORITY		3. DISTRIBUTION/AVAILABILITY OF REPORT Approved for public release; distribution unlimited	
2b. DECLASSIFICATION/DOWNGRADING SCHEDULE		5. MONITORING ORGANIZATION REPORT NUMBER(S) AFWAL-TR-85-4031	
4. PERFORMING ORGANIZATION REPORT NUMBER(S) UDR-TR-85-10		7a. NAME OF MONITORING ORGANIZATION Air Force Wright Aeronautical Laboratories Materials Laboratory (AFWAL/MLPO)	
6a. NAME OF PERFORMING ORGANIZATION Univ. of Dayton Research Inst.* Kent State University†	6b. OFFICE SYMBOL (If applicable) UDRI, KSU	7b. ADDRESS (City, State and ZIP Code) Wright-Patterson Air Force Base, Ohio 45433	
6c. ADDRESS (City, State and ZIP Code) * Dayton, Ohio 45469 * Kent, Ohio 44242		9. PROCUREMENT INSTRUMENT IDENTIFICATION NUMBER F33615-81-C-5095	
8a. NAME OF FUNDING/SPONSORING ORGANIZATION Materials Laboratory	8b. OFFICE SYMBOL (If applicable) AFWAL/ML	10. SOURCE OF FUNDING NOS.	
8c. ADDRESS (City, State and ZIP Code) Wright-Patterson Air Force Base, Ohio 45433		PROGRAM ELEMENT NO. 61102F	PROJECT NO. 2306
11. TITLE (Include Security Classification) A Theory of Exciton Photoluminescence...Si:(Al,Ga)		TASK NO. Q1	WORK UNIT NO. 11
12. PERSONAL AUTHOR(S) David S. Moroi, Melvin C. Ohmer, and David H. Brown			
13a. TYPE OF REPORT Interim Technical	13b. TIME COVERED FROM June 83 TO Aug 84	14. DATE OF REPORT (Yr. Mo., Day) February 1985	15. PAGE COUNT 118
16. SUPPLEMENTARY NOTATION			
17. COSATI CODES		18. SUBJECT TERMS (Continue on reverse if necessary and identify by block number)	
FIELD	GROUP	SUB. GR.	photoluminescence, excitons, neutral acceptors, free exciton capture cross section, rate equations, oscillator strength, thermal release rate, bound exciton decay rate, wavenumber
20	12		
19. ABSTRACT (Continue on reverse if necessary and identify by block number) Rate equations for the densities of free excitons and excitons bound to two types of neutral acceptors in silicon are solved for steady state in the absence of saturation. These rate equations contain the terms for the tunneling of an exciton bound to one type of neutral impurity to another, and explicitly include reverse tunneling. The tunneling rates are calculated using a simple model of an exciton in a one-dimensional semi-infinite double potential well. The energy eigenvalue equation for an exciton in this potential well is derived for estimating the exciton tunneling time. The steady-state solutions of the rate equations yield an expression for the ratio of the bound exciton luminescence intensity as a function of the impurity concentrations. The relative photoluminescence intensities for the systems Si:(B,In), Si:(Al,In), Si:(Ga,In), Si:(B,Al), Si:(B,Ga), and Si:(Al,Ga) are calculated for various values for the relative free exciton capture cross section ratios. This model predicts no exciton tunneling for any of the above systems for the low impurity concentration range, of 10^{12} - 10^{14} cm ⁻³ . For the systems CONTINUED			
20. DISTRIBUTION/AVAILABILITY OF ABSTRACT UNCLASSIFIED/UNLIMITED <input checked="" type="checkbox"/> SAME AS RPT <input type="checkbox"/> DTIC USERS <input type="checkbox"/>		21. ABSTRACT SECURITY CLASSIFICATION Unclassified	
22a. NAME OF RESPONSIBLE INDIVIDUAL David W. Fischer		22b. TELEPHONE NUMBER (Include Area Code) (513) 255-4474	22c. OFFICE SYMBOL AFWAL/MLPO

19. Abstract (Continued)

with large differences in the bound exciton energy levels such as Si:(B,In), Si:(Al,In), and Si:(Ga,In), and having indium concentrations exceeding 10^{15}cm^{-3} , it predicts quenching of shallow impurity bound exciton luminescence, because the forward exciton tunneling rate from the shallow level to the deep level of indium dominates and the reverse exciton tunneling rate from indium to the shallow impurities is negligible. For the systems with small differences in the bound exciton energy levels such as Si:(B,Al) and Si:(B,Ga), the theory predicts enhancement of shallow impurity bound exciton luminescence beyond certain concentrations depending upon the free exciton capture cross section ratios because in these cases the reverse exciton tunneling rate dominates. For the system Si:(Al,Ga) in which the difference in the bound exciton energy levels is very small, gallium bound exciton luminescence dominates when the gallium concentration exceeds 10^{16}cm^{-3} if the aluminum free exciton capture cross section is less than the gallium free exciton capture cross section. The energy eigenvalue equation for an exciton in a one-dimensional finite double potential well is derived for future use.

SUMMARY

Rate equations for the densities of free excitons and excitons bound to two types of neutral acceptors in silicon are solved for steady state in the absence of saturation. These rate equations explicitly include the terms for reverse and forward tunneling of bound excitons from one type of neutral impurity to another. The tunneling rates are calculated using a simple model of an exciton in a one-dimensional semi-infinite double potential well. The energy eigenvalue equation for an exciton in this potential well is derived for estimating the exciton tunneling time. The steady-state solutions of the rate equations yield an expression for the ratio of the bound exciton luminescence intensity as a function of the impurity concentrations. The relative photoluminescence intensities for the systems Si:(B,In), Si:(Al,In), Si:(Ga,In), Si:(B,Al), Si:(B,Ga), and Si(Al,Ga) are calculated for various values of the relevant free exciton capture cross section ratios. This model predicts no exciton tunneling for any of the above systems for the low impurity concentration range of 10^{12} - 10^{14} cm^{-3} . For the systems with large differences in the bound exciton energy levels such as Si:(B,In), Si:(Al,In), and Si:(Ga,In), and having indium concentrations exceeding 10^{15} cm^{-3} , it predicts quenching of shallow impurity bound exciton luminescence because the forward exciton tunneling rate from the shallow level to the deep level of indium dominates and the reverse exciton tunneling rate from indium to the shallow impurities is negligible. For the systems with small differences in the bound exciton energy levels such as Si:(B,Al) and Si:(B,Ga), the theory predicts enhancement of shallow impurity

bound exciton luminescence beyond certain concentrations depending upon the free exciton capture cross section ratios because in these cases the reverse exciton tunneling rate dominates. For the system Si:(Al,Ga) in which the difference in the bound exciton energy levels is very small, gallium bound exciton luminescence dominates when the gallium concentration exceeds 10^{16}cm^{-3} if the aluminum free exciton capture cross section is less than the gallium free exciton capture cross section. The energy eigenvalue equation for an exciton in a one-dimensional finite double potential well is derived for future use.

FOREWORD

Materials requirements for silicon-based devices are becoming ever more stringent as VHSIC-related applications become more important to Air Force research. Photoluminescence (PL) has been shown to be an effective method for impurity and defect concentration determination in the 10^{11} - 10^{13} cm^{-3} range. However, recent experimental and theoretical evidence indicates that the PL method may have limited usefulness as a quantitative technique for impurity concentrations above 10^{15} cm^{-3} . This paper establishes a theoretical framework for examining the exciton tunneling problem in doubly-doped silicon and thus establishes a "window of applicability" for quantitative concentration measurements in silicon.

One of the authors (D. S. Moroi) would like to thank the AFOSR for supporting the preliminary part of the work under the 1982 USAF-SCEEE Summer Faculty Research Program, Contract No. F49620-82-C-0035 and Universal Energy Systems for funding the project for the summer months of 1983 under Contract No. F33615-82-C-5001 and Task No. 729-074. He would like to extend his appreciation to the Laser and Optical Materials Branch, Electromagnetic Materials Division, the Materials Laboratory of the AFWAL for providing him with the opportunity to spend the very worthwhile and rewarding summers. It is our pleasure to thank Dr. Patrick M. Hemenger for providing useful references and inspiring discussions. His collaboration, guidance, and continuing encouragement during the course of research is appreciated. We are also thankful to Dr. Frank Szmulowicz for

numerous stimulating discussions on modelling exciton tunneling. Finally, we want to thank Mr. David O'Quinn for his fine work in producing many of the figures for the tunneling factors and Ms. Niki Maxwell for a fine job of typing the manuscript.

TABLE OF CONTENTS

SECTION		PAGE
I	INTRODUCTION	1
II	A THEORY OF PHOTOLUMINESCENCE FOR A DOUBLY-DOPED SEMICONDUCTOR INCLUDING EXCITON TUNNELING	4
	1. IMPURITY DISTRIBUTION	4
	2. THE RATE EQUATIONS AND STEADY STATE SOLUTIONS	6
	3. THE INTENSITY RATIO OF BOUND EXCITON LUMINESCENCE	8
III	TUNNELING RATE AND ENERGY EIGENVALUE EQUATION FOR AN EXCITON IN A ONE DIMENSIONAL SEMI-INFINITE DOUBLE POTENTIAL WELL	10
	1. TUNNELING RATE CALCULATION	10
	2. DERIVATION FOR THE ENERGY EIGENVALUE EQUATION	14
IV	TUNNELING RATE AND ENERGY EIGENVALUE EQUATION FOR AN EXCITON IN A ONE DIMENSIONAL FINITE DOUBLE POTENTIAL WELL	15
V	NUMERICAL RESULTS AND DISCUSSIONS	16
	REFERENCES	26

STRATIONS

LIST OF
(C

	PAGE	FIGURE
y atoms in a doubly-	5	6a
ional semi-infinite SDW).	10	6b
2c:		6c
rations, N_i , of each of n is 10^{12} - 10^{20} cm^{-3} . The ollowing a figure numeral ional plot of the tunnel- given free exciton cap- for the system Si:(i,j) centration N_j of impurity ations N_i of impurity i. Immediately following a two different views of ot of the tunneling factor exciton capture cross- ion of N_i and N_j .		7a
		7b
		7c
as functions of N_{In} for	28	8a
$\sigma_B/\sigma_{In} = 0.1$ as a function	29	8b
for $\sigma_B/\sigma_{In} = 0.1$ as a	30	8c
d McGill for $\sigma_B/\sigma_{In} = 0.1$ given N_B .	31	9a
Mitchard and McGill for on of N_B and N_{In} .	32	9b
) by Mitchard and McGill nction of N_B and N_{In} .	33	9c
.05 as functions of N_{In}	34	10a
$\sigma_{Al}/\sigma_{In} = 0.05$ as a	35	10b
for $\sigma_{Al}/\sigma_{In} = 0.05$ as a	36	10c

LIST OF ILLUSTRATIONS
(Continued)

FIGURE		PAGE
11a	R(Ga,In) for $\sigma_{\text{Ga}}/\sigma_{\text{In}} = 0.2$ as functions of N_{In} for given N_{Ga} .	52
11b	One view of R(Ga,In) for $\sigma_{\text{Ga}}/\sigma_{\text{In}} = 0.2$ as a function of N_{Ga} and N_{In} .	53
11c	Another view of R(Ga,In) for $\sigma_{\text{Ga}}/\sigma_{\text{In}} = 0.2$ as a function of N_{Ga} and N_{In} .	54
12a	R(Ga,In) for $\sigma_{\text{Ga}}/\sigma_{\text{In}} = 1.4$ as functions of N_{In} for given N_{Ga} .	55
12b	One view of R(Ga,In) for $\sigma_{\text{Ga}}/\sigma_{\text{In}} = 1.4$ as a function of N_{Ga} and N_{In} .	56
12c	Another view of R(Ga,In) for $\sigma_{\text{Ga}}/\sigma_{\text{In}} = 1.4$ as a function of N_{Ga} and N_{In} .	57
13a	R(Ga,In) for $\sigma_{\text{Ga}}/\sigma_{\text{In}} = 5$ as functions of N_{In} for given N_{Ga} .	58
13b	One view of R(Ga,In) for $\sigma_{\text{Ga}}/\sigma_{\text{In}} = 5$ as a function of N_{Ga} and N_{In} .	59
13c	Another view of R(Ga,In) for $\sigma_{\text{Ga}}/\sigma_{\text{In}} = 5$ as a function of N_{Ga} and N_{In} .	60
14a	R(Ga,In) for $\sigma_{\text{Ga}}/\sigma_{\text{In}} = 20$ as functions of N_{In} for given N_{Ga} .	61
14b	One view of R(Ga,In) for $\sigma_{\text{Ga}}/\sigma_{\text{In}} = 20$ as a function of N_{Ga} and N_{In} .	62
14c	Another view of R(Ga,In) for $\sigma_{\text{Ga}}/\sigma_{\text{In}} = 20$ as a function of N_{Ga} and N_{In} .	63
15a	R(B,Al) for $\sigma_{\text{B}}/\sigma_{\text{Al}} = 0.005$ as functions of N_{Al} for given N_{B} .	64
15b	One view of R(B,Al) for $\sigma_{\text{B}}/\sigma_{\text{Al}} = 0.005$ as a function of N_{B} and N_{Al} .	65
15c	Another view of R(B,Al) for $\sigma_{\text{B}}/\sigma_{\text{Al}} = 0.005$ as a function of N_{B} and N_{Al} .	66



LIST OF ILLUSTRATIONS
(Continued)

FIGURE		PAGE
16a	R(B,A1) for $\sigma_B/\sigma_{A1} = 0.02$ as functions of N_{A1} for given N_B .	67
16b	One view of R(B,A1) for $\sigma_B/\sigma_{A1} = 0.02$ as a function of N_B and N_{A1} .	68
16c	Another view of R(B,A1) for $\sigma_B/\sigma_{A1} = 0.02$ as a function of N_B and N_{A1} .	69
17a	R(B,A1) for $\sigma_B/\sigma_{A1} = 1/14$ as functions of N_{A1} for given N_B .	70
17b	One view of R(B,A1) for $\sigma_B/\sigma_{A1} = 1/14$ as a function of N_B and N_{A1} .	71
17c	Another view of R(B,A1) for $\sigma_B/\sigma_{A1} = 1/14$ as a function of N_B and N_{A1} .	72
18a	R(B,A1) for $\sigma_B/\sigma_{A1} = 0.5$ as functions of N_{A1} for given N_B .	73
18b	One view of R(B,A1) for $\sigma_B/\sigma_{A1} = 0.5$ as a function of N_B and N_{A1} .	74
18c	Another view of R(B,A1) for $\sigma_B/\sigma_{A1} = 0.5$ as a function of N_B and N_{A1} .	75
19a	R(B,A1) for $\sigma_B/\sigma_{A1} = 2$ as functions of N_{A1} for given N_B .	76
19b	One view of R(B,A1) for $\sigma_B/\sigma_{A1} = 2$ as a function of N_B and N_{A1} .	77
19c	Another view of R(B,A1) for $\sigma_B/\sigma_{A1} = 2$ as a function of N_B and N_{A1} .	78
20a	R(B,A1) for $\sigma_B/\sigma_{A1} = 20$ as functions of N_{A1} for given N_B .	79
20b	One view of R(B,A1) for $\sigma_B/\sigma_{A1} = 20$ as a function of N_B and N_{A1} .	80
20c	Another view of R(B,A1) for $\sigma_B/\sigma_{A1} = 20$ as a function of N_B and N_{A1} .	81

LIST OF ILLUSTRATIONS
(Continued)

FIGURE		PAGE
21a	R(B,Ga) for $\sigma_B/\sigma_{Ga} = 0.005$ as functions of N_{Ga} for given N_B .	82
21b	One view of R(B,Ga) for $\sigma_B/\sigma_{Ga} = 0.005$ as a function of N_B and N_{Ga} .	83
21c	Another view of R(B,Ga) for $\sigma_B/\sigma_{Ga} = 0.005$ as a function of N_B and N_{Ga} .	84
22a	R(B,Ga) for $\sigma_B/\sigma_{Ga} = 0.02$ as functions of N_{Ga} for given N_B .	85
22b	One view of R(B,Ga) for $\sigma_B/\sigma_{Ga} = 0.02$ as a function of N_B and N_{Ga} .	86
22c	Another view of R(B,Ga) for $\sigma_B/\sigma_{Ga} = 0.02$ as a function of N_B and N_{Ga} .	87
23a	R(B,Ga) for $\sigma_B/\sigma_{Ga} = 1/14$ as functions of N_{Ga} for given N_B .	88
23b	One view of R(B,Ga) for $\sigma_B/\sigma_{Ga} = 1/14$ as a function of N_B and N_{Ga} .	89
23c	Another view of R(B,Ga) for $\sigma_B/\sigma_{Ga} = 1/14$ as a function of N_B and N_{Ga} .	90
24a	R(B,Ga) for $\sigma_B/\sigma_{Ga} = 0.5$ as functions of N_{Ga} for given N_B .	91
24b	One view of R(B,Ga) for $\sigma_B/\sigma_{Ga} = 0.5$ as a function of N_B and N_{Ga} .	92
24c	Another view of R(B,Ga) for $\sigma_B/\sigma_{Ga} = 0.5$ as a function of N_B and N_{Ga} .	93
25a	R(B,Ga) for $\sigma_B/\sigma_{Ga} = 2$ as functions of N_{Ga} for given N_B .	94
25b	One view of R(B,Ga) for $\sigma_B/\sigma_{Ga} = 2$ as a function of N_B and N_{Ga} .	95
25c	Another view of R(B,Ga) for $\sigma_B/\sigma_{Ga} = 2$ as a function of N_B and N_{Ga} .	96

LIST OF ILLUSTRATIONS
(Continued)

FIGURE		PAGE
26a	R(B,Ga) for $\sigma_B/\sigma_{Ga} = 20$ as functions of N_{Ga} for given N_B .	97
26b	One view of R(B,Ga) for $\sigma_B/\sigma_{Ga} = 20$ as a function of N_B and N_{Ga} .	98
26c	Another view of R(B,Ga) for $\sigma_B/\sigma_{Ga} = 20$ as a function of N_B and N_{Ga} .	99
27a	R(Al,Ga) for $\sigma_{Al}/\sigma_{Ga} = 0.05$ as functions of N_{Ga} for given N_{Al} .	100
27b	One view of R(Al,Ga) for $\sigma_{Al}/\sigma_{Ga} = 0.05$ as a function of N_{Al} and N_{Ga} .	101
27c	Another view of R(Al,Ga) for $\sigma_{Al}/\sigma_{Ga} = 0.05$ as a function of N_{Al} and N_{Ga} .	102
28a	R(Al,Ga) for $\sigma_{Al}/\sigma_{Ga} = 0.2$ as functions of N_{Ga} for given N_{Al} .	103
28b	One view of R(Al,Ga) for $\sigma_{Al}/\sigma_{Ga} = 0.2$ as a function of N_{Al} and N_{Ga} .	104
28c	Another view of R(Al,Ga) for $\sigma_{Al}/\sigma_{Ga} = 0.2$ as a function of N_{Al} and N_{Ga} .	105
29a	R(Al,Ga) for $\sigma_{Al}/\sigma_{Ga} = 1$ as functions of N_{Ga} for given N_{Al} .	106
29b	One view of R(Al,Ga) for $\sigma_{Al}/\sigma_{Ga} = 1$ as a function of N_{Al} and N_{Ga} .	107
29c	Another view of R(Al,Ga) for $\sigma_{Al}/\sigma_{Ga} = 1$ as a function of N_{Al} and N_{Ga} .	108
30a	R(Al,Ga) for $\sigma_{Al}/\sigma_{Ga} = 2$ as functions of N_{Ga} for given N_{Al} .	109
30b	One view of R(Al,Ga) for $\sigma_{Al}/\sigma_{Ga} = 2$ as a function of N_{Al} and N_{Ga} .	110
30c	Another view of R(Al,Ga) for $\sigma_{Al}/\sigma_{Ga} = 2$ as a function of N_{Al} and N_{Ga} .	111

LIST OF ILLUSTRATIONS
(Concluded)

FIGURE		PAGE
31a	$R(\text{Al}, \text{Ga})$ for $\sigma_{\text{Al}}/\sigma_{\text{Ga}} = 10$ as functions of N_{Ga} for given N_{Al} .	112
31b	One view of $R(\text{Al}, \text{Ga})$ for $\sigma_{\text{Al}}/\sigma_{\text{Ga}} = 20$ as a function of N_{Al} and N_{Ga} .	113
31c	Another view of $R(\text{Al}, \text{Ga})$ for $\sigma_{\text{Al}}/\sigma_{\text{Ga}} = 20$ as a function of N_{Al} and N_{Ga} .	114
32a	$R(\text{Al}, \text{Ga})$ for $\sigma_{\text{Al}}/\sigma_{\text{Ga}} = 50$ as functions of N_{Ga} for given N_{Al} .	115
32b	One view of $R(\text{Al}, \text{Ga})$ for $\sigma_{\text{Al}}/\sigma_{\text{Ga}} = 50$ as a function of N_{Al} and N_{Ga} .	116
32c	Another view of $R(\text{Al}, \text{Ga})$ for $\sigma_{\text{Al}}/\sigma_{\text{Ga}} = 50$ as a function of N_{Al} and N_{Ga} .	117

LIST OF TABLES

TABLE		PAGE
1	Bound Exciton Ionization Energies, Wavenumbers, Potential Depths, Potential Widths, Total Decay Rates, Forward and Reverse Tunneling Coefficients	18
2	$R^{(0)}(\text{Al,In})$ and $R(\text{Al,In})$ With Various $\sigma_{\text{Al}}/\sigma_{\text{In}}$ for $N_{\text{Al}} = 3.03 \times 10^{15} \text{ cm}^{-3}$ and $N_{\text{In}} = 9.93 \times 10^{16} \text{ cm}^{-3}$	20

SECTION I
INTRODUCTION

Characterization of semiconductor materials in terms of their electromagnetic properties is important to the development of semiconductor devices and various electrical and optical techniques¹ have been utilized to study those electromagnetic properties. Particularly, recent progress in the technology of integrated circuits demands near-perfect crystals of silicon and requires, therefore, a great improvement in the methods of analysis for minute amounts of impurities and defects in silicon since they drastically change its electromagnetic properties.

Recently, attempts have been made to use photoluminescence (PL) as a quantitative tool for measuring impurity concentrations. Tajima² obtained boron and phosphorus concentrations in silicon crystals by PL analysis at liquid-helium temperature. Nakayama et al.³ measured and analyzed the low temperature exciton luminescence of silicon on the basis of rate equations describing the formation and decay kinetics of free excitons (FE), bound excitons (BE) and bound multiexciton complexes. Tajima and Nomura⁴ applied the PL technique to the quantitative analysis of shallow impurities incorporated intentionally and unintentionally in silicon epitaxial layers. Mitchard and McGill⁵ used PL to determine relative concentrations in the Si:(B,In) system while Brown et al.⁶ investigated the optical and electrical properties of the systems Si:(In,Al) using PL, Hall effect transport, infrared absorption, and photoconductivity measurements. In both papers, it was observed that the luminescence from the shallower acceptor (B or Al) of a two-acceptor system may be quenched when

the concentration of the deeper acceptor (In) exceeds certain critical values ($>10^{16} \text{cm}^{-3}$).⁵⁻⁶ In other words, no aluminum nor boron bound exciton luminescence was observed despite high concentrations of Al and B in the samples used. It is believed that the forward tunneling of bound excitons to In bound states is responsible for the quenching of the B and Al luminescence. Consequently, it appears that PL may not be particularly useful for determining the concentration of a second impurity in the presence of another dopant at much higher concentrations.

The main goal of this research project is to understand the electromagnetic properties of multiply-doped silicon, and, in particular, to provide a theory interpreting the experimental results on PL from the Si:(In,Al) system by Brown, et al.⁶, as well as predicting the reverse exciton tunneling for the systems Si:(B,Al), Si:(B,Ga), and Si:(Al,Ga). We do not attempt to solve the PL problem using the exact Schrödinger equation for an exciton because of its complexity; instead, we use the simplest model to obtain the PL intensity ratio for the doubly-doped semiconductor, leaving more complicated and sophisticated models for later investigations.

In the next section, we present a general PL theory for doubly-doped semiconductors; this theory takes into account forward and reverse exciton tunneling, impurity distributions, the resulting rate equations, and their steady-state solutions in the absence of saturation. We calculate in Section III the forward and reverse exciton tunneling rates using a simple model of a BE in a one-dimensional semi-infinite double potential well (OSDW) using standard methods of quantum mechanics⁷. The exciton

energy eigenvalue equation is also derived for estimating the tunneling time. In Section IV, we calculate the tunneling rate and derive the energy eigenvalue equation for a BE in a one-dimensional finite double potential well (OFDW) for future use. The numerical results and discussion along with recommendations and suggestions for further work are presented in Section V.

SECTION II

A THEORY OF PHOTOLUMINESCENCE FOR A DOUBLY-DOPED SEMICONDUCTOR INCLUDING EXCITON TUNNELING

1. IMPURITY DISTRIBUTION

To study the concentration effect on luminescence of two impurity atoms in a semiconductor, we consider here some direct interactions⁸ between an exciton bound to impurity atom "1" (A_1) and its nearest neighbor neutral impurity atom "2" (A_2) which results in tunneling of the exciton from the atom A_1 to the atom A_2 (due to overlap of the wavefunctions for the A_1 BE and A_2 BE) and its reverse tunneling. From here on, we will use the subscript "1" and "2" for quantities associated with impurity atom "1" with shallow BE energy levels and with impurity atom "2" with deep BE energy levels, respectively; e.g., N_1 = the concentration of B atoms, I_2 = the intensity of PL from the In BE, σ_1 = the FE capture cross section by impurity atom "1".

We calculate first the probability that the nearest-neighbor atom A_2 is between r and $r + dr$ from a given atom A_1 as shown in Fig. 1

$$P_2(r)dr = 4\pi r^2 dr N_2 \exp\left[-\frac{4}{3}\pi r^3 N_2\right] \quad (1)$$

where

$4\pi r^2 dr N_2$ = The probability that an atom A_2 is between r and $r + dr$ from a given atom A_1

$\exp\left[-\frac{4}{3}\pi r^3 N_2\right]$ = The probability that there is no atom A_2 between the atom A_1 and r (obtained from the Poisson distribution).

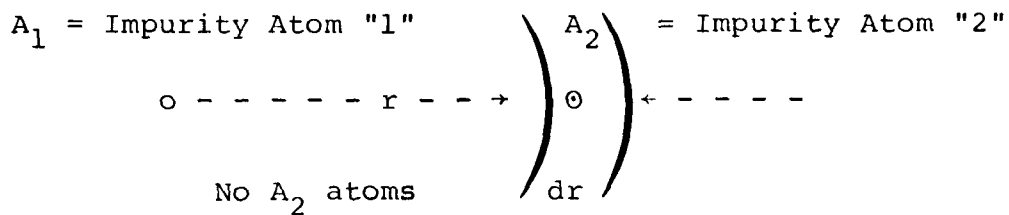


Figure 1. Configuration of impurity atoms in a doubly-doped semiconductor.

Note that

$$\int_0^{\infty} P_2(r) dr = 1 \quad . \quad (2)$$

The average value of r for a given A_2 concentration is

$$\langle r \rangle_2 = \int_0^{\infty} r P_2(r) dr = (3/4\pi N_2)^{-1/3} \Gamma(4/3) \quad (3)$$

where $\Gamma(x)$ is the gamma function⁹. For $N_2 = 10^{16} \text{ cm}^{-3}$ we find $\langle r \rangle_2 = 257 \text{ \AA}$. Considering that the Si BE Bohr radius is 43 \AA , it is reasonable to assume that direct interaction effects are important.

Now the density of atoms A_1 with a nearest-neighbor atom A_2 between r and $r+dr$ is given by

$$N_1(r) = N_1 P_2(r) \quad , \quad (4)$$

so that

$$\int_0^{\infty} N_1(r) dr = N_1 \int_0^{\infty} P_2(r) dr = N_1 \quad (5)$$

Simply switching the subscript "2" to subscript "1" in Eqs. (1) and (4), we obtain the probability that the nearest-neighbor atom A_1 is between r and $r+dr$ from a given atom A_2 as well as the density of A_2 atoms.

2. THE RATE EQUATIONS AND STEADY STATE SOLUTIONS

We use a model for the formation and decay kinetics of FE and BE including forward and reverse BE tunneling to derive a formula for the relative intensity of PL from two dopants in a semiconductor as a function of their concentrations. For this purpose, we start with the rate equations for the densities of the FE and BE⁸.

$$\frac{dn_{FE}}{dt} = g - (v_{FE} + \gamma_1 + \gamma_2)n_{FE} + \rho_1 n_1 + \rho_2 n_2 \quad , \quad (6)$$

$$\frac{\partial n_1(r)}{\partial t} = \gamma_1(r)n_{FE} - \{v_1 + \rho_1 + \Omega_1(r)\}n_1(r) + \Omega_2(r)n_2(r) \quad , \quad (7)$$

$$\frac{\partial n_2(r)}{\partial t} = \gamma_2(r)n_{FE} - \{v_2 + \rho_2 + \Omega_2(r)\}n_2(r) + \Omega_1(r)n_1(r) \quad . \quad (8)$$

Here

- g = the free exciton (FE) generation rate
- n_{FE} = the FE density
- v_{FE} = the FE decay rate
- n_j = the density of excitons bound to impurity atom j ($j = 1$ or 2); e.g., "1" = Al, "2" = In
- $n_i(r)$ = the density of excitons bound to impurity atom i with a nearest-neighbor impurity atom j ($\neq i$) between r and $r + dr$
- γ_i = the FE capture rate by impurity atom i
- $\gamma_i(r)$ = the FE capture rate by impurity atom i with nearest-neighbor impurity atom j ($\neq i$) between r and $r + dr$
- v_i = the BE _{i} decay rate
- ρ_i = the thermal release rate of BE _{i}
- $\Omega_i(r)$ = the distance dependent exciton tunneling rate from impurity atom i to impurity atom j ($\neq i$) .

Integrating Eq. (13) over r , we obtain

$$\begin{aligned} n_i &= \int_0^{\infty} n_i(r) dr \\ &= \xi_i n_{FE} \left\{ 1 + \frac{\gamma_j}{\gamma_i} J_j - J_i \right\} \end{aligned} \quad (17)$$

where

$$J_i = \int_0^{\infty} P_j(r) w_i(r) \{1 + w_1(r) + w_2(r)\}^{-1} dr \quad (18)$$

with

$$P_j(r) = 4\pi r^2 N_j \exp\left(-\frac{4\pi}{3} r^3 N_j\right) \quad (1)$$

3. THE INTENSITY RATIO OF BOUND EXCITON LUMINESCENCE

Using Eq. (17) we have the ratio of PL intensity of BE_i to that of FE

$$\frac{I_i}{I_{FE}} = \frac{f_i n_i}{f_{FE} n_{FE}} = \frac{f_i}{f_{FE}} \xi_i \left\{ 1 + \frac{\gamma_j}{\gamma_i} J_j - J_i \right\} \quad (19)$$

where f_i is the BE_i oscillator strength and f_{FE} is the FE oscillator strength. With the help of Eq. (19), we have the intensity ratio of BE luminescence

$$\frac{I_1}{I_2} = R_{12} \frac{N_1}{N_2}, \quad (20)$$

where

$$R_{12} = R_{12}^{(0)} R(1,2) \quad (21)$$

with

$$R_{12}^{(0)} = \frac{f_1}{f_2} \left\{ \frac{\xi_1 N_2}{\xi_2 N_1} \right\} = \frac{f_1}{f_2} \frac{\sigma_1 / (\nu_1 + \rho_1)}{\sigma_2 / (\nu_2 + \rho_2)} \quad (22)$$

= the value of R_{12} in the absence of exciton tunneling,

$$R(1,2) = \frac{1 + \eta^{-1} \cdot J_2 - J_1}{1 + \eta \cdot J_1 - J_2} \quad (23)$$

and

$$= \frac{\gamma_1}{\gamma_2} = \frac{\sigma_1 N_1}{\sigma_2 N_2} \quad (24)$$

We name $R(1,2)$ in Eq. (23) the "tunneling factor" of a BE from impurity 1 to impurity 2. It has the following characteristics: no BE tunneling will occur if $R(1,2) = 1$, the forward BE tunneling from the shallow impurity to the deep impurity dominates if $R(1,2) < 1$, and the reverse BE tunneling from the deep impurity to the shallow impurity dominates if $R(1,2) > 1$. We point out here that Eq. (21) contains the vital information on PL from a doubly-doped semiconductor which depends on the impurity concentrations as well as parameters such as the FE and BE oscillator strengths and the FE capture cross sections.



SECTION III
 TUNNELING RATE AND ENERGY EIGENVALUE EQUATION
 FOR AN EXCITON IN A ONE DIMENSIONAL
 SEMI-INFINITE DOUBLE POTENTIAL WELL

Before we compare this theory with the experimental results, we must calculate the exciton tunneling rates $\Omega_i(r)$ in Eqs. (16), (18), and (23). The general topic of tunneling in solids has been considered extensively in the literature^{10,11}.

1. TUNNELING RATE CALCULATION

Here we treat the exciton, a correlated electron-hole pair, as a single particle and assume that it moves in a OSDW, as shown in Fig. 2. It is assumed that the exciton is initially in potential well "1" (Region I in Fig. 2).

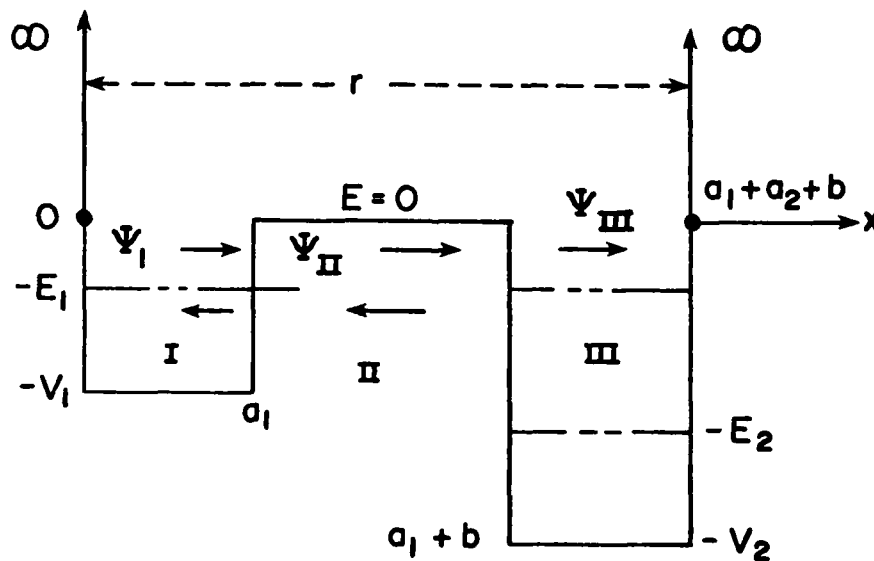


Figure 2. An exciton in one-dimensional semi-infinite double potential well (OSDW).

The motion of an exciton with effective mass m in the potential well shown in Fig. 2 is governed by the Schrodinger equation

$$\frac{\hbar^2}{2m} \frac{d^2\psi}{dx^2} + (E - V)\psi = 0 \quad , \quad (25)$$

with the solutions

$$\begin{aligned} \psi_{\text{I}}(x) &= Ae^{ik_1x} + Be^{-ik_1x} \quad , \quad 0 \leq x \leq a_1 \\ \psi_{\text{II}}(x) &= Ce^{-\kappa x} + De^{\kappa x} \quad , \quad a_1 \leq x \leq a_1 + b \\ \psi_{\text{III}}(x) &= Ee^{ik_2x} \quad , \quad a_1 + b \leq x \leq a_1 + a_2 + b \end{aligned} \quad (26)$$

where

$$\begin{aligned} k_i &= \sqrt{2m(V_i - E)/\hbar} \\ \kappa &= \sqrt{2mE/\hbar} \\ m &= 0.6m_e \end{aligned} \quad (27)$$

and constants A, \dots, E are to be determined by the boundary conditions. The boundary conditions between regions I and II, and II and III yield

$$\begin{aligned} E/A &= 4i\zeta_1 e^{i(a_1 - a')} / \Delta_1 \\ \Delta_1 &= e^{-\kappa b} (1 + i\zeta_1)(1 + i\zeta_2) - e^{\kappa b} (1 - i\zeta_1)(1 - i\zeta_2) \\ \alpha_i &= k_i a_i \quad , \quad a' = k_2(a_1 + b) \quad , \quad \zeta_i = k_i / \kappa \end{aligned} \quad (28)$$

A transmission coefficient T can be calculated by taking the ratio of the current density of particles transmitted through the barrier, J_{III} , and the incident current density, J_{I} ,

$$\begin{aligned}
T &= J^{III}/J_I = (k_2/k_1) (E/A)^2 & (29) \\
&= rk_1 k_2 \kappa^2 / \Delta \\
\Delta &= \kappa^4 |\Delta_1|^2 / 4 \\
&= (k_1^2 + \kappa^2) (k_2^2 + \kappa^2) \sinh^2(\kappa b) + \kappa^2 (k_1^2 + k_2^2)
\end{aligned}$$

The tunneling rate from well "1" to well "2" is defined as the transmission coefficient divided by the period of classical oscillations within potential well "1":

$$\begin{aligned}
\Omega_1(r) &= T / (2ma_1/k_1) \\
&= \Omega_1 e^{-2\kappa r}
\end{aligned}$$

where

$$\Omega_1 = \frac{2hk_1}{ma_1} \frac{4k_1 k_2 \kappa^2}{(k_1^2 + \kappa^2) (k_2^2 + \kappa^2)} e^{2\kappa(a_1 + a_2)} \quad (30)$$

$$r = a_1 + a_2 + b \quad .$$

In arriving at Eq. (30), we have ignored the term with $e^{-\kappa b}$ in Eq. (29) assuming a large separation of two wells. The reverse tunneling rate is obtained by exchanging subscripts 1 \leftrightarrow 2 in Eq. (30) multiplied by a Boltzmann factor $\exp(-\Delta E/kT)$ with $\Delta E = E_1 - E_2$ (the difference in the BE energy levels in two wells).

The tunneling rate from impurity atom A_1 to impurity atom A_2 by Eq. (30) is overestimated for the approximate concentration range below $N_2 = 10^{17} \text{ cm}^{-3}$ for the actual three-dimensional problem. We discuss below how to remedy this problem. It is reasonable to assume that 12 impurity atoms A_2 are distributed at equi-distance $\langle r \rangle_2$ from each other on the spherical shell of radii $\langle r \rangle_2$ and $\langle r \rangle_2 + dr$ centered at the atom A_1 , which is analogous

to a close hexagonal packing of atoms in a solid. The total width of the potential wells of the 12 impurity atoms A_2 on the shell does not occupy the entire region of the spherical shell, if the concentration of the atoms A_2 is less than approximately 10^{17} cm^{-3} . Taking account of this fact, the more accurate expression for the tunneling rate is given by

$$\Omega_1^{(3)} = C_1 \Omega_1(r) \quad (31)$$

where

$$C_1 = 6 \left[1 - \sqrt{1 - (a_2 / \langle r \rangle_2)^2} \right] = 6 \left[1 - \sqrt{1 - \frac{a_2}{\Gamma(\frac{4}{3})} \left(\frac{4\pi N_2}{3} \right)^{1/3}} \right]^2$$

for $N_2 \lesssim 10^{17} \text{ cm}^{-3}$ (32)

$$C_1 = 1 \quad \text{for} \quad N_2 \gtrsim 10^{17} \text{ cm}^{-3}$$

For concentrations greater than about 10^{17} cm^{-3} , the correction factor C_1 becomes unity due to overlap of the potential wells.

The relationship between the depth, width, and the energy eigenvalue for the exciton in an isolated semi-infinite well is given by

$$\tan(k_i a_i) + k_i / \kappa = 0 \quad (33)$$

We assume that the reverse tunneling from well "2" to well "1" will take place after the exciton in well "2" is raised from its deeper energy level E_2 to a shallower energy level E_1 by thermal excitation.

The tunneling rate may be calculated by various other means: e.g. the semiclassical approximation by Wentzel, Kramers, and Brillouin (the WKB approximation)⁷ yields a tunneling rate similar to Eq. (30). In general, the tunneling rate depends

on a dominant factor $\exp(-2\kappa r)$ regardless of the model used because the wavefunction representing a BE behaves as $\exp(-\kappa r)$ after tunneling through a potential barrier.

2. DERIVATION FOR THE ENERGY EIGENVALUE EQUATION

Here we derive the energy eigenvalue equation for an exciton in an OSDW in order to compute the BE_1 tunneling time. The wavefunctions in the three regions which satisfy the appropriate boundary conditions are

$$\begin{aligned}\psi_I &= A'\sin(k_1x) \\ \psi_{II} &= B'e^{-\kappa x} + C'e^{\kappa x} \\ \psi_{III} &= D'\sin(k_2(a_1 + a_2 + b - x))\end{aligned}\tag{34}$$

By eliminating the constants A' , B' , C' , and D' from the four equations for the boundary conditions ($\psi_I(a_1) = \psi_{II}(a_1)$, $\psi_I'(a_1) = \psi_{II}'(a_1)$; $\psi_{II}(a_1 + b) = \psi_{III}(a_1 + b)$, $\psi_{II}'(a_1 + b) = \psi_{III}'(a_1 + b)$), we have the exciton energy eigenvalue equation

$$F_1 F_2 = e^{-2\kappa b}\tag{35}$$

where

$$F_i = \frac{\tan(k_i a_i) + k_i/\kappa}{\tan(k_i a_i) - k_i/\kappa}\tag{36}$$

Equation (35) reduces to Eq. (33) for a large separation, b , of the two wells.

SECTION IV
TUNNELING RATE AND ENERGY EIGENVALUE EQUATION
FOR AN EXCITON IN ONE DIMENSIONAL FINITE
DOUBLE POTENTIAL WELL

We give here the tunneling rate of an exciton in a OFDW and the energy eigenvalue equation for future use. The exciton tunneling rate is

$$\begin{aligned} u_1(r) &= \Omega_1' e^{-2\kappa r} \\ \Omega_1' &= \Omega_1 e^{-\kappa(a_1 + a_2)} \\ r &= \frac{1}{2}(a_1 + a_2) + b \end{aligned} \quad (37)$$

The realistic tunneling rate is obtained by multiplying Eq. (37) by the correction factor given in Eq. (32) as in the case for the OSDW.

The energy eigenvalue equation is

$$G_1 G_2 = e^{-2\kappa b} \quad (38)$$

where

$$\begin{aligned} G_i &= \left\{ 2 \cot(k_i a_i) - \left(\frac{k_i}{\kappa} - \frac{\kappa}{k_i} \right) \right\} / \left\{ \frac{k_i}{\kappa} + \frac{\kappa}{k_i} \right\} \\ &= \left\{ 1 - \frac{k_i}{\kappa} \tan\left(\frac{k_i a_i}{2}\right) \right\} \left\{ 1 + \frac{\kappa}{k_i} \tan\left(\frac{k_i a_i}{2}\right) \right\} / \tan\left(\frac{k_i a_i}{2}\right) \left\{ \frac{k_i}{\kappa} + \frac{\kappa}{k_i} \right\} \end{aligned} \quad (39)$$

SECTION V
NUMERICAL RESULTS AND DISCUSSIONS

It is convenient to introduce the forward tunneling coefficient w_i ($= w_{ij}$) which is defined by

$$w_i = w_{ij} = \Omega_i / (\nu_i + \rho_i) \quad (40)$$

where $(\nu_i + \rho_i)$ is the total decay rate of BE_i , i.e., the sum of the BE_i decay rate and thermal release rate of BE_i , each of which is estimated using the experimental value of the BE lifetime at 4.2K.^{5,12} It turns out that ν_i , the thermal release rate, is negligible for all cases with the exception of the BE for boron at this temperature. We have used the experimental values of ionization energies determined by Lipari et al.¹³ to estimate the BE ionization energies with the help of the Haynes rule. There are still four parameters a_1 , a_2 , V_1 , and V_2 (the widths and depths of the two potential wells) to be determined before calculating the tunneling coefficients; however, the energy eigenvalue equation for each separate well (Eq. (33)) effectively reduces the number of unknowns to two. For the system Si:(B,In), we have fixed the numerical value of one parameter, a_B , to match the values of $R(B,In)$ obtained by Mitchard and McGill⁵ for the boron concentration range $N_B = 10^{12} - 10^{14} \text{ cm}^{-3}$ and the indium concentration range $N_{In} = 10^{12} - 10^{15} \text{ cm}^{-3}$ and approximated the other, a_{In} , as the first Bohr radius in the context of the hydrogenic BE model. For the rest of the systems, we have determined the shapes of the potential wells using a similar process. The numerical values of the BE ionization energy (E), wavenumber (κ), potential depth (V), potential width (a), total decay rate ($\nu + \rho$), forward tunneling coefficient (w_{ij}) and reverse

tunneling coefficient (w_{ji}) for each system are summarized in Table 1 for the BE model presented in Section III (an exciton in a OSDW).

Note here that the reverse tunneling coefficients w_{ji} are calculated with the help of Eq. (40) exchanging the subscript $i \leftrightarrow j$ multiplied by the Boltzmann factors. As seen in Table 1, the reverse tunneling coefficients w_{ji} for the systems Si:(B,In), Si:(Al,In) and Si:(Ga,In) are extremely small and thus neglected for evaluating their tunneling factors $R(i,j)$.

With few exceptions, the FE capture cross sections by neutral acceptors in silicon are not well known. We take $\sigma_B/\sigma_{In} = 0.1$ ^{5,14} for the system Si:(B,In). For the system Si:(Al,In), we have estimated $\sigma_{Al}/\sigma_{In} = 1.4$, using a linear relationship between the reciprocal of the FE capture time¹⁵ and the FE capture cross section. However, we also examine four other values 0.05, 0.2, 5, and 20 for σ_{Al}/σ_{In} to evaluate the tunneling factor $R(Al,In)$ because of uncertainty in the FE capture cross section ratio. We use the same set of values for the σ_{Ga}/σ_{In} rate in the system Si:(Ga,In) as that for the system Si:(Al,In) because aluminum and gallium have similar electronic properties in Si. For the systems Si:(B,Al) and Si:(B,Ga), we take the set of values 0.005, 0.02, 1/14, 0.5, 2, and 20 for their FE capture cross section ratios. Finally, for the system Si:(Al,Ga), we examine values of 0.05, 0.2, 1, 2, 10, and 50 for the σ_{Al}/σ_{Ga} ratio.

TABLE 1

BOUND EXCITON IONIZATION ENERGIES, WAVENUMBERS, POTENTIAL DEPTHS,
 POTENTIAL WIDTHS, TOTAL DECAY RATES,
 FORWARD AND REVERSE TUNNELING COEFFICIENTS

Impurity	E (meV)	K (10^6 cm^{-1})	V (meV)	a (\AA)	$\nu + \rho$ (10^6 s^{-1})	w_{BIn} (10^{10})	w_{AlIn} (10^{10})	w_{GaIn} (10^{10})	w_{BAL} (10^{10})	w_{BGa} (10^{10})	w_{AlGa} (10^{10})
B	4.583	2.580	6.377	160.0	1.270	3.966			174.0	125.89	
Al	7.042	3.198	11.43	98.0	13.23		0.2635		0.0597*		14.61
Ga	7.416	3.281	12.33	92.0	13.02			0.2612			6.178*
In	15.694	4.774	44.67	34.0	370.4	1.406×10^{-14} *	3.296×10^{-12} *	7.974×10^{-12} *			

* The reverse tunneling coefficients w_{ji} are calculated with the help of Eq. (40) exchanging the subscript $i \leftrightarrow j$ multiplied by the Boltzmann factor.

ions for the tunneling factor are plotted in Fig. 3a, as a function of N_B (10^{12} - 10^{20} cm^{-3}). Similar plots for N_B and N_{In} . Similar plots for N_B and N_{In} by Mitchard and McGill⁵ are shown. For the boron concentration the indium concentration range tunneling factors $R(B,In)$ and $R_{mm}(B,In)$ are plotted against each other because the potential barrier heights $\phi_{Si:(B,In)}$ have been chosen to be the same for the above concentration ranges. In the above ranges, however, $R(B,In)$ decreases more rapidly than $R_{mm}(B,In)$. The tunneling coefficient of $R(B,In)$ is that of 10^7 by Mitchard and McGill⁵ in the exponential factor for the tunneling rate. In other words, the present tunneling rate and thus stronger luminescence than that predicted by Mitchard and McGill⁵ at concentrations below 10^{14} cm^{-3} , both for boron and indium, which implies no BE tunneling. Figs. 3b, 3c, 4b, and 4c indicate $R(B,In) = 1$. (a) for the system Si:(Al,In) and (b) for the system Si:(Al,In) with cross section ratios of $\sigma_{Al}/\sigma_{In} = 0.05$ and 0.2 and are plotted in Figs.

5a-9c. For all the values of σ_{Al} there is no BE tunneling if both aluminum and indium concentrations are less than 10^{14} cm^{-3} . Comparison of Figs. 8a ($\sigma_{Al}/\sigma_{In} = 0.05$) and 9a ($R(Al,In)$ vs N_{Al}) shows that there is more BE tunneling at a given aluminum concentration for a larger value of σ_{Al}/σ_{In} . In Table 2, $R^{(0)}(Al,In)$ and the tunneling factor $R(Al,In)$ for $N_{Al} = 3.03 \times 10^{15}$ cm^{-3} are plotted against σ_{Al}/σ_{In} in order to compare the theory and experiment. The values of $R^{(0)}(Al,In)$ are calculated using the relative oscillator strengths of σ_{Al} and σ_{In} from Mitchell et al.¹⁶ The theory predicts very

TABLE 2
 $R^{(0)}(Al,In)$ AND $R(Al,In)$
 FOR $N_{Al} = 3.03 \times 10^{15}$ cm^{-3} AND
 $N_{In} = 10^{15}$ cm^{-3}

σ_{Al}/σ_{In}	0.05	0.2
$R^{(0)}(Al,In)$	0.0875	0.350
$R(Al,In)$	0.000537	0.000534

factors for the above concentration ranges. In the help of Eqs. (20) and (21), the relative PL intensity for the system Si:(Al,In) is

$$\frac{I_{Al}}{I_{In}} = R^{(0)}(Al,In)$$

Referring to Table 2, Eq. (41) gives the relative PL intensity

$$\frac{I_{Al}}{I_{In}} = 3.57 \times 10^{-4} \quad (42)$$

which is still below the sensitivity of the experiment to observe PL from aluminum. Thus it confirms the experimental results by Brown et al.⁶ that no aluminum BE luminescence should be observed at these concentrations.

The tunneling factors $R(Ga, In)$ for the system $Si:(Ga, In)$ are calculated for the $\sigma_{Ga}/\sigma_{In} = 0.05, 0.2, 1.4, 5,$ and 20 and plotted in Figs. 10a-14c. These figures are very similar to those for the system $Si:(Al, In)$, i.e. they indicate no BE tunneling from gallium to indium if the concentrations are below 10^{14} cm^{-3} , and strong quenching of gallium bound exciton luminescence for In concentrations beyond 10^{17} cm^{-3} .

For the systems $Si:(B, Al)$ and $Si:(B, Ga)$, we have calculated the tunneling factors $R(B, Al)$ and $R(B, Ga)$ for the FE capture cross section ratios $\sigma_B/\sigma_{Al} = \sigma_B/\sigma_{Ga} = 0.005, 0.02, 1/14, 0.5, 2,$ and 20 , and plotted them in Figs. 15a-20c and Figs. 21a-26c, respectively. The figures corresponding to the same FE capture cross section are very similar to each other. Once again they show no BE tunneling from the shallow impurity to the deep impurity if their concentrations are below 10^{14} cm^{-3} . For $\sigma_B/\sigma_{Al} = \sigma_B/\sigma_{Ga} = 0.005$, however, Figs. 15a and 21a show very little quenching of boron bound exciton luminescence and rather an enhancement if $N_B < 10^{14} \text{ cm}^{-3}$, $N_{Al} > 10^{16} \text{ cm}^{-3}$ and $N_{Ga} > 3 \times 10^{16} \text{ cm}^{-3}$. The finite values of the reverse tunneling coefficients are responsible for this phenomenon (see Table 1). In other words, for a small value of the FE capture cross-section ratio, the reverse tunneling from the deeper impurity to the shallower impurity starts to dominate the forward tunneling from the shallower

impurity to the deeper impurity for the above concentrations, resulting in only slight quenching of the shallow impurity bound exciton luminescence. For $\sigma_B/\sigma_{Al} = \sigma_B/\sigma_{Ga} = 20$, Figs. 20a and 26a show considerable quenching of boron bound exciton luminescence if $N_B < 10^{14} \text{ cm}^{-3}$ and $N_{Al} = N_{Ga} = 3 \times 10^{16} \text{ cm}^{-3}$ and enhancement if $N_B < 10^{14} \text{ cm}^{-3}$ and the extremely high concentrations of $N_{Al} = N_{Ga} = 10^{20} \text{ cm}^{-3}$. For a large value of the FE capture cross-section ratio, a large number of excitons are captured by the shallower impurity, most of them are lost to the deeper impurity via forward BE tunneling, and the smaller number of excitons captured by the deeper impurity stay there because of the small reverse BE tunneling coefficients, if $N_B < 10^{14} \text{ cm}^{-3}$ and $N_{Al} = N_{Ga} = 3 \times 10^{16} \text{ cm}^{-3}$. Thus considerable quenching of boron bound exciton luminescence occurs at these concentrations. For the extremely high concentrations of $N_{Al} = N_{Ga} = 10^{20} \text{ cm}^{-3}$, the reverse tunneling from the deeper impurity to the shallower impurity starts to dominate the forward tunneling and enhances the shallower impurity bound exciton luminescence. Once again, the plateau regions of Figs. 15b,c - 26b,c indicate the regions exhibiting no BE tunneling.

The results of the calculations for the tunneling factors $R(Al,Ga)$ for the system $Si:(Al,Ga)$ with the FE capture cross-section ratios $\sigma_{Al}/\sigma_{Ga} = 0.05, 0.2, 1, 2, 10, \text{ and } 50$ are plotted in Figs. 27a - 32c. Figures 27a and 28a show no quenching of aluminum bound exciton luminescence and its enhancement if $N_{Al} < 10^{14} \text{ cm}^{-3}$ and $N_{Ga} > 3 \times 10^{15} \text{ cm}^{-3}$ due to the fact that the forward and reverse tunneling coefficients are of the same order of magnitude and the difference in their BE energy levels is very

small. For $\sigma_{Al}/\sigma_{Ga} > 1$, slight quenching of aluminum bound exciton luminescence occurs at certain gallium concentrations; e.g. $N_{Ga} = 3 \times 10^{15} \text{ cm}^{-3}$ for $\sigma_{Al}/\sigma_{Ga} = 1$ and $N_{Ga} = 3 \times 10^{16} \text{ cm}^{-3}$ for $\sigma_{Al}/\sigma_{Ga} = 50$ (see Figs. 29a and 32a). Figs. 29a and 32a also show enhancement of aluminum bound exciton luminescence if $N_{Ga} > 10^{16} \text{ cm}^{-3}$ for $\sigma_{Al}/\sigma_{Ga} = 1$ and $N_{Ga} > 6 \times 10^{17} \text{ cm}^{-3}$ for $\sigma_{Al}/\sigma_{Ga} = 50$, because the reverse tunneling starts to dominate beyond these concentrations.

Finally, to ensure the occurrence of BE tunneling, we have estimated the tunneling time of a BE from one potential well to another for the system Si:(B,In) at $N_{In} = 10^{16} \text{ cm}^{-3}$ by two different methods:

1. The reciprocal of the tunneling rate (Eq. (30)) gives the tunneling time of $1.14 \times 10^{-11} \text{ s}$.
2. Eq. (35) with the help of time-dependent perturbation theory yields the tunneling time of $1.10 \times 10^{-11} \text{ s}$. Since the tunneling time at $N_{In} = 10^{16} \text{ cm}^{-3}$ is much less than the boron BE decay time of 10^{-6} s (Auger lifetime)^{12,17}, BE tunneling will occur before decay.

We summarize the results of the present calculation by pointing out that PL can be used as a quantitative tool to measure the impurity concentrations in a doubly doped semiconductor if their concentrations are less than 10^{14} cm^{-3} because the theory predicts no BE tunneling for all the systems considered here. As a result, PL can be an excellent quantitative tool for evaluating high purity silicon production and processing steps such



as silane and polycrystalline Si purity analysis, as well as monitoring the compositions of epitaxial silicon films. The silicon materials industry is currently exploiting the PL technique for these purposes.

We conclude this section with the following recommendations and suggestions:

1. In order to confirm the predicted reverse BE tunneling from a deeper impurity to a shallower impurity when there is a small difference in their ionization energies, we recommend, for example, measuring the relative PL intensity I_B/I_{Ga} at $N_B = 10^{13} \text{ cm}^{-3}$ and $N_{Ga} = 10^{17} - 10^{18} \text{ cm}^{-3}$ for the system Si:(B,Ga) or the corresponding Si:(B,Al) system.

2. Since, as indicated in Eq. (23), the tunneling factor $R(1,2)$ strongly depends on the FE capture cross-section ratio, σ_1/σ_2 , it would be very useful to measure and/or calculate that ratio accurately, perhaps using a model analogous to positronium capture by a neutral atom.

3. Historically, minority lifetime killer dopants, e.g. zirconium¹⁸ have been added to Si in an attempt to improve detector performance in radiation environments. It is possible that, for excitons in Si, a deep acceptor could play an analogous role in a more benign fashion.

4. Since current silicon growth and processing technology has not yet reached the point where all defects save the major dopants are eliminated, it would be a valuable extension of this work to consider the exciton tunneling problem in a multi-component material. Also, due to the increased attention devoted to Si counter-doped extrinsic detectors, it would be useful to evaluate

compensation effects by appropriately including donor bound exciton capture and transfer in the rate equations used in this model. These modifications, while useful in assessing the viability of PL in quantitative determinations of physically realistic materials, are outside the scope of the present investigation.

REFERENCES

1. P. Blood and J. W. Orton, "The Electrical Characterization of Semiconductors," Rep. Prog. Phys., Vol. 41, pp. 157-257, 1978.
2. M. Tajima, "Determination of Boron and Phosphorus Concentration in Silicon by Photoluminescence Analysis," Appl. Phys. Lett., Vol. 32, pp. 719-721, 1978.
3. H. Nakayama, T. Nishino, and Y. Hamakawa, "Analysis of the Exciton Luminescence of Silicon for Characterization of the Content of Impurities," Jpn. J. Appl. Phys., Vol. 19, pp. 501-511, 1980.
4. M. Tajima and M. Nomura, "Photoluminescence Analysis of Impurities in Epitaxial Silicon Crystals," Jpn. J. Appl. Phys., Vol. 20, pp. L697-L700, 1981.
5. G. S. Mitchard and T. G. McGill, "Determination of Relative Impurity Concentrations Using Photoluminescence: A Case Study of the Si:(B,In) System," Appl. Phys. Lett., Vol. 37, pp. 959-961, 1980.
6. D. H. Brown, M. C. Ohmer, K. D. Beasley, J. J. Rome, G. J. Brown, and D. W. Fischer, "Optical and Electrical Characterization of Multiply-doped Silicon: A Study of the Si:(In,Al) System," J. Appl. Phys., Vol. 53, pp. 8793-8797, 1982.
7. L. D. Landau and E. M. Lifshitz, Quantum Mechanics--Non-relativistic Theory (Pergamon Press, New York, 1958), pp. 171-178.
8. G. S. Mitchard, "Low Temperature Photoluminescence Properties of Silicon and Silicon-Germanium Alloys," Ph.D. Thesis, California Institute of Technology, 1981 (unpublished).
9. P. J. Davis, in Handbook of Mathematical Functions with Formulas, Graphs, and Mathematical Tables, edited by M. Abramowitz and I. A. Stegun (U.S. Government Printing Office, Washington, D.C., 1970), p. 255.
10. D. L. Dexter, "A Theory of Sensitized Luminescence in Solids," J. Chem. Phys., Vol. 21, pp. 836-850, 1953.
11. L. O. Kane, in Tunneling Phenomena in Solids, edited by E. Burnstein and S. Lundquist (Plenum Press, New York, 1969), pp. 1-11.
12. S. A. Lyon, G. C. Osbourn, D. L. Smith, and T. C. McGill, "Bound Exciton Life Time for Acceptors in Si," Solid State Comm., Vol. 23, pp. 425-428, 1977.

13. N. O. Lipari, A. Baldereschi, and M. L. Thewalt, "Central Cell Effects on Acceptor Spectra in Si and Ge," Solid State Commun., Vol. 33, pp. 277-279, 1980.
14. R. M. Feenstra and T. C. McGill, "Exciton Capture Cross Sections of Indium and Boron Impurities in Silicon," Solid State Commun., Vol. 36, pp. 1039-1045, 1980.
15. K. R. Elliott, "Optical Determination of the Properties of Excitons Bound to Impurities in Semiconductors," Ph.D. Thesis, California Institute of Technology, 1980.
16. K. R. Elliott, G. C. Osbourn, D. L. Smith, and T. C. McGill, "Bound-Exciton Absorption in Si:Al, Si:Ga, and Si:In," Phys. Rev. B, Vol. 17, pp. 1808-1815, 1978.
17. W. Schmid, "Auger Lifetimes for Excitons Bound to Neutral Donors and Acceptors in Si," Phys. Stat. Sol. (b), Vol. 84, pp. 529-540, 1977.
18. S. Mayer, U.S. Patent No. 3,444,100 (1969).

NOTE TO ACCOMPANY FIGURES 3 THROUGH 32

The range of the concentrations, N_i , of each of two impurities in silicon is $10^{12} - 10^{20} \text{ cm}^{-3}$. The letter "a" immediately following a figure numeral refers to the two dimensional plot of the tunneling factors $R(i,j)$ for a given free exciton capture cross section ratio for the system Si:(i,j) as a function of the concentration N_j of impurity j for the given concentrations N_i of impurity i. The letters "b" and "c" immediately following a figure numeral refer to two different views of the three-dimensional plot of the tunneling factor $R(i,j)$ for a given free exciton capture cross-section ratio as a function of N_i and N_j .

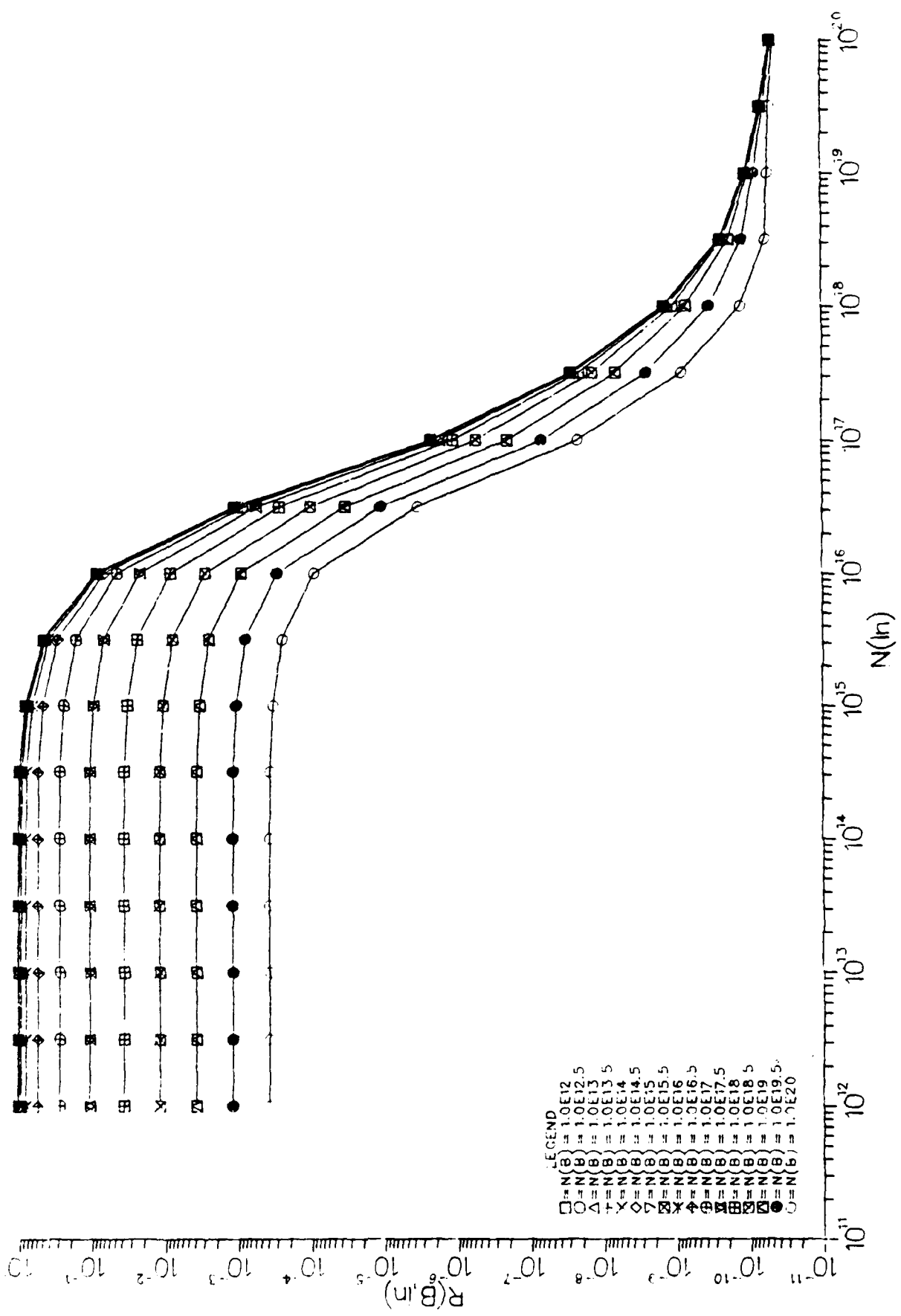


Figure 3a. $R(B, In)$ for $\beta_B/\beta_{In} = 0.1$ as functions of N_{In} for given N_B .

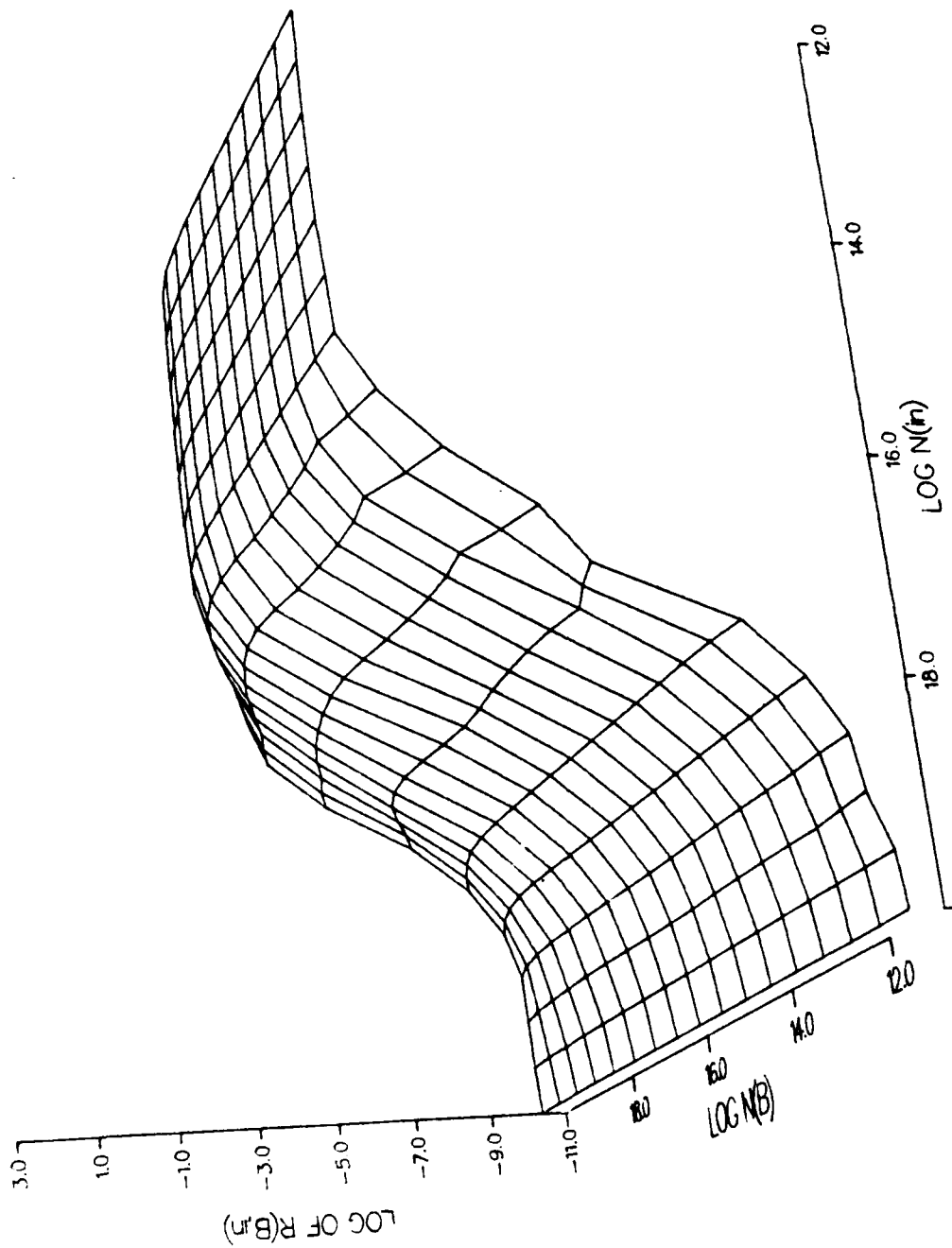


Figure 3c. Another view of $R(B, In)$ for $\sigma_B/\sigma_{In} = 0.1$ as a function of N_B and N_{In} .

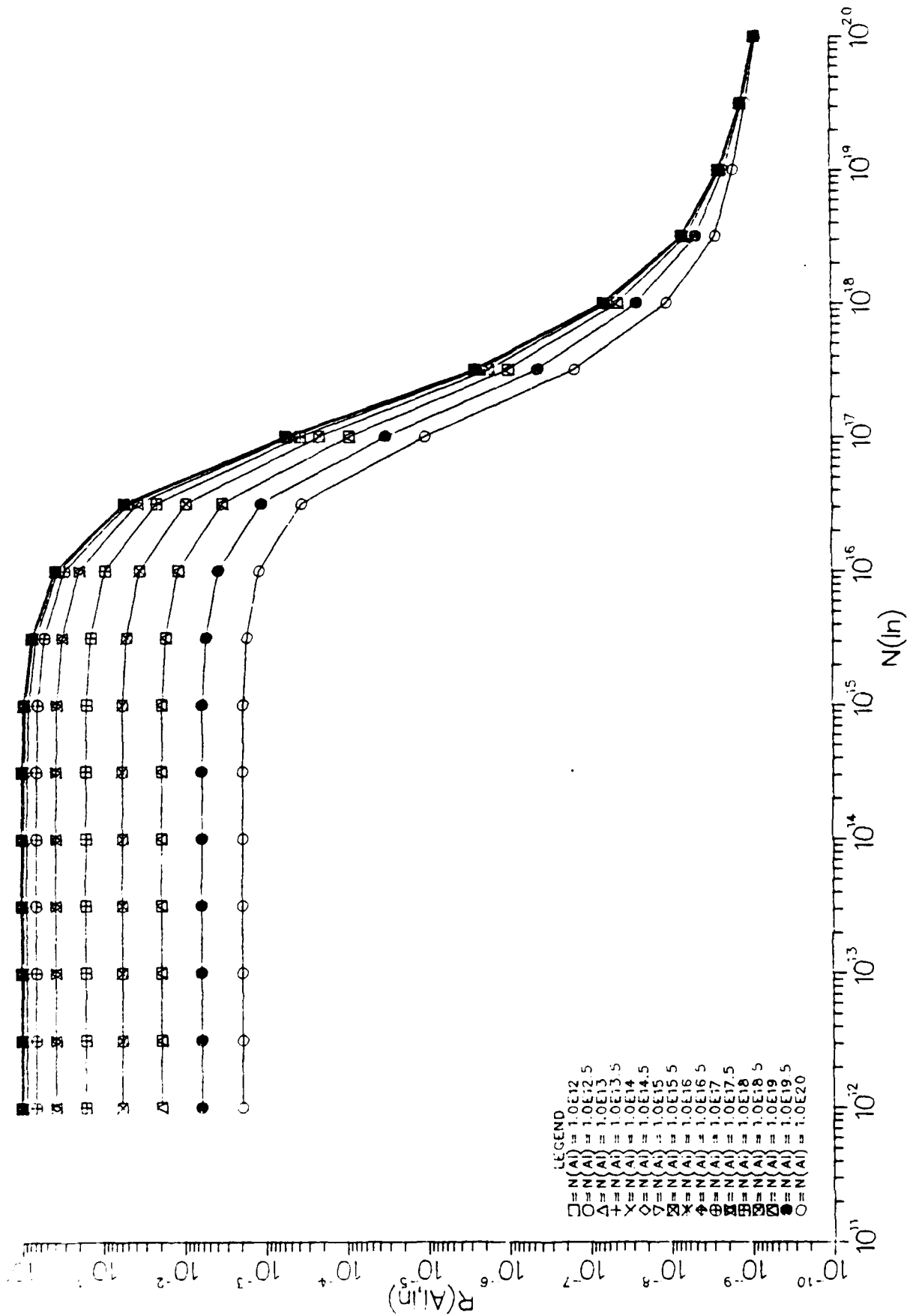


Figure 5a. $R(Al, In)$ for $\sigma_{Al/\sigma_{In}} = 0.05$ as functions of N_{In} for given N_{Al} .

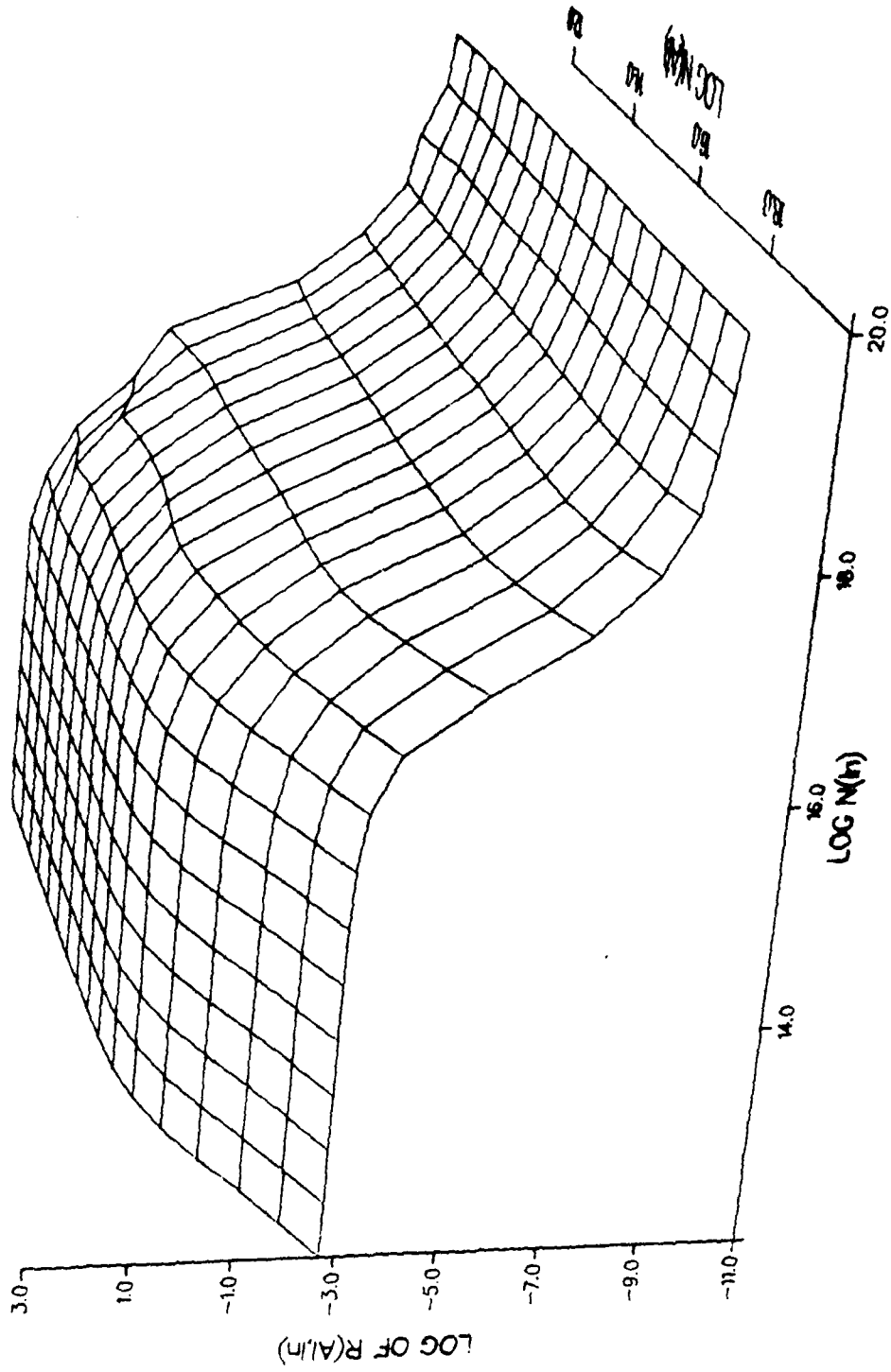


Figure 5b. One view of $R(AI, In)$ for $\sigma_{AI}/\sigma_{In} = 0.05$ as a function of N_{AI} and N_{In} .

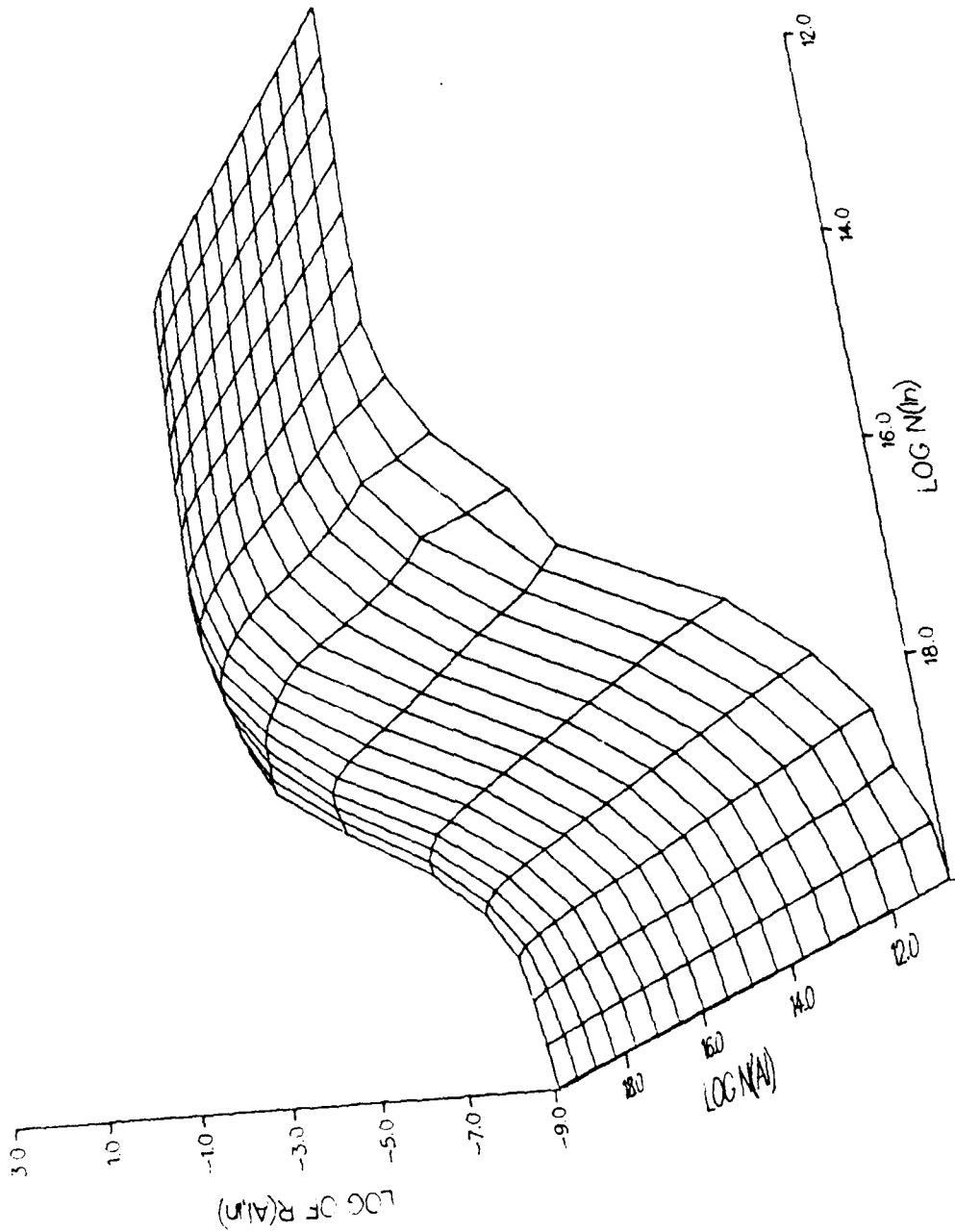


Figure 5c. Another view of $R(AI, In)$ for $\sigma_{AI/\sigma In} = 0.05$ as a function of N_{AI} and N_{In} .

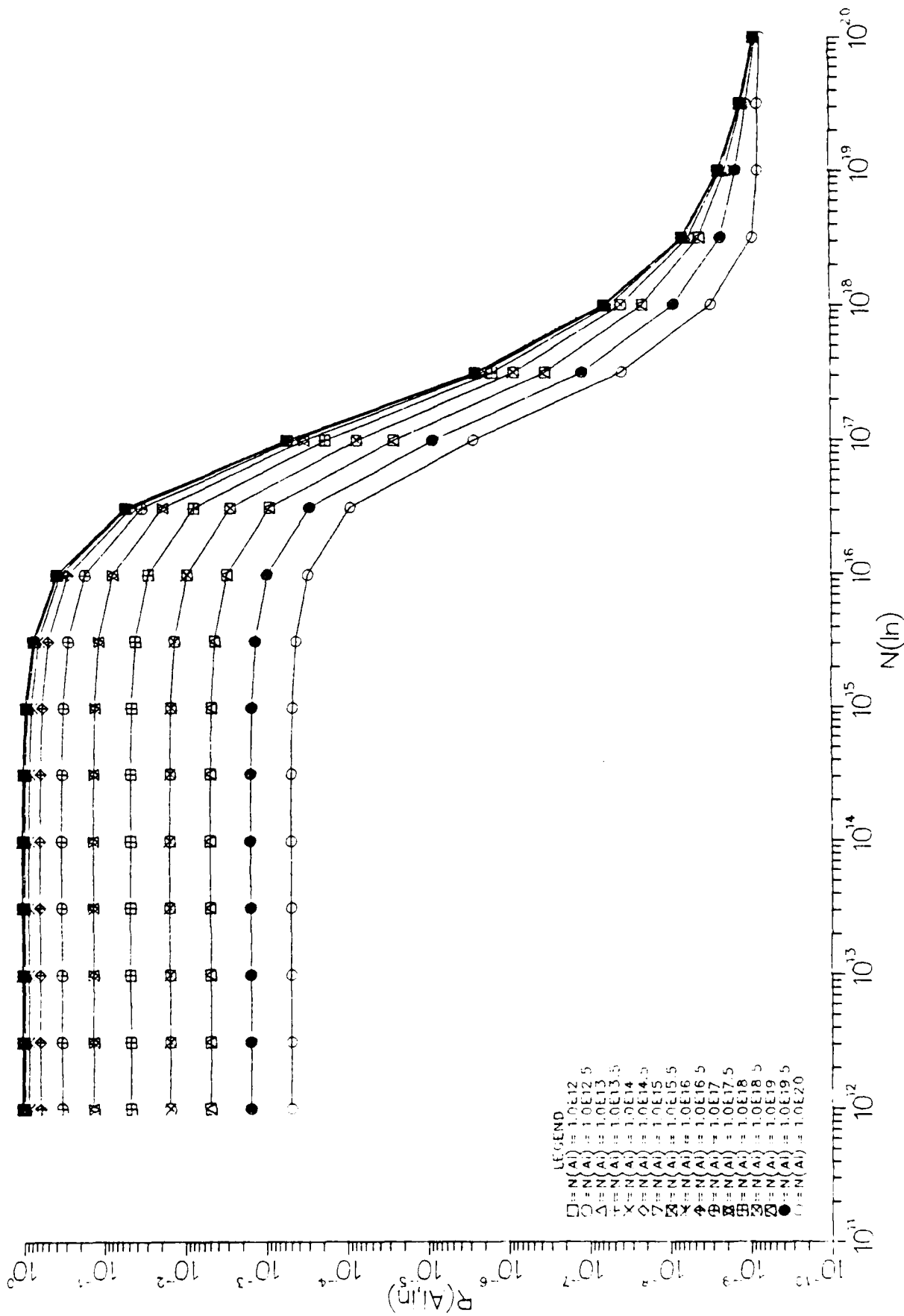
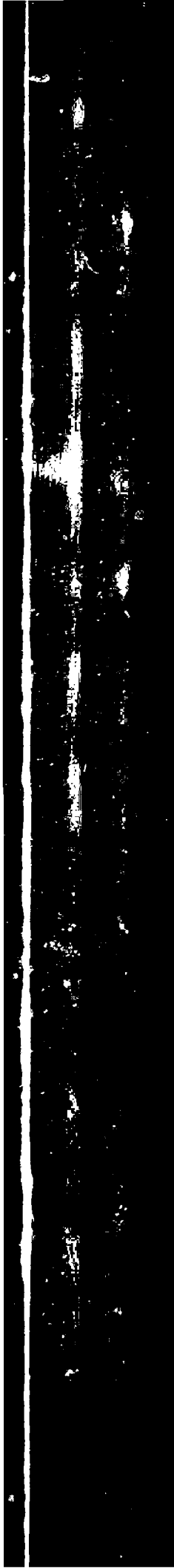


Figure 6a. $R(Al, In)$ for $N_{Al}/N_{In} = 0.2$ as functions of N_{In} for given N_{Al} .



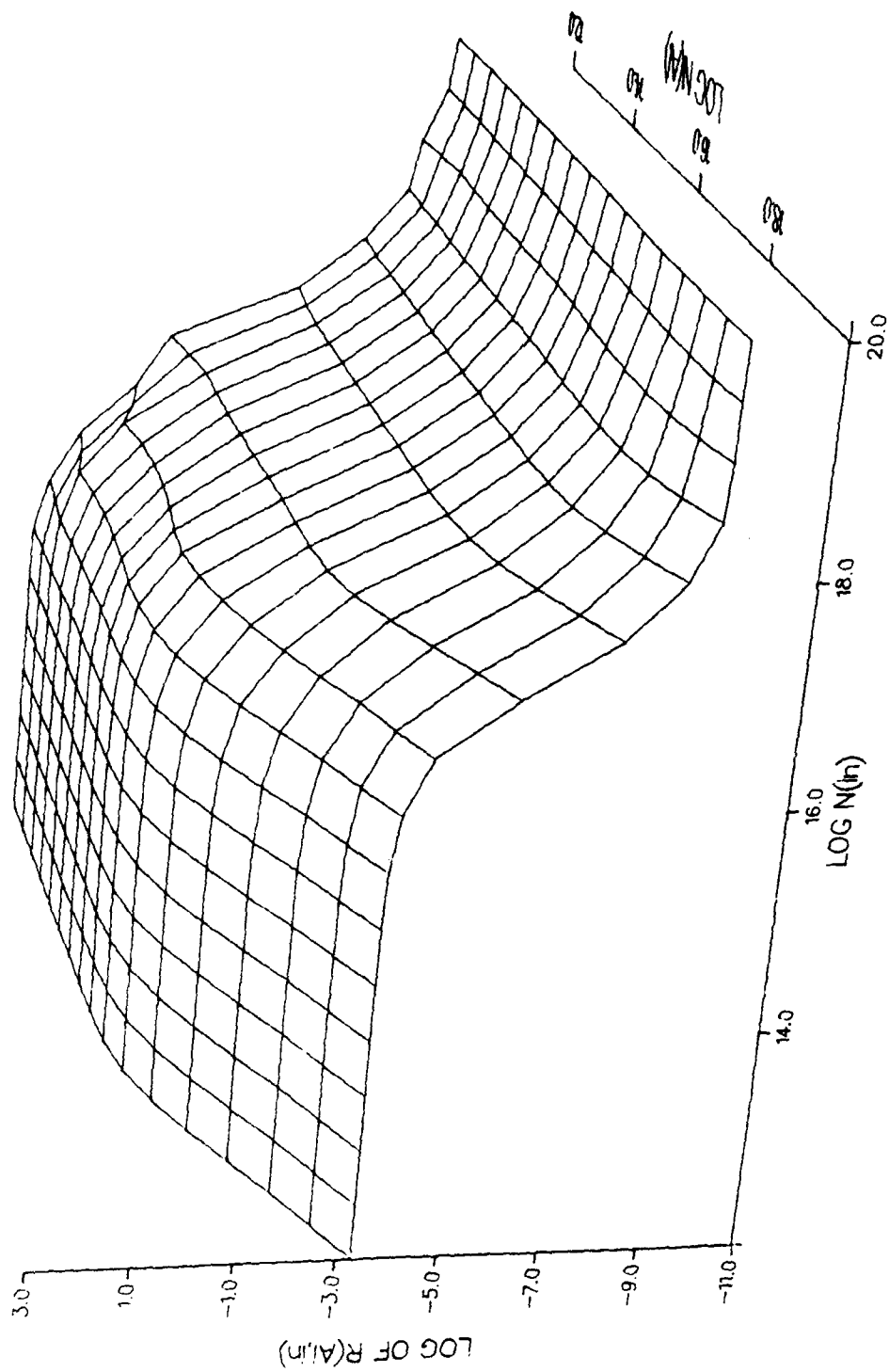


Figure 6b. One view of $R(AI, In)$ for $\sigma_{AI}/\sigma_{In} = 0.2$ as a function of N_{AI} and N_{In} .

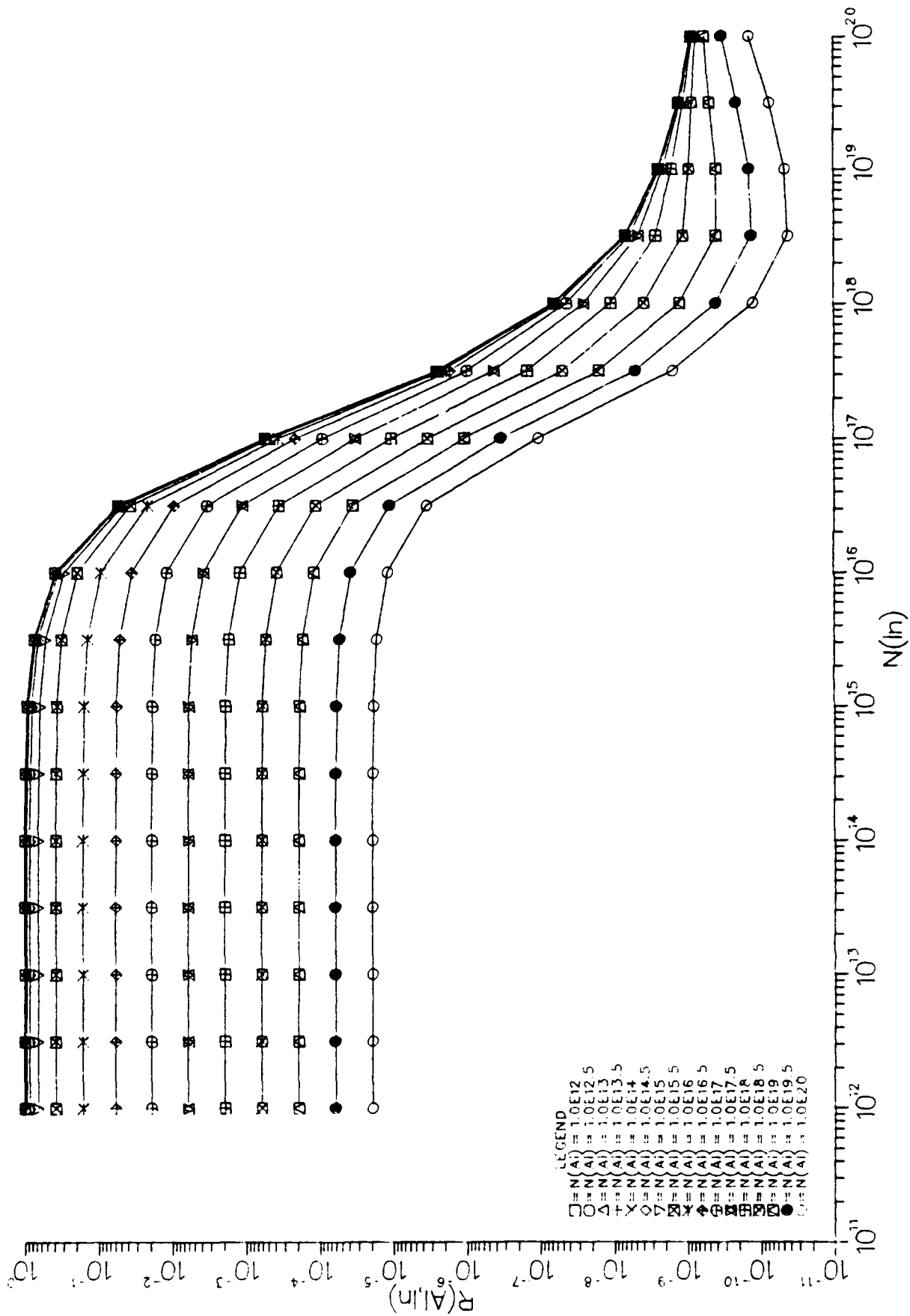


Figure 8a. $R(AI, In)$ for $\rho_{AI}/\rho_{In} = 5$ as functions of N_{In} for given N_{AI} .

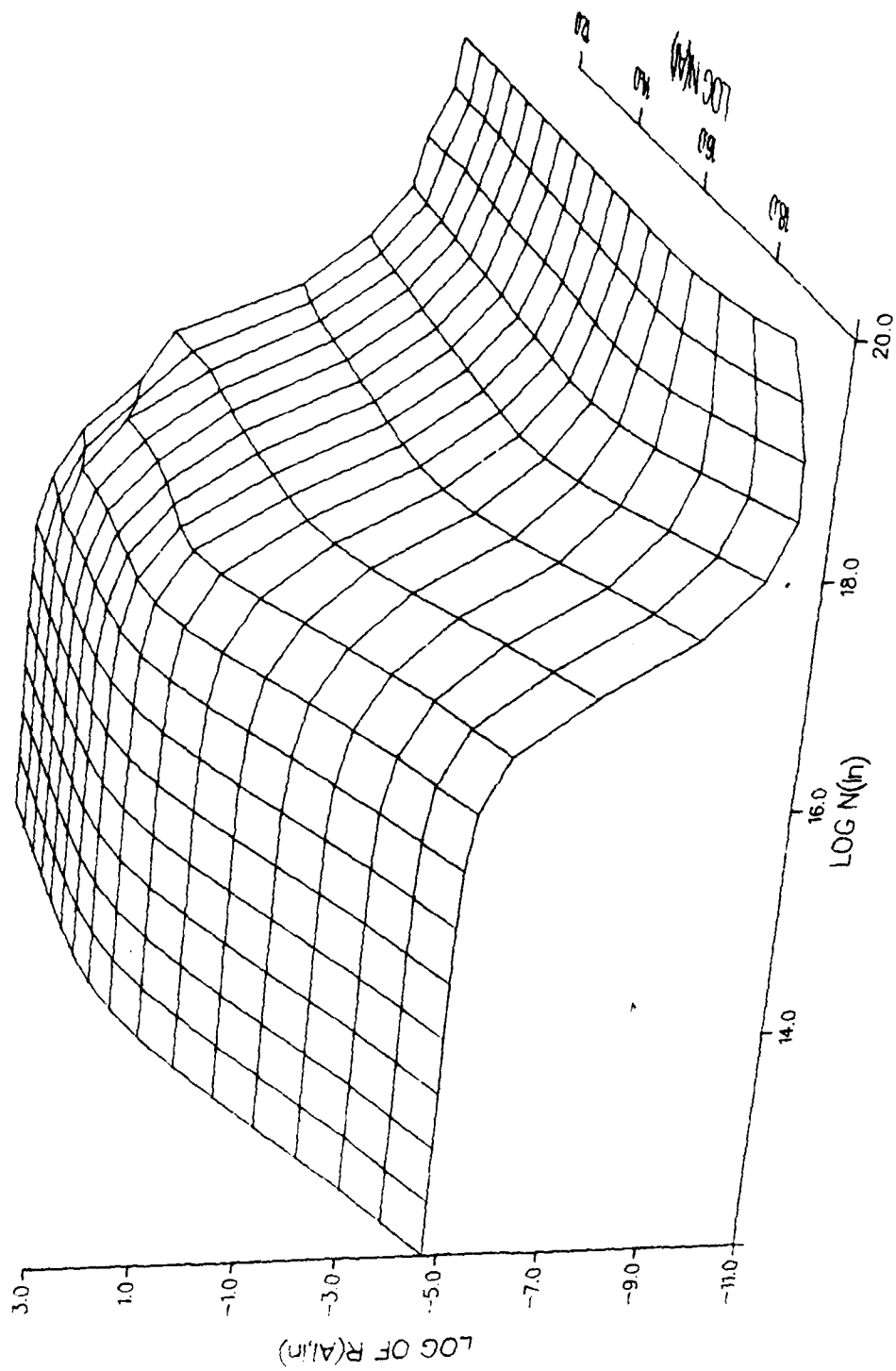


Figure 8c. Another view of $R(Al, In)$ for $\sigma_{Al/\sigma In} = 5$ as a function of N_{Al} and N_{In} .

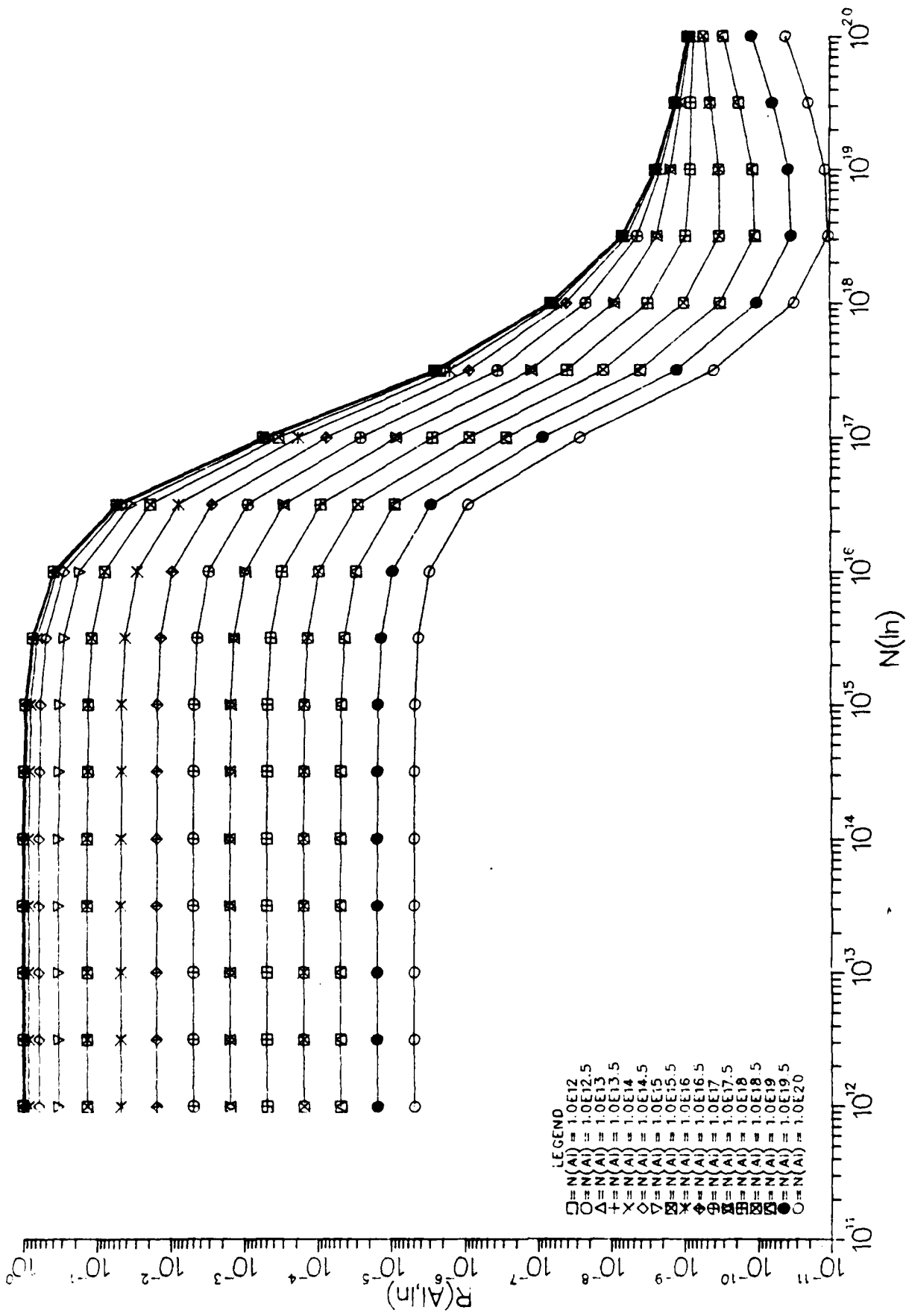


Figure 9a. $R(AI, In)$ for $\sigma_{AI/\sigma_{In}} = 20$ as functions of N_{In} for given N_{AI} .

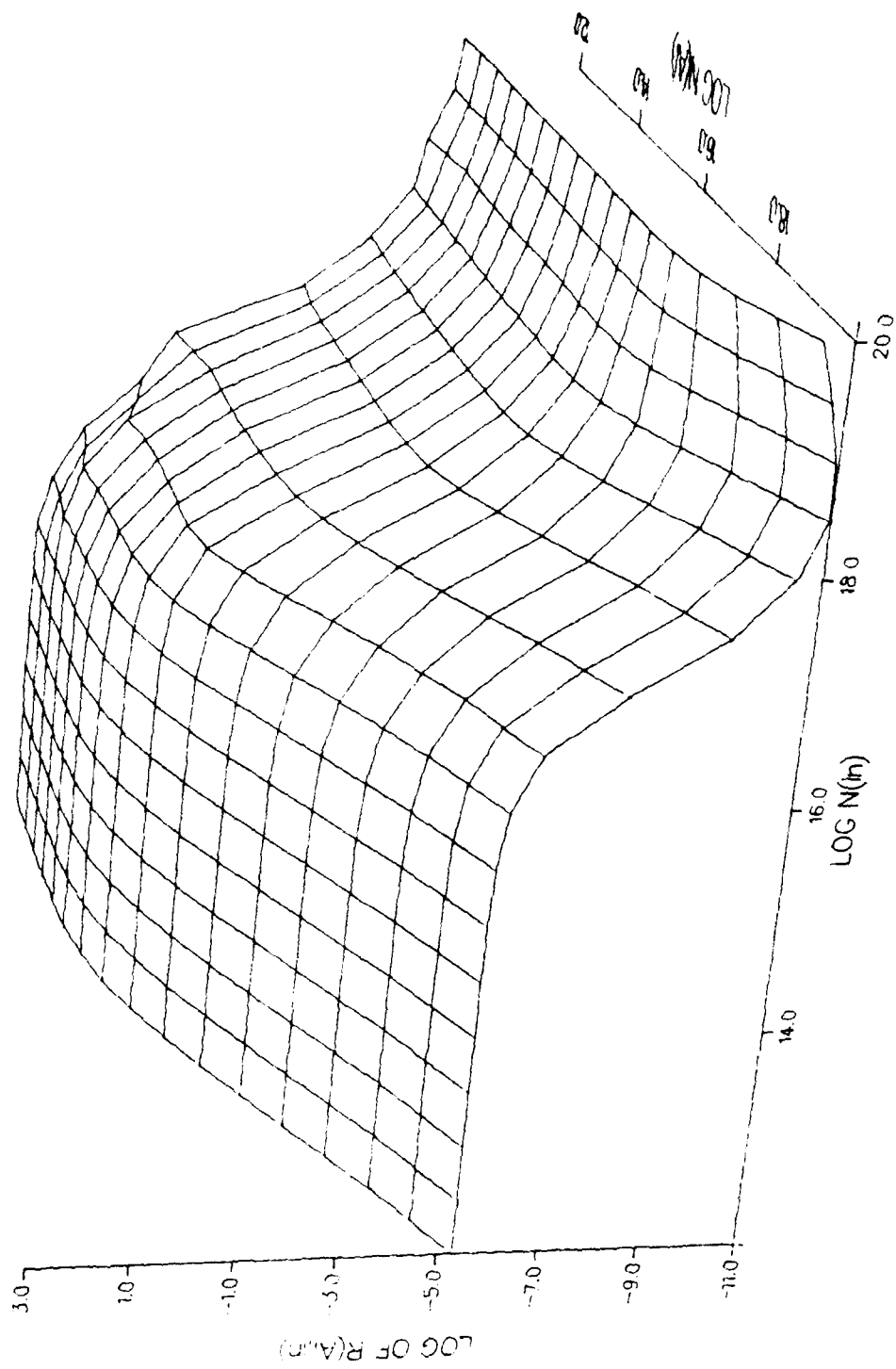


Figure 9b. One view of $R(A, In)$ for $N_{Al}/N_{In} = 20$ as a function of N_{Al} and N_{In} .

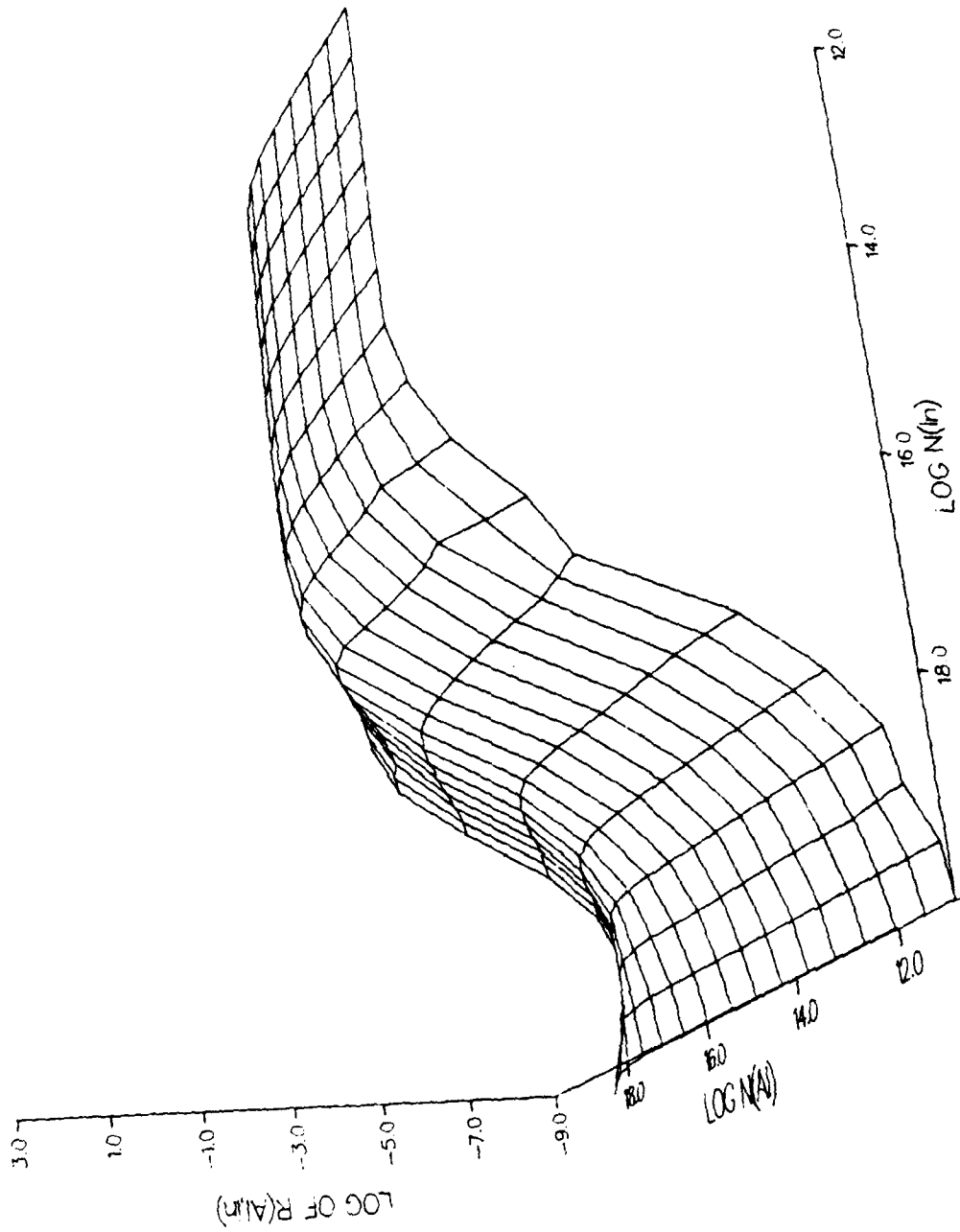


Figure 9c. Another view of $R(AI, In)$ for $J_{AI}^{u_{In}} = 20$ as a function of N_{AI} and N_{In} .

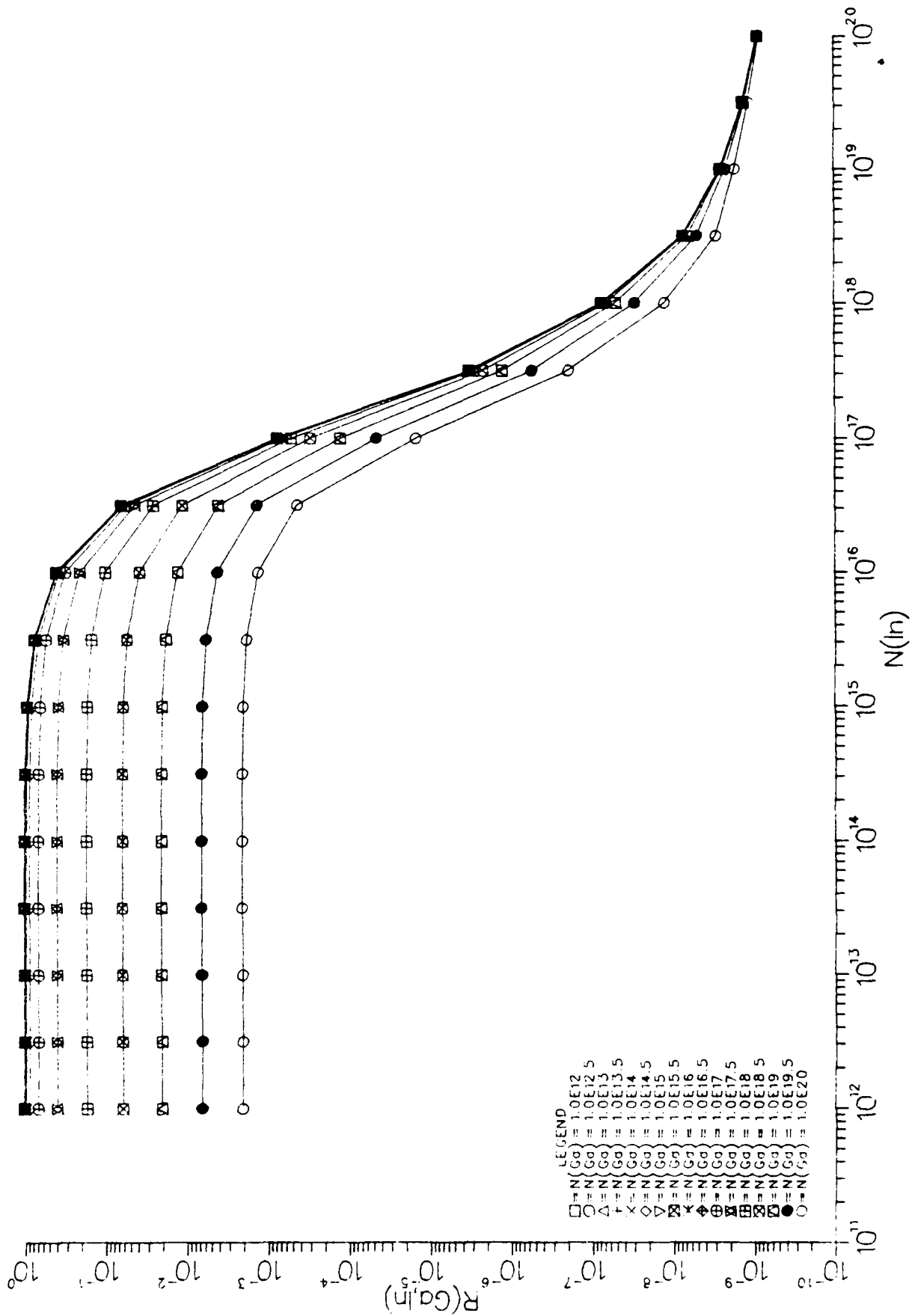


Figure 10a. $R(\text{Ga}, \text{In})$ for $\text{Ga}/\text{In} = 0.05$ as functions of N_{In} for given N_{Ga} .

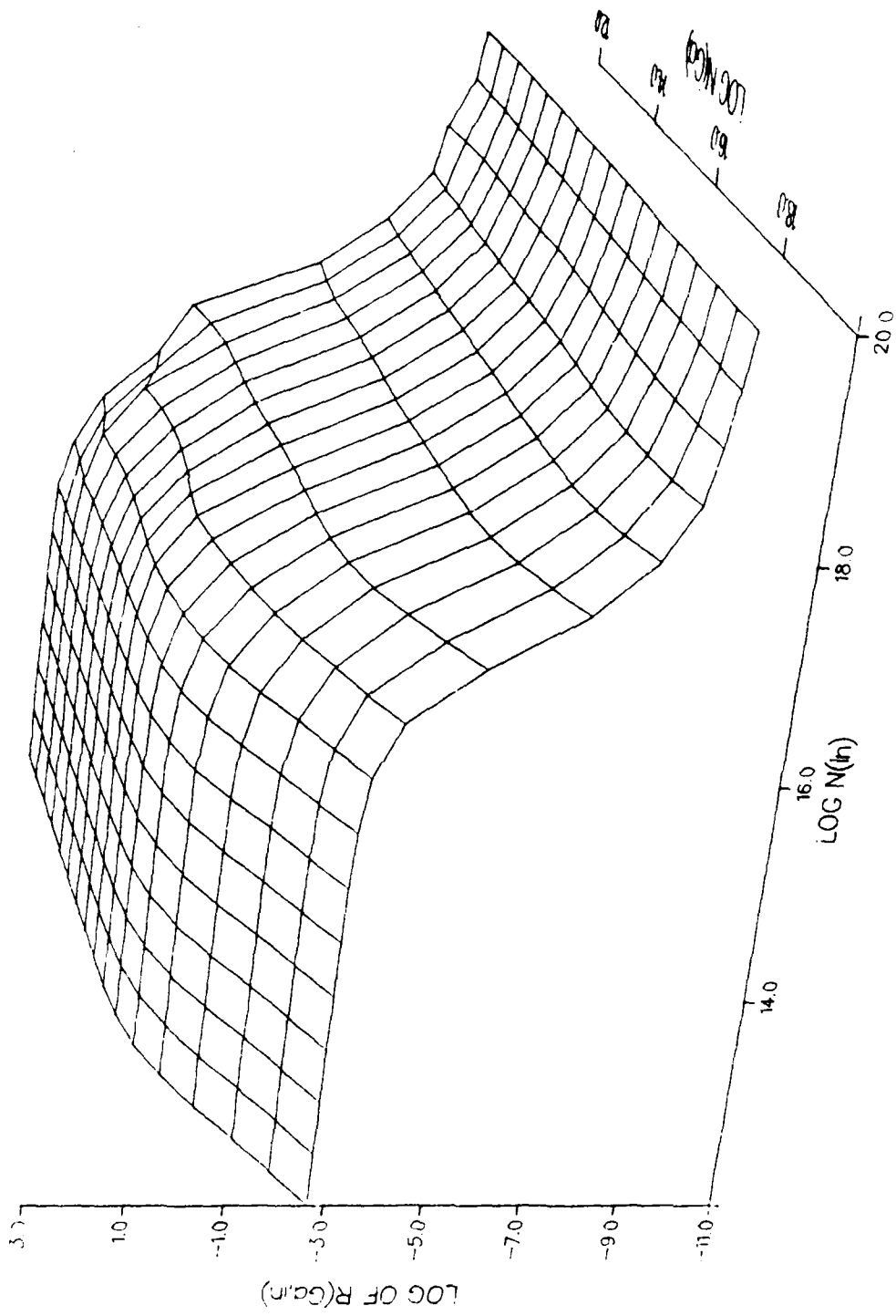


Figure 10b. One view of $R(\text{Ga}, \text{In})$ for $\frac{N_{\text{Ga}}}{N_{\text{In}}} = 0.05$ as a function of N_{Ga} and N_{In} .

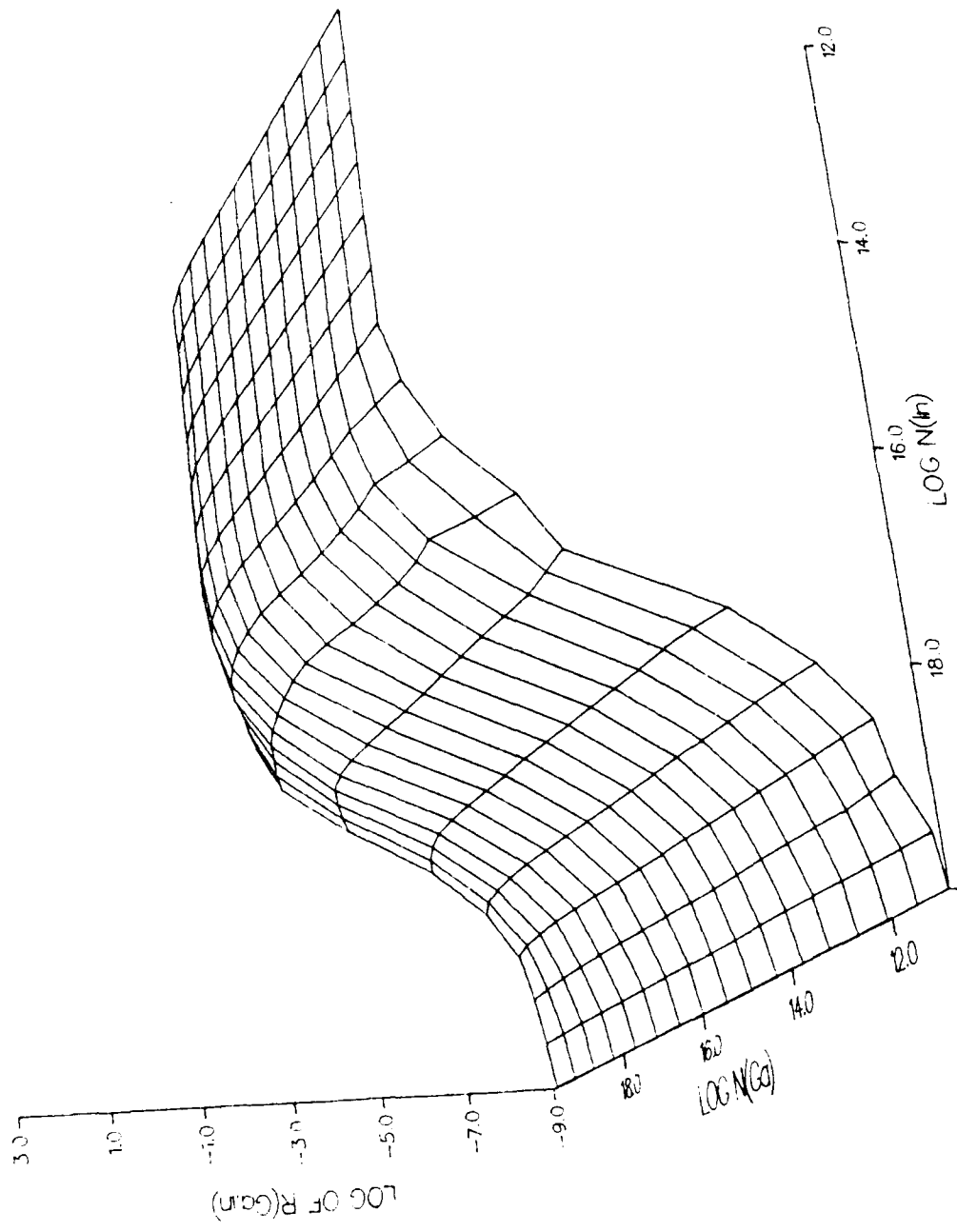


Figure 10c. Another view of $R(\text{Ga}, \text{In})$ for $\gamma_{\text{Ga}/\text{In}} = 0.05$ as a function of N_{Ga} and N_{In} .



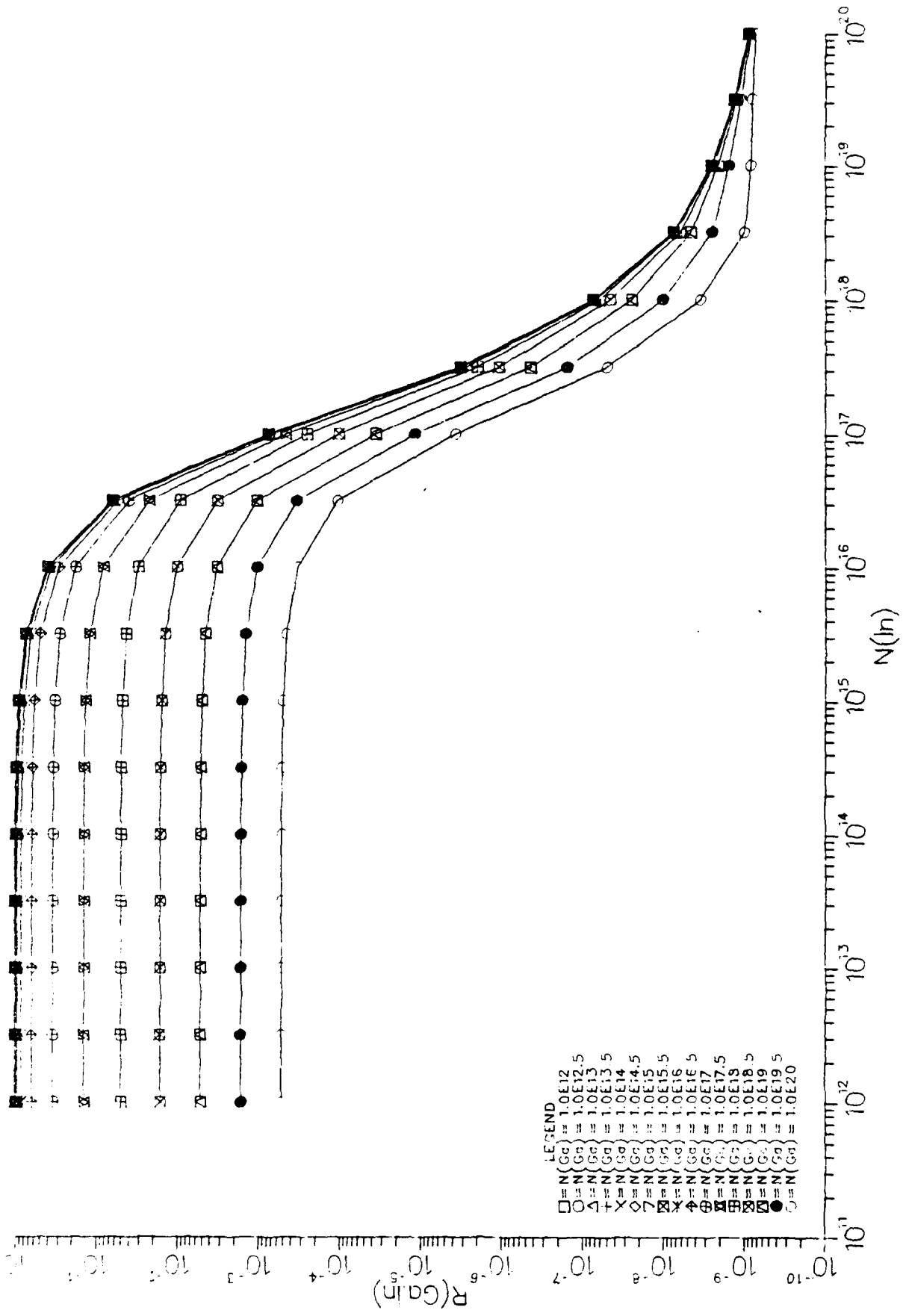


Figure 11a. $R(\text{Ga}, \text{In})$ for $N_{\text{Ga}}/N_{\text{In}} = 0.2$ as functions of N_{In} for given N_{Ga} .

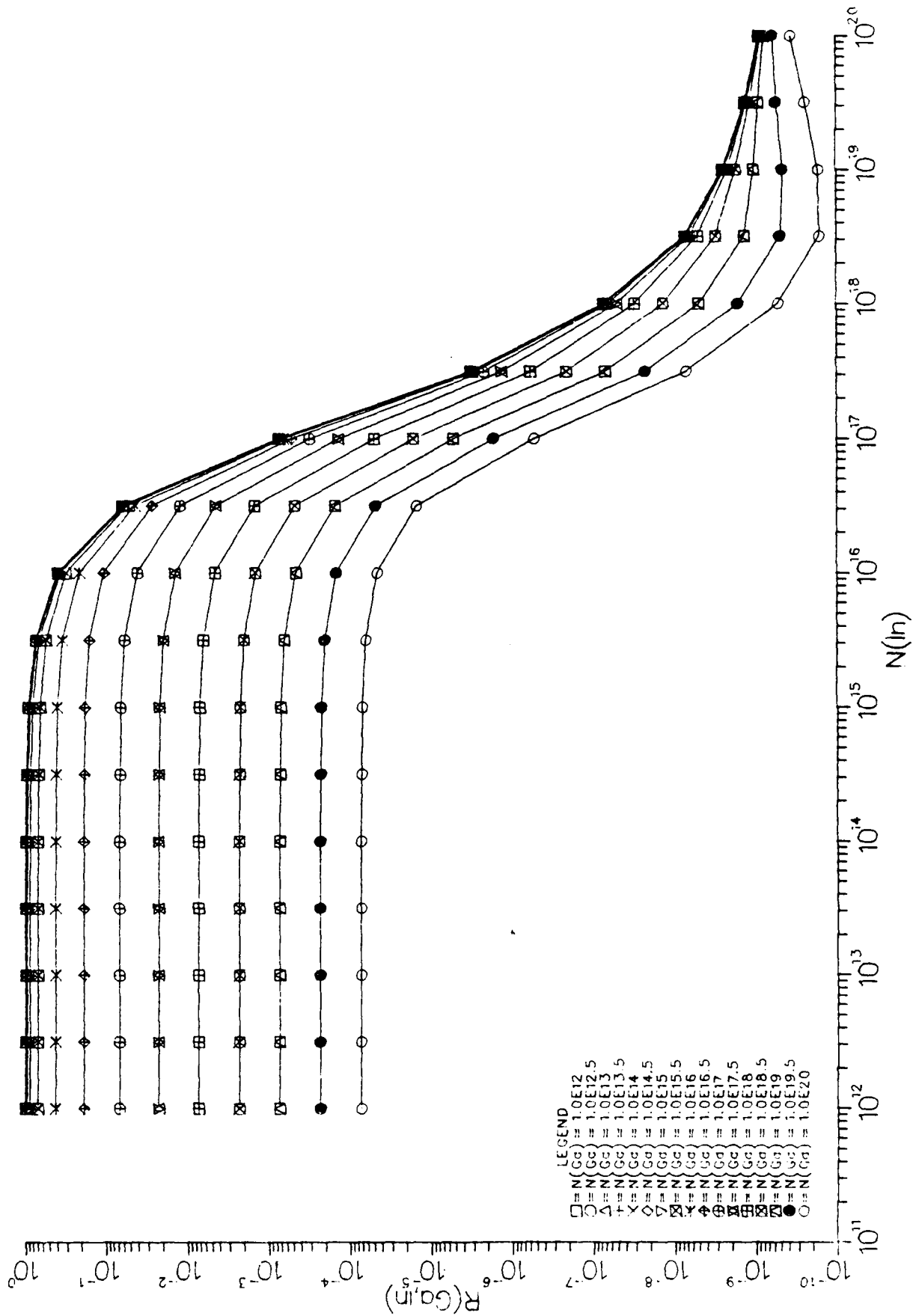


Figure 12a. $R(\text{Ga}, \text{In})$ for $\sigma_{\text{Ga}}/\sigma_{\text{In}} = 1.4$ as functions of N_{In} for given N_{Ga} .

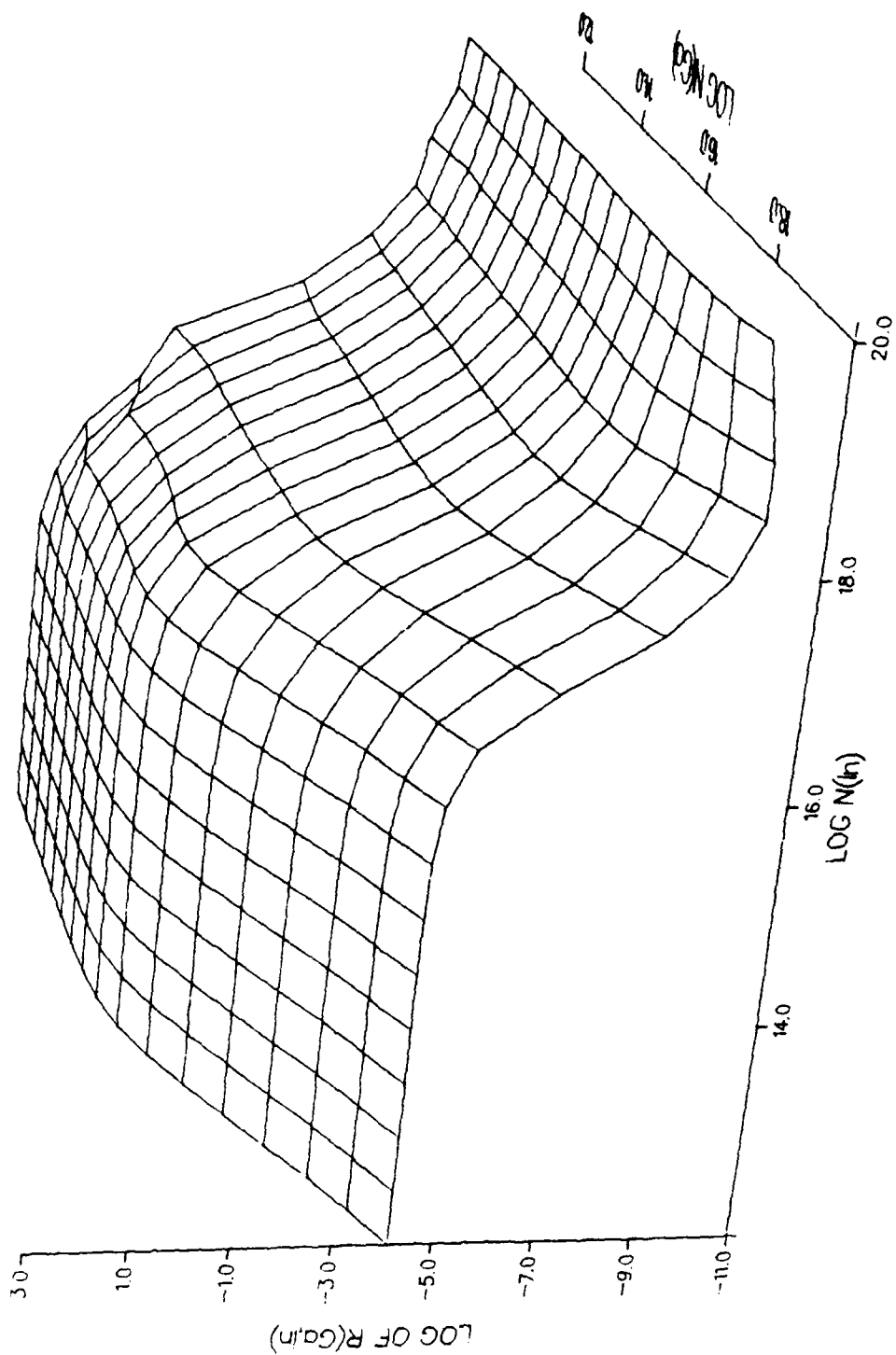


Figure 12b. One view of $R(\text{Ga}, \text{In})$ for $\sigma_{\text{Ga}}/\sigma_{\text{In}} = 1.4$ as a function of N_{Ga} and N_{In} .

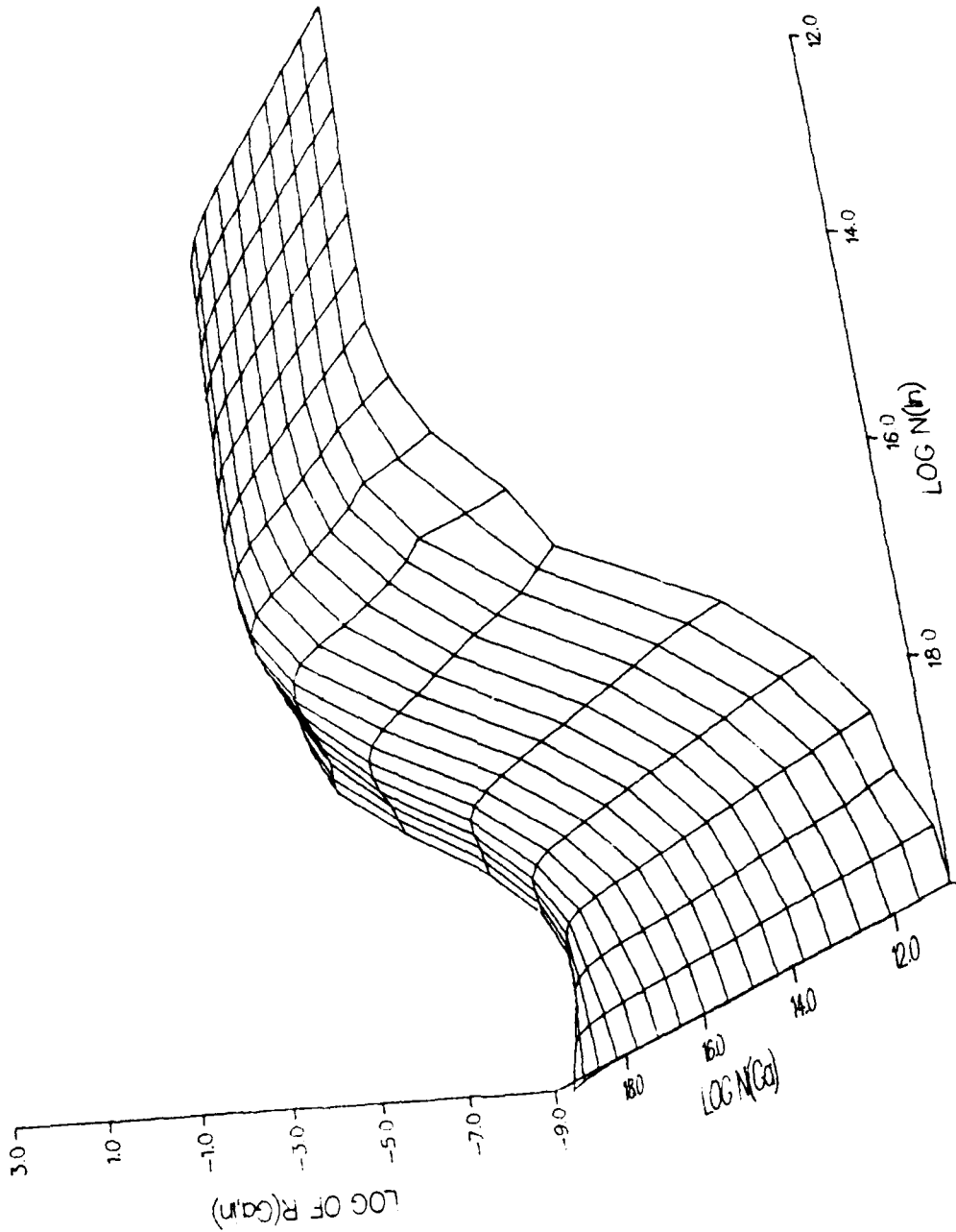


Figure 12c. Another view of $R(\text{Ga}, \text{In})$ for $\sigma_{\text{Ga}}/\sigma_{\text{In}} = 1.4$ as a function of N_{Ga} and N_{In} .

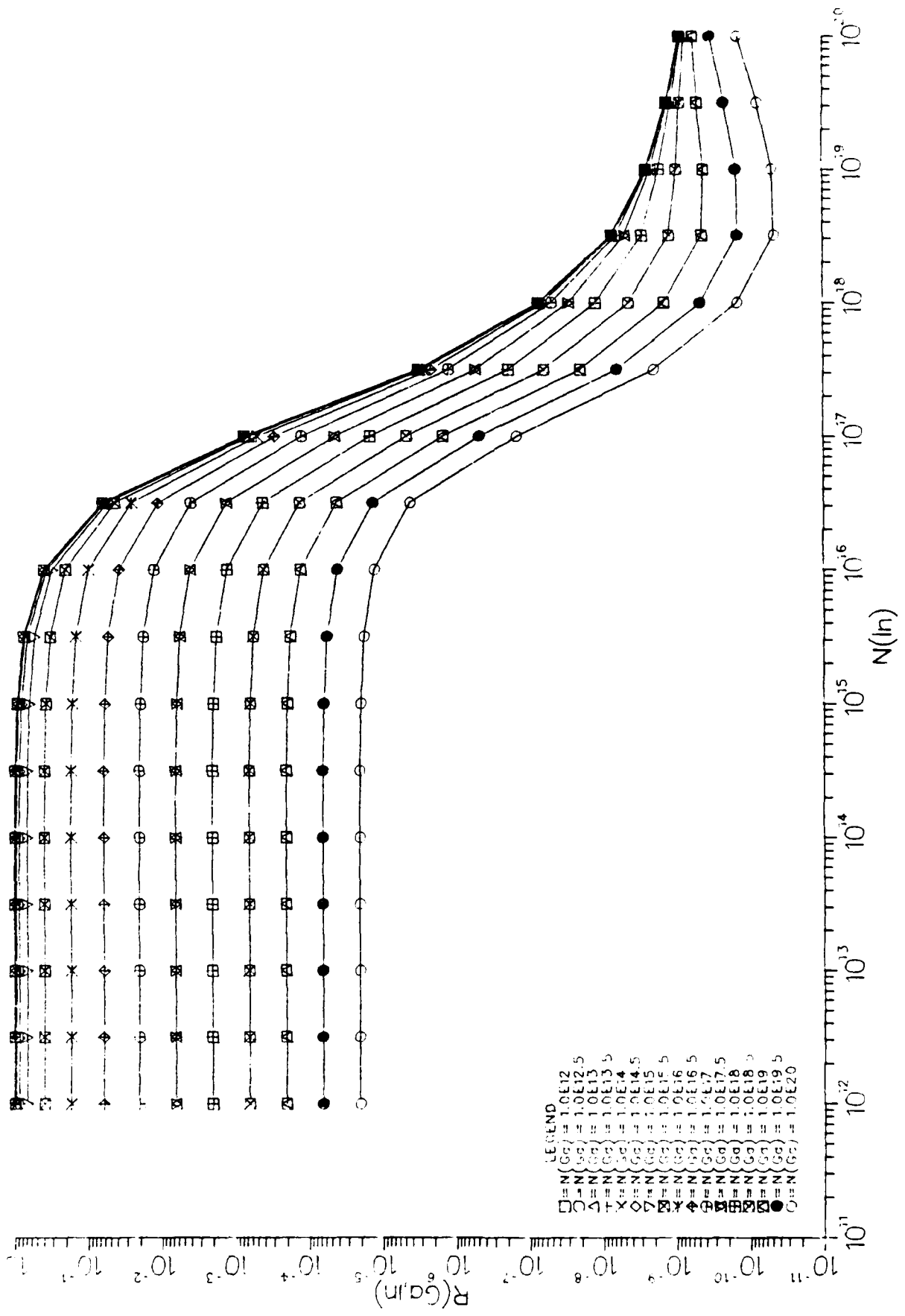


Figure 13a. $R(\text{Ga}, \text{In})$ for $\sigma_{\text{Ga}/\sigma_{\text{In}}} = 5$ as functions of N_{In} for given N_{Ga} .

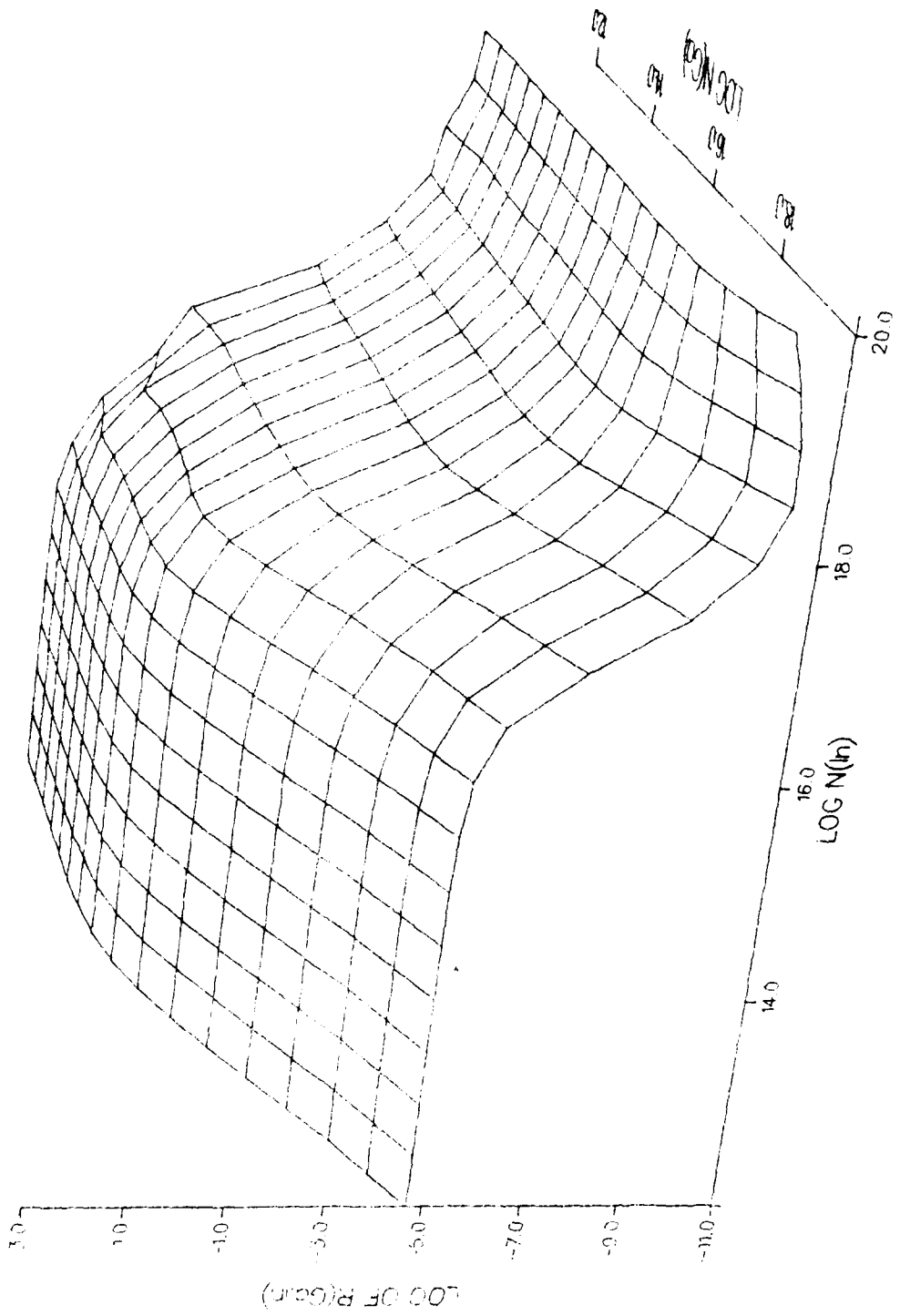


Figure 13b. One view of $R(\text{Ga}, \text{In})$ for $\sigma_{\text{Ga}}/\sigma_{\text{In}} = 5$ as a function of N_{Ga} and N_{In} .

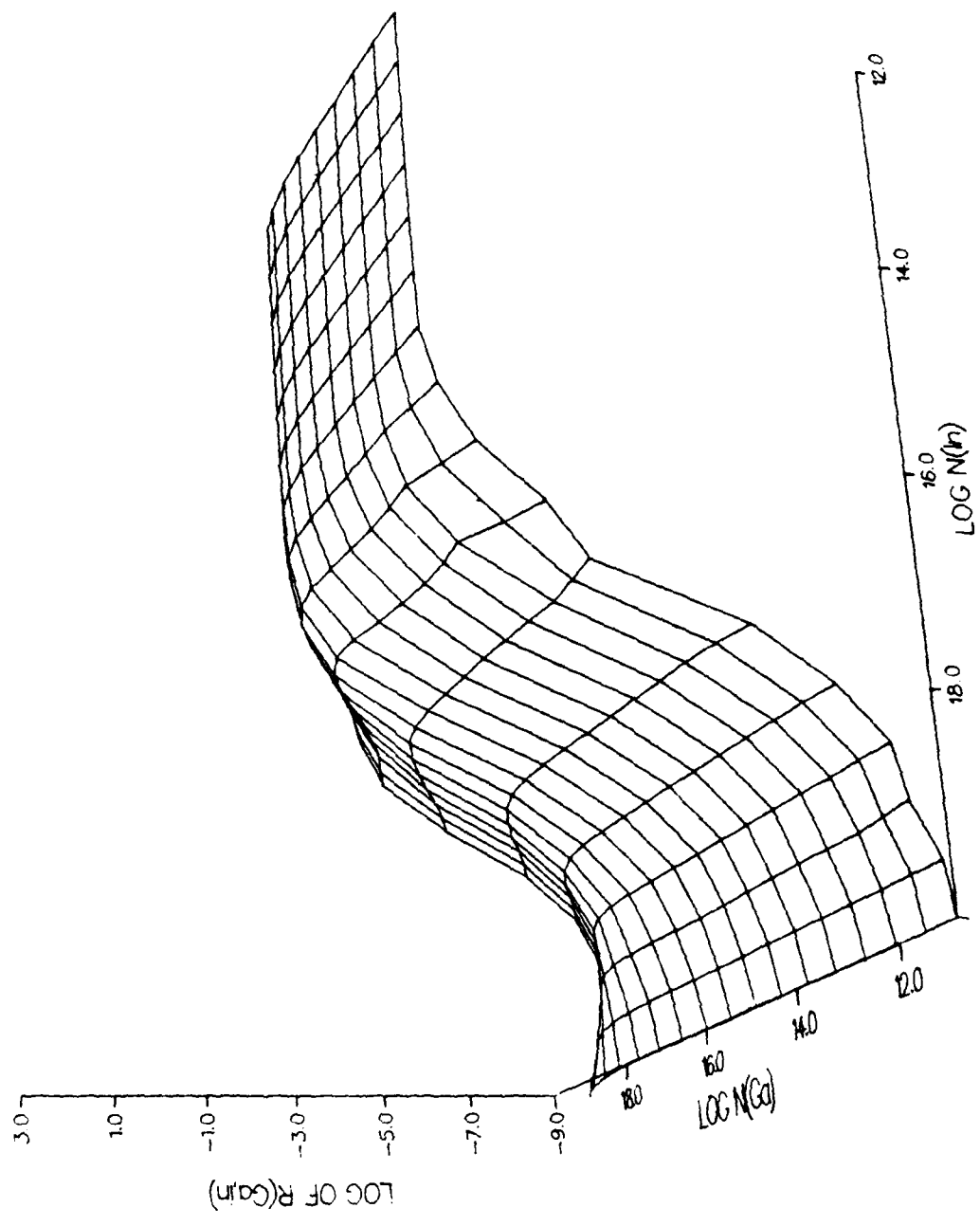


Figure 13c. Another view of $R(\text{Ga}, \text{In})$ for $\sigma_{\text{Ga}}/\sigma_{\text{In}} = 5$ as a function of N_{Ga} and N_{In} .

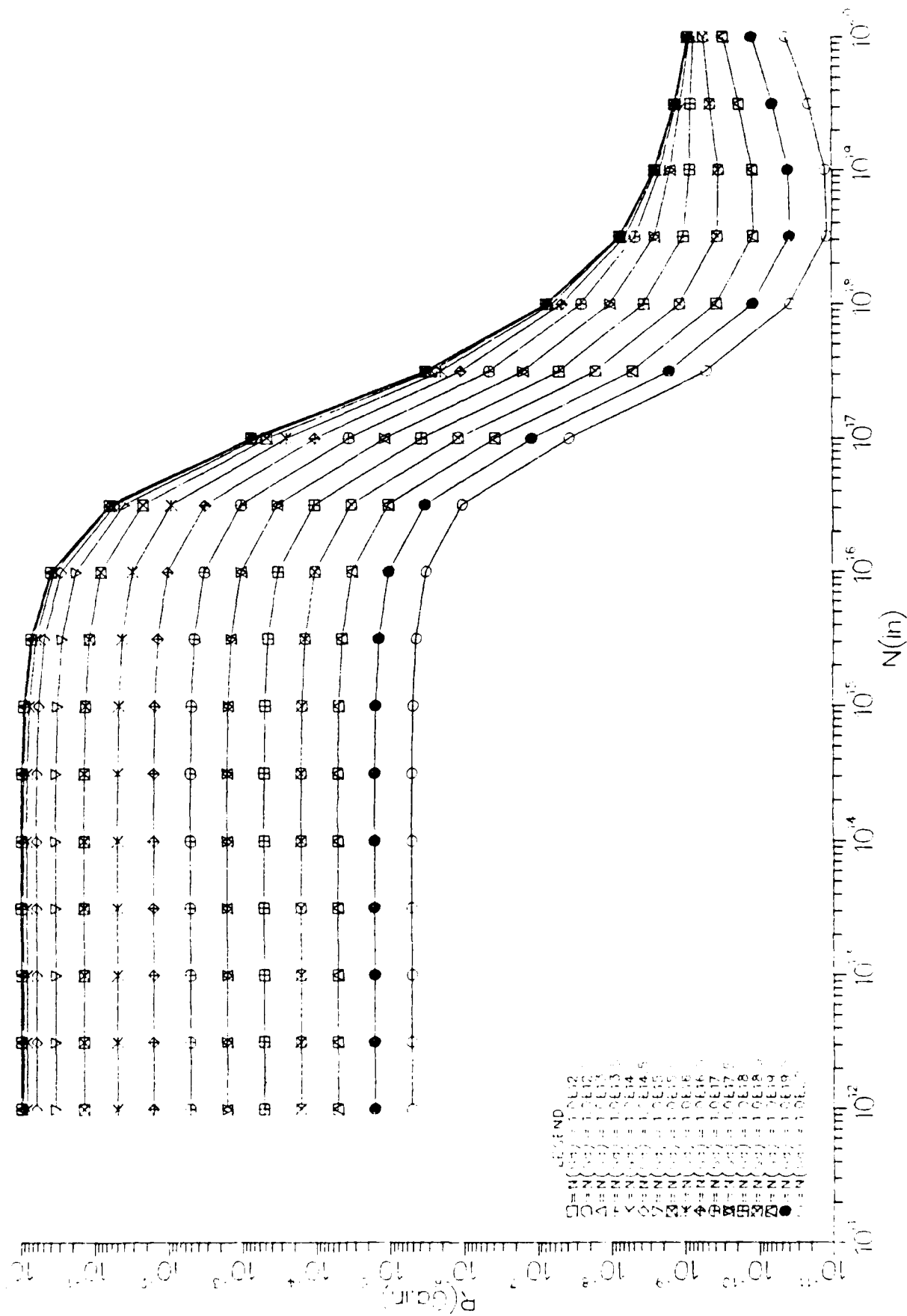


Figure 14a. $R(Ga, In)$ for $N(Ga) = 20$ as functions of $N(In)$ for given $N(Ga)$.

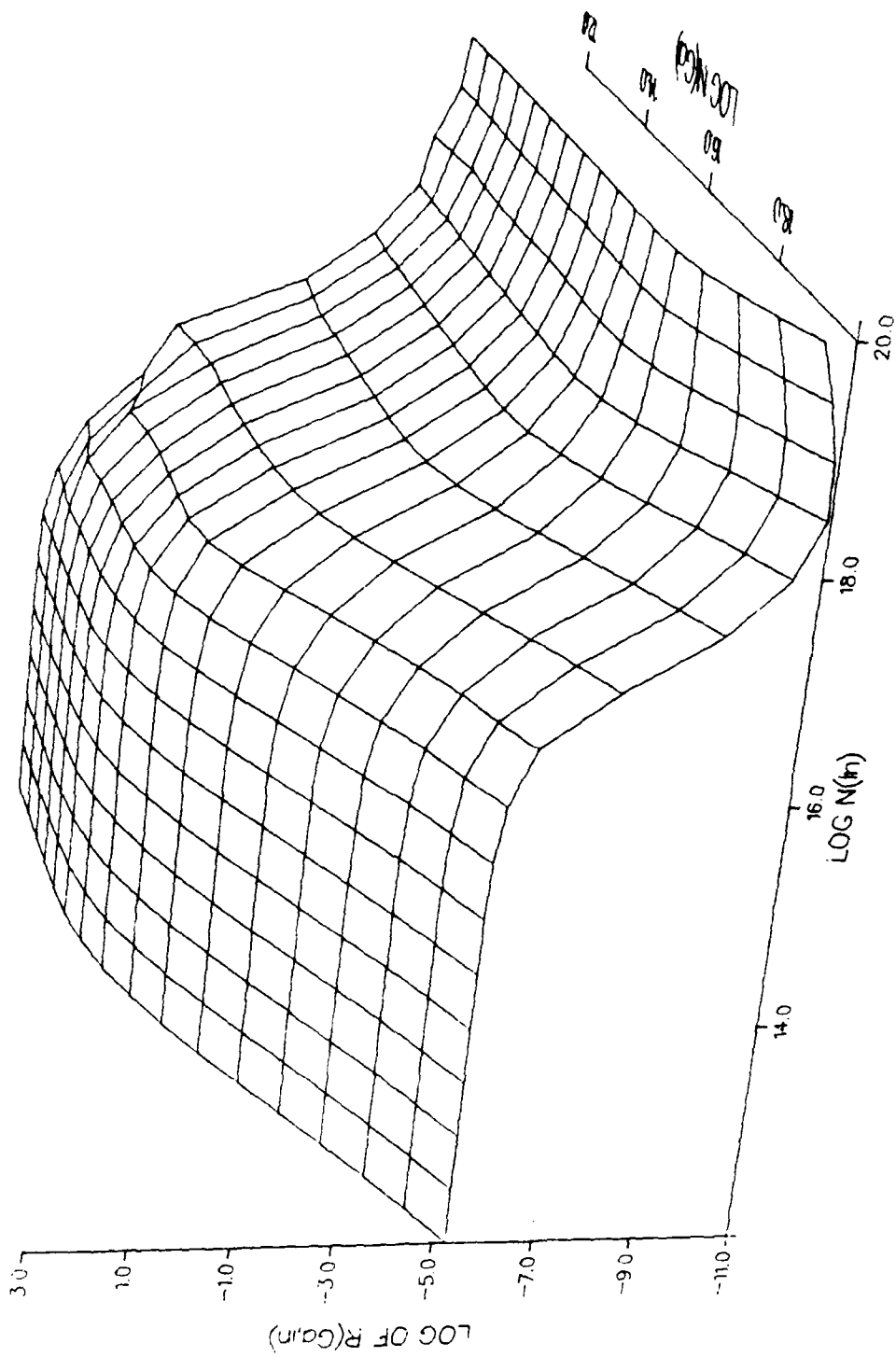


Figure 14b. One view of $R(\text{Ga}, \text{In})$ for $\sigma_{\text{Ga}}/\sigma_{\text{In}} = 20$ as a function of N_{Ga} and N_{In} .

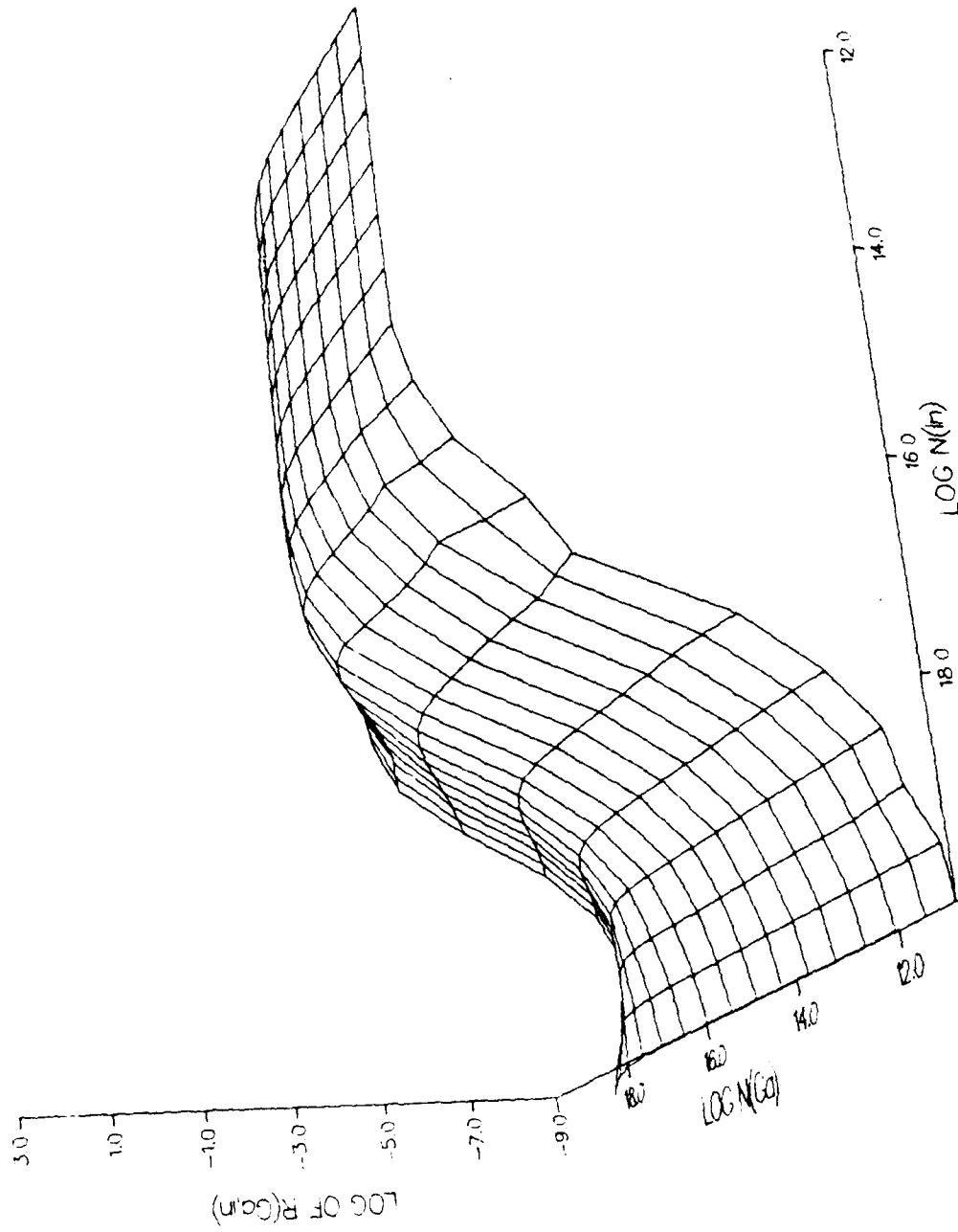


Figure 14c. Another view of $R(\text{Ga}, \text{In})$ for $N_{\text{Ga}}/N_{\text{In}} = 20$ as a function of N_{Ga} and N_{In} .

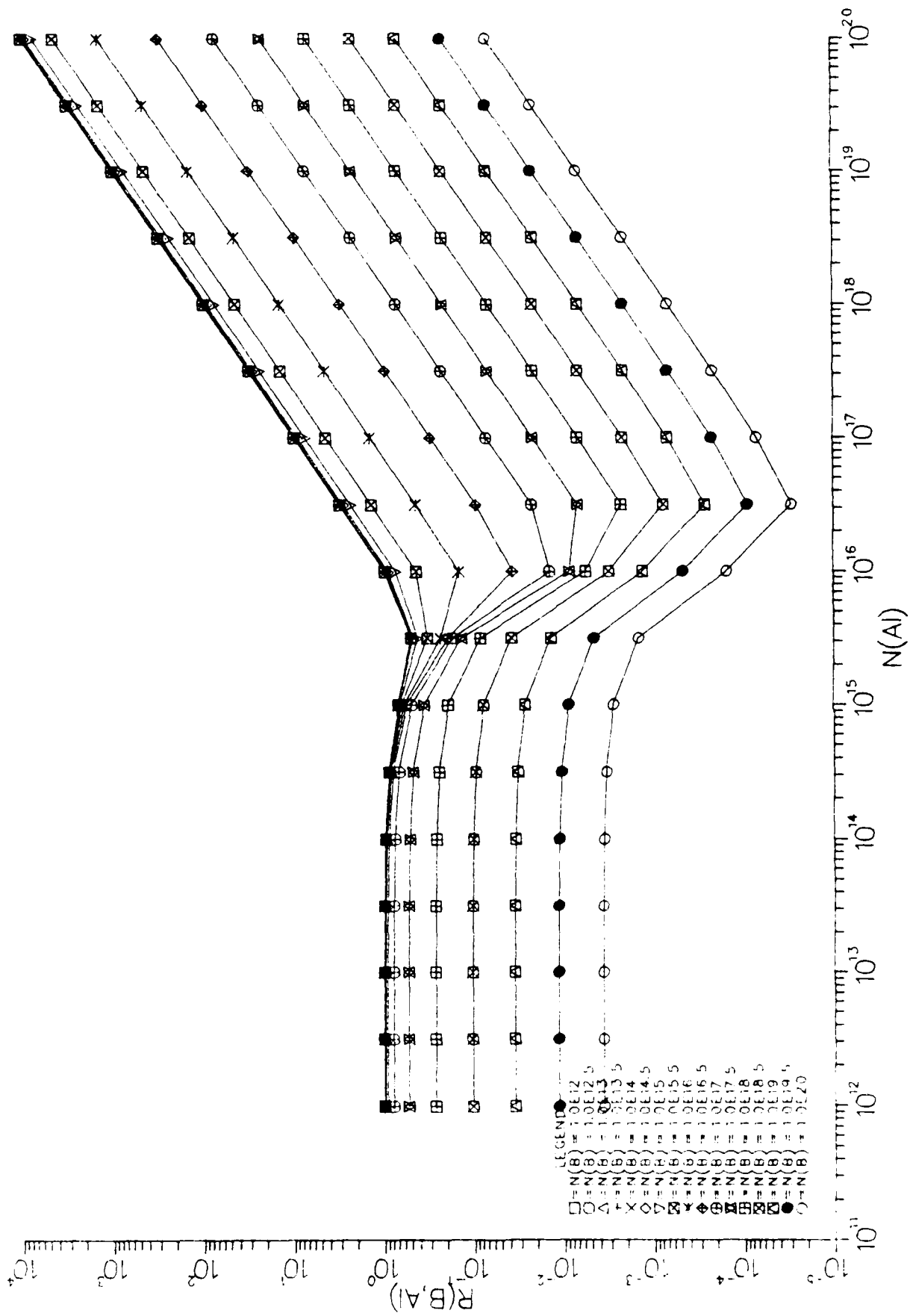


Figure 15a. $R(B, A1)$ for $B/A1 = 0.005$ as functions of N_{A1} for given N_B .

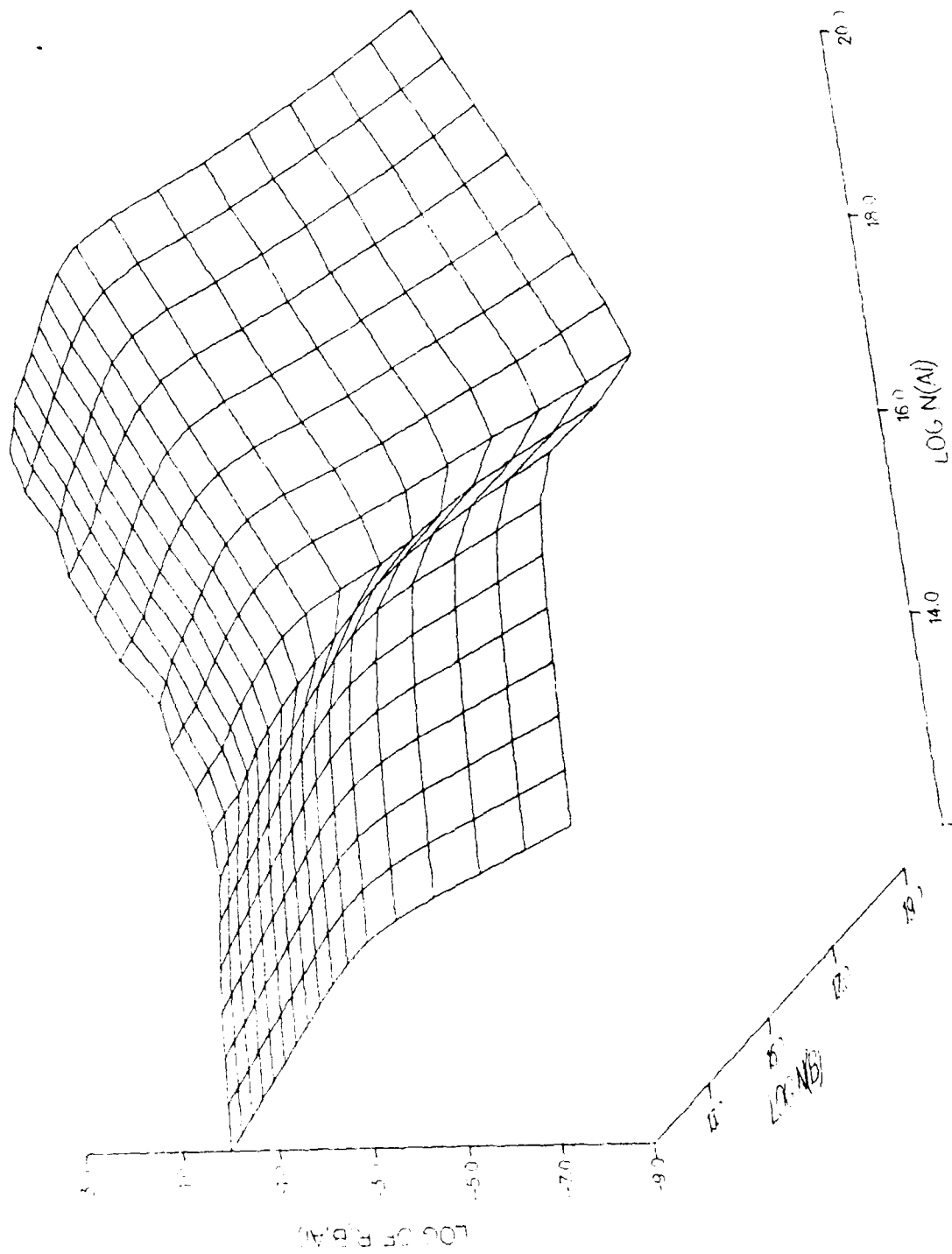
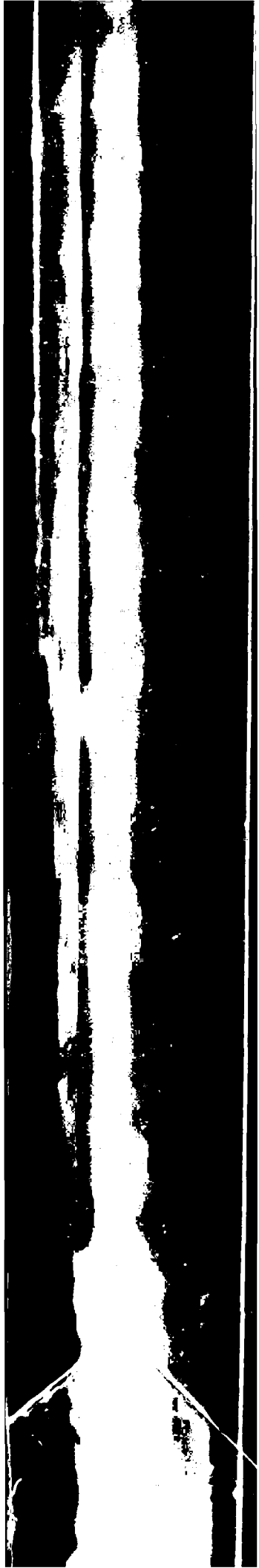


Figure 15b. One view of $R(B, Al)$ for $\log N(Al) = 0.005$ as a function of N_B and N_{Al} .



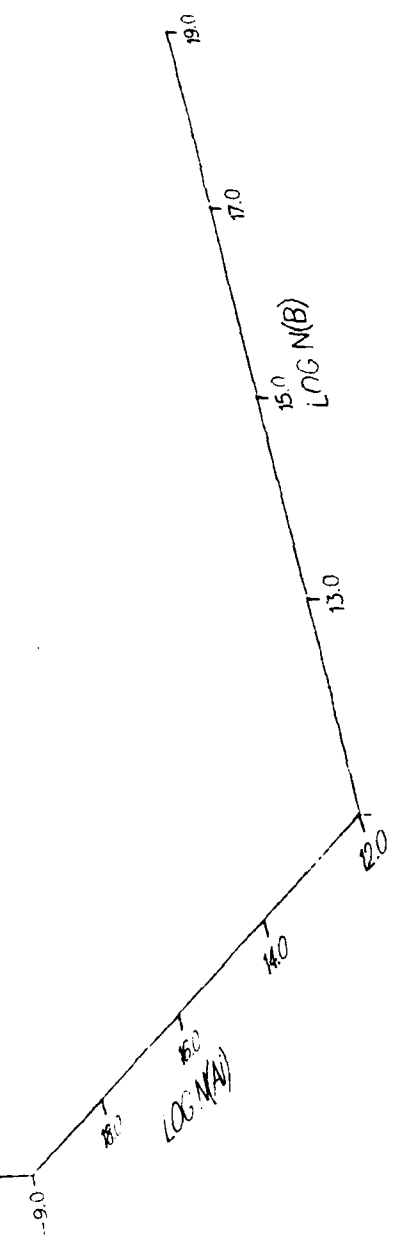
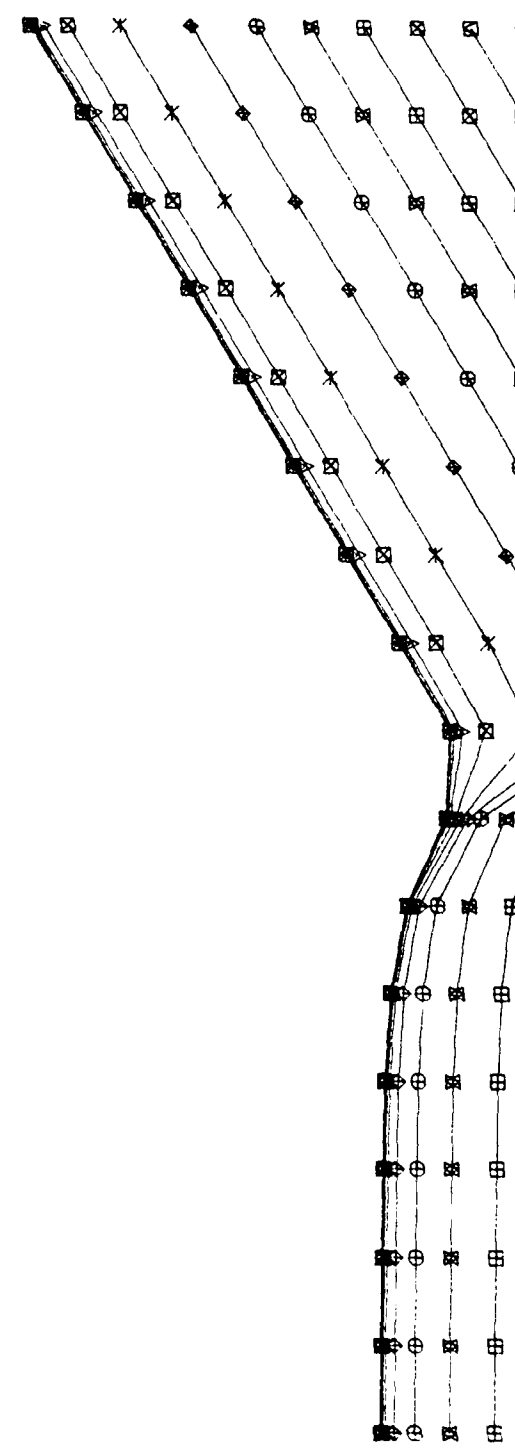


Figure 15c. Another view of $R(B, A_1)$ for $\sigma_B / \sigma_{A_1} = 0.005$ as a function of N_B and N_{A_1} .

$B(A_1)$
 10^4
 10^3
 10^2
 10^1



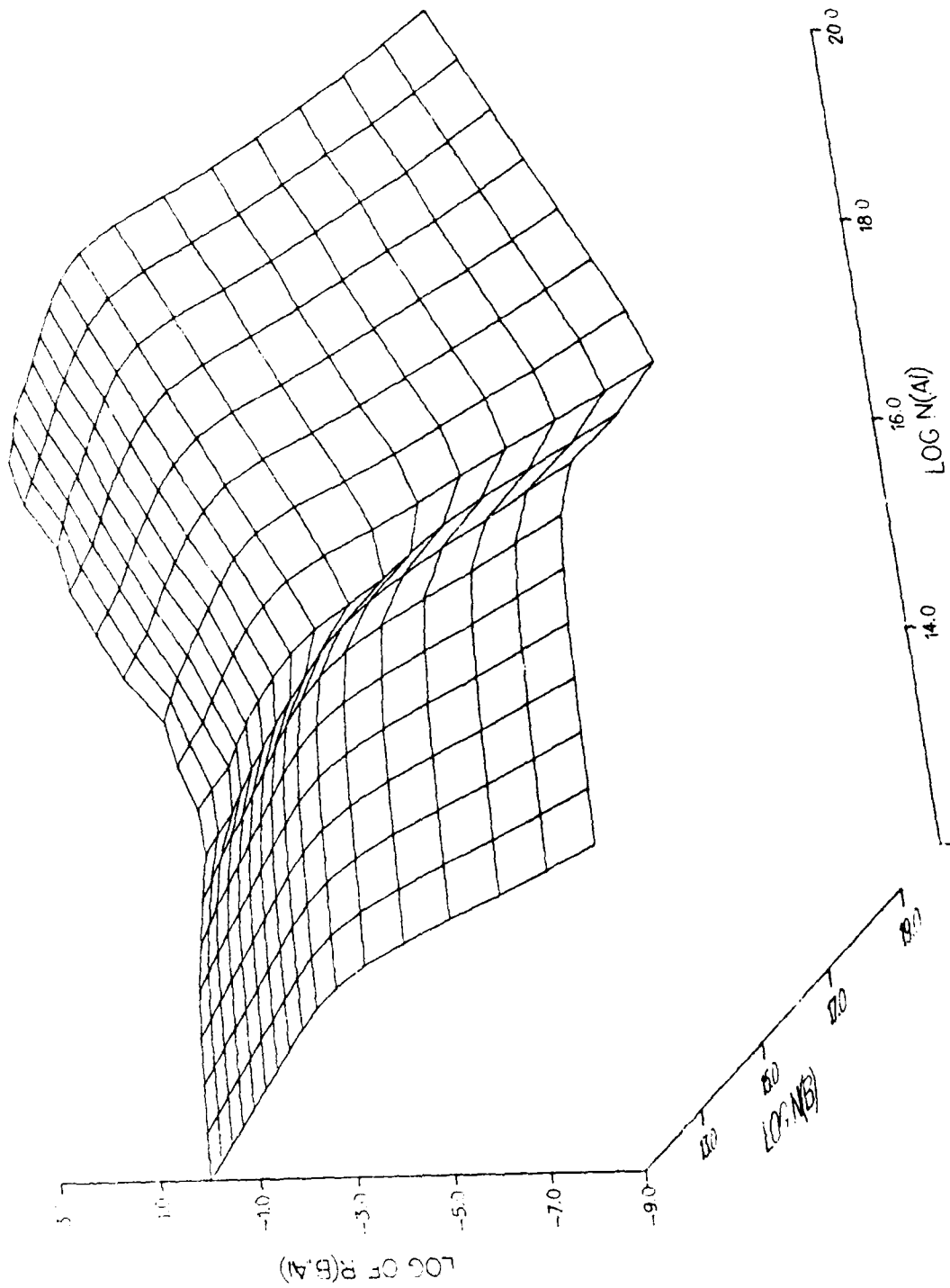


Figure 16b. One view of $R(B,Al)$ for $\sigma_B/\sigma_{Al} = 0.02$ as a function of N_B and N_{Al} .

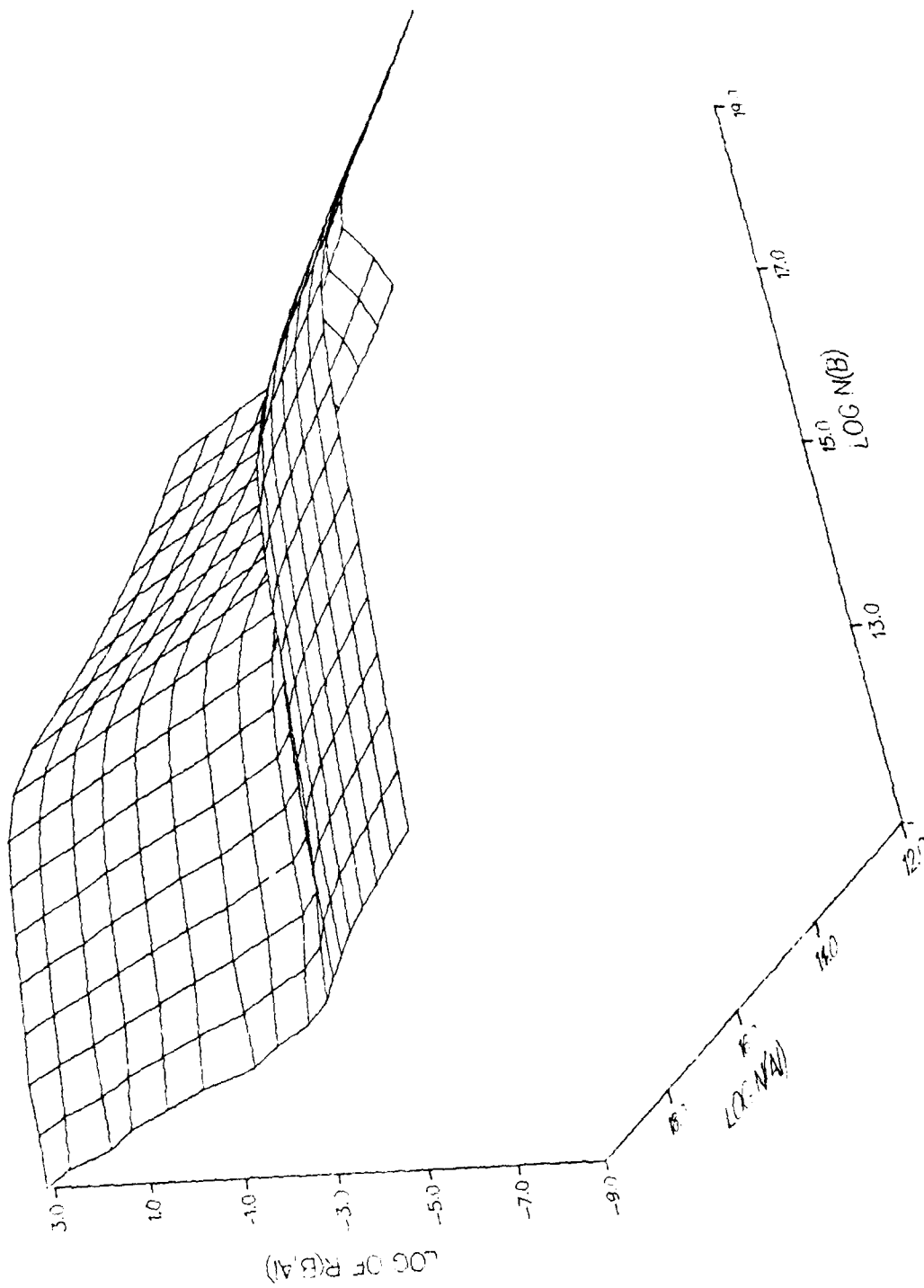


Figure 16c. Another view of $R(B,Al)$ for $J_B/J_{Al} = 0.02$ as a function of N_B and N_{Al} .

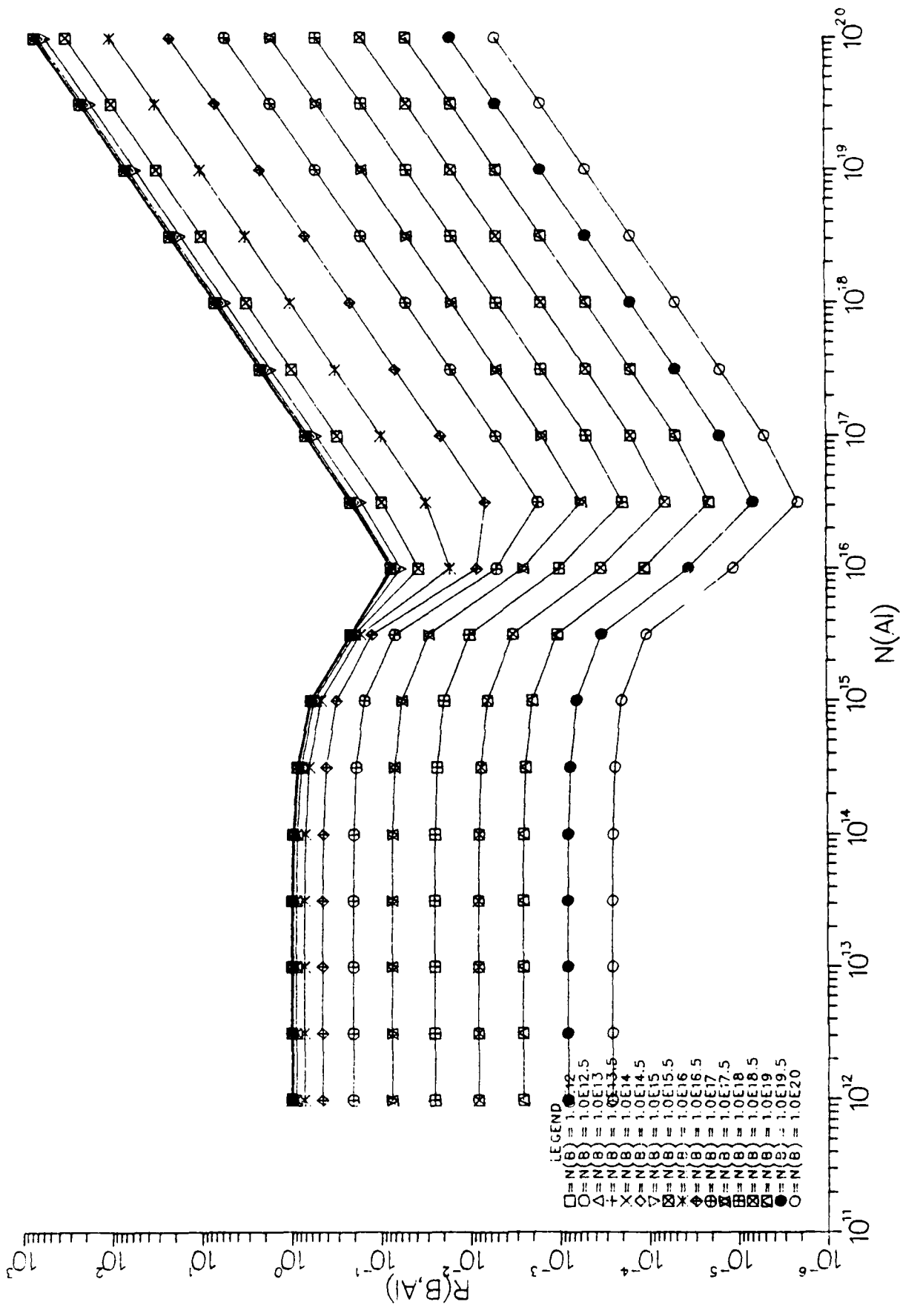


Figure 17a. $R(B, Al)$ for $\sigma_{B/Al} = 1/14$ as a function of N_B and N_{Al} .

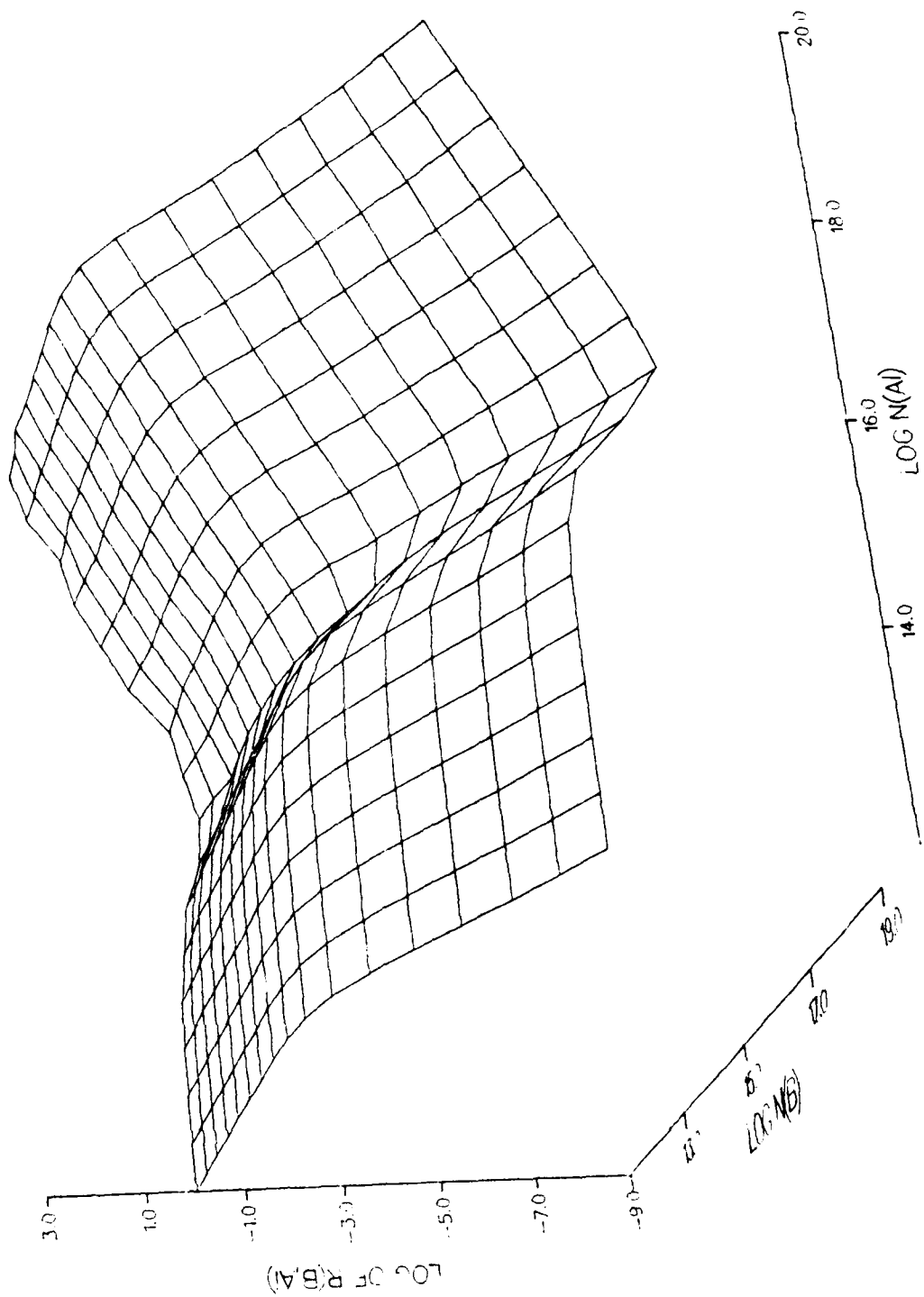


Figure 17b. One view of $R(B,Al)$ for $\sigma_{B/Al} = 1/14$ as a function of N_B and N_{Al} .

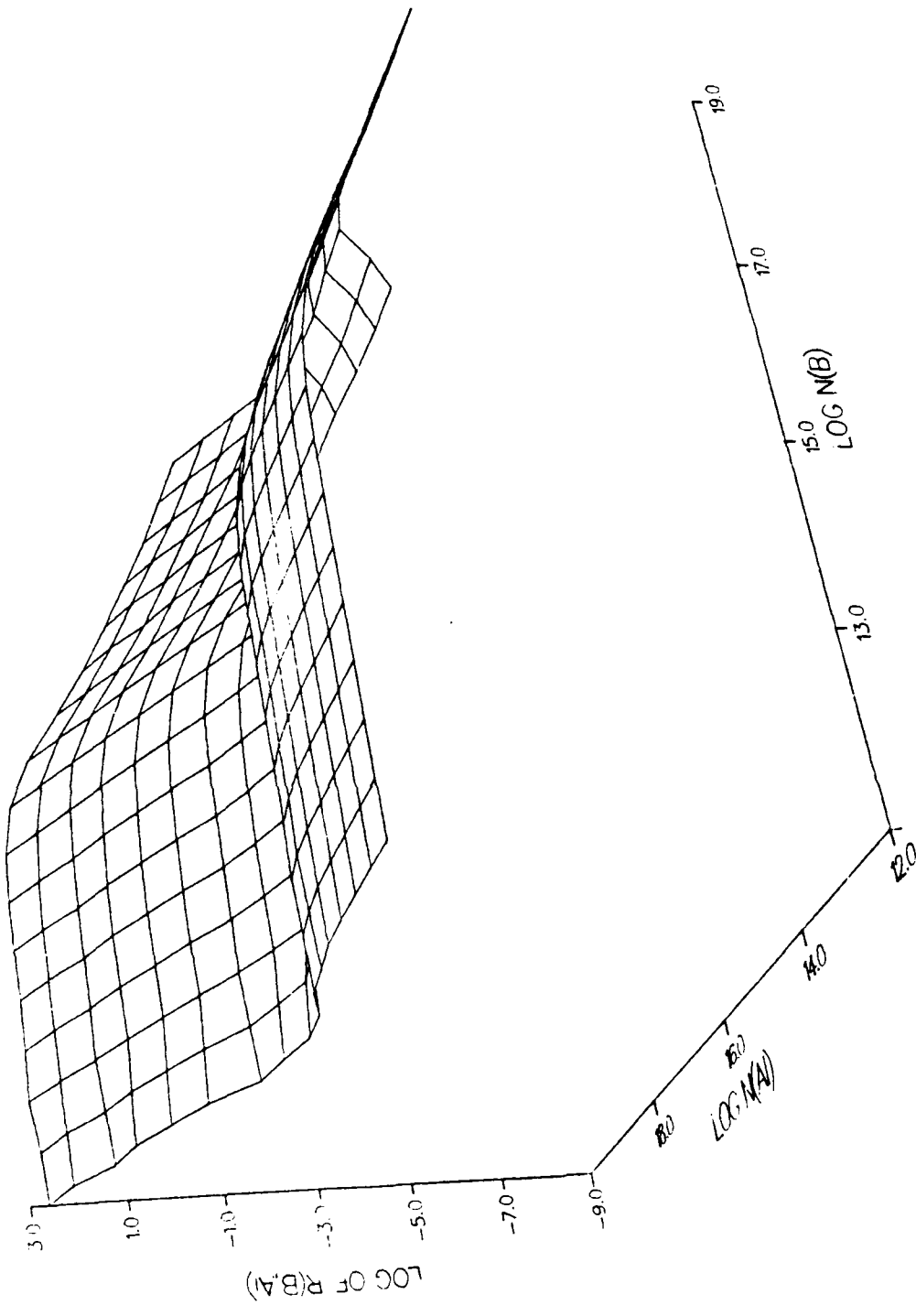


Figure 17c. Another view of $R(B,Al)$ for $\sigma_{B/\sigma_{Al}} = 1/14$ as a function of N_B and N_{Al} .

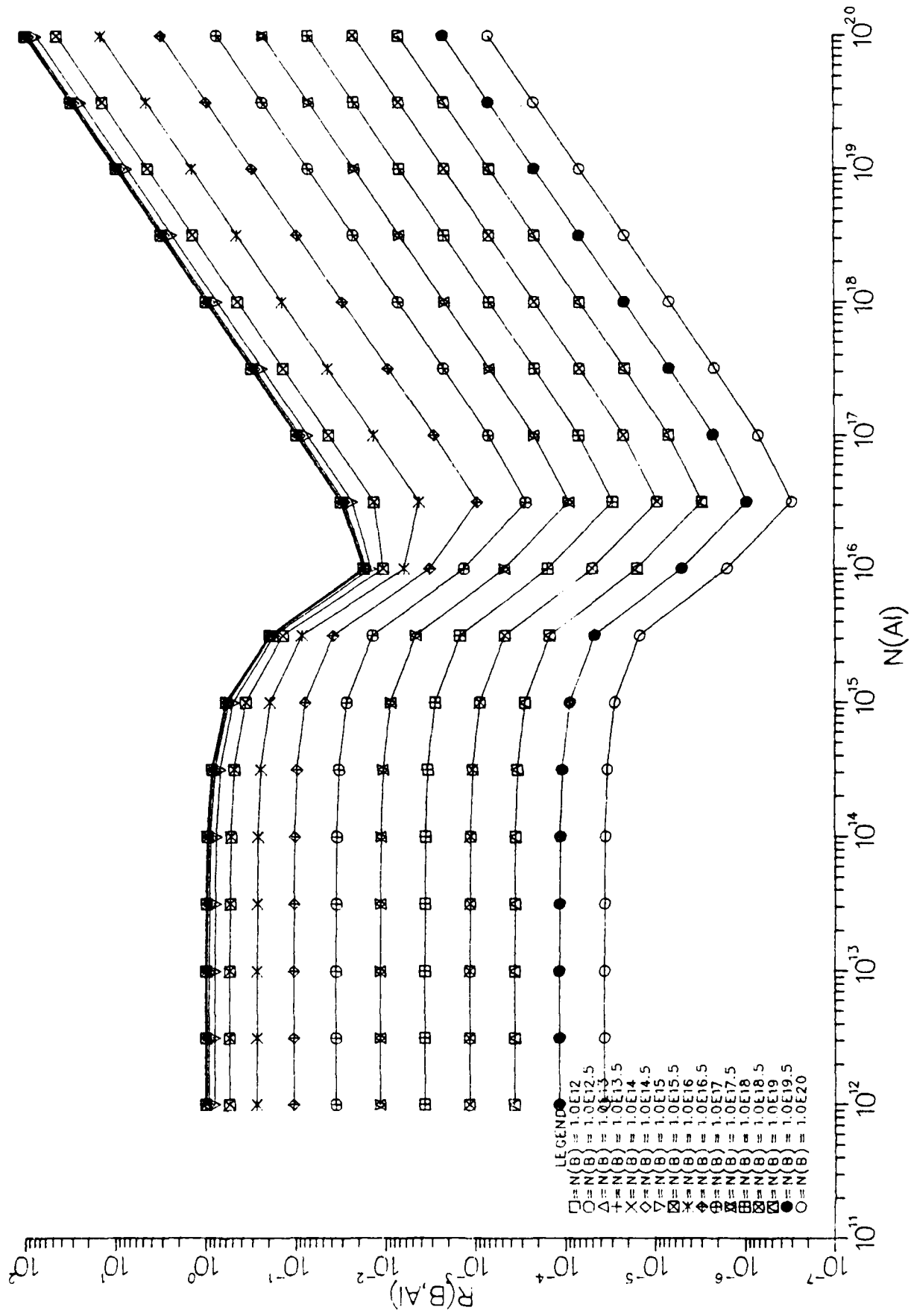


Figure 18a. $R(B,Al)$ for $\beta_{B/Al} = 0.5$ as functions of N_{Al} for given N_B .

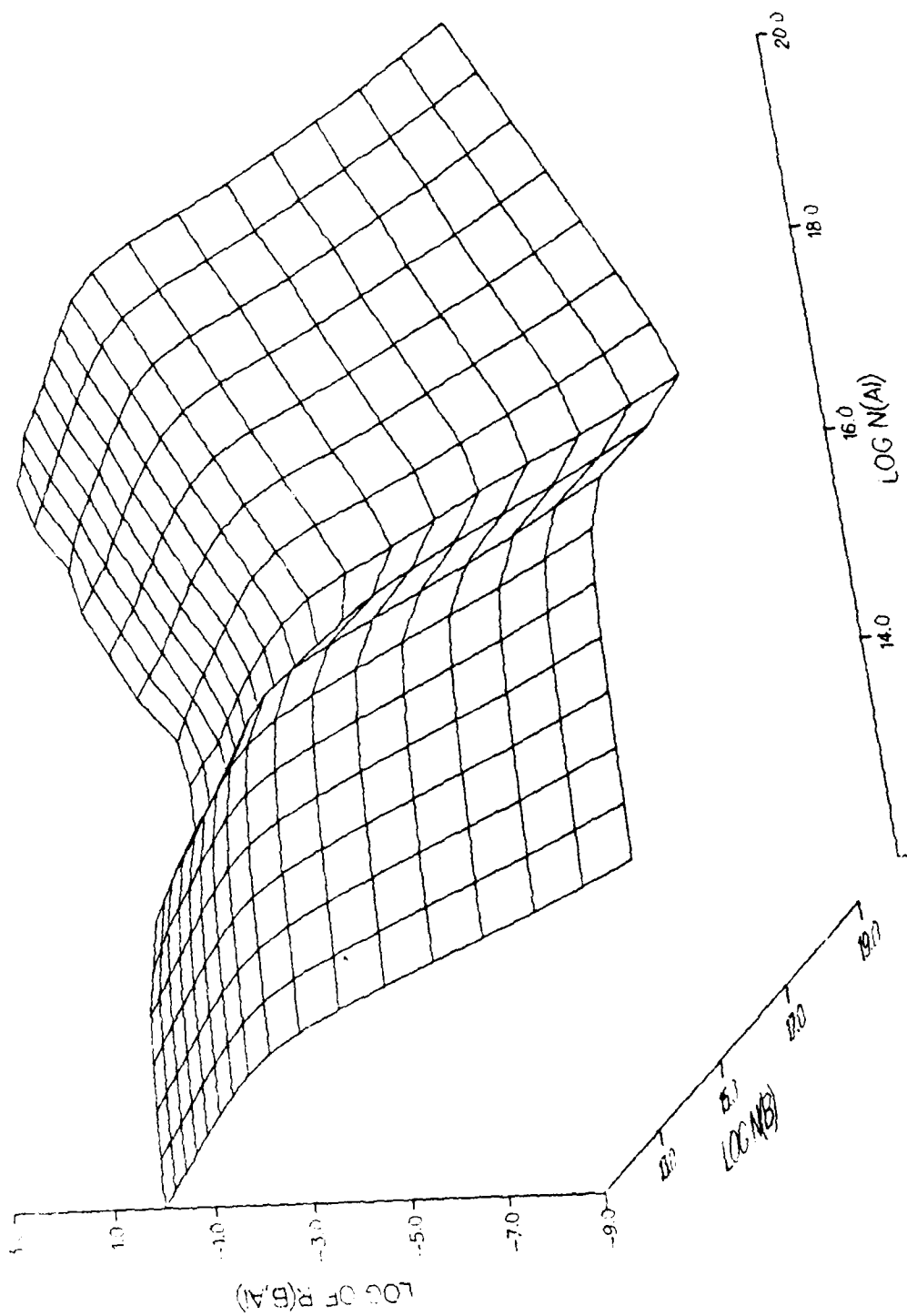


Figure 18b. One view of $R(B,A)$ for $\sigma_B/\sigma_{A1} = 0.5$ as a function of N_B and N_{A1} .

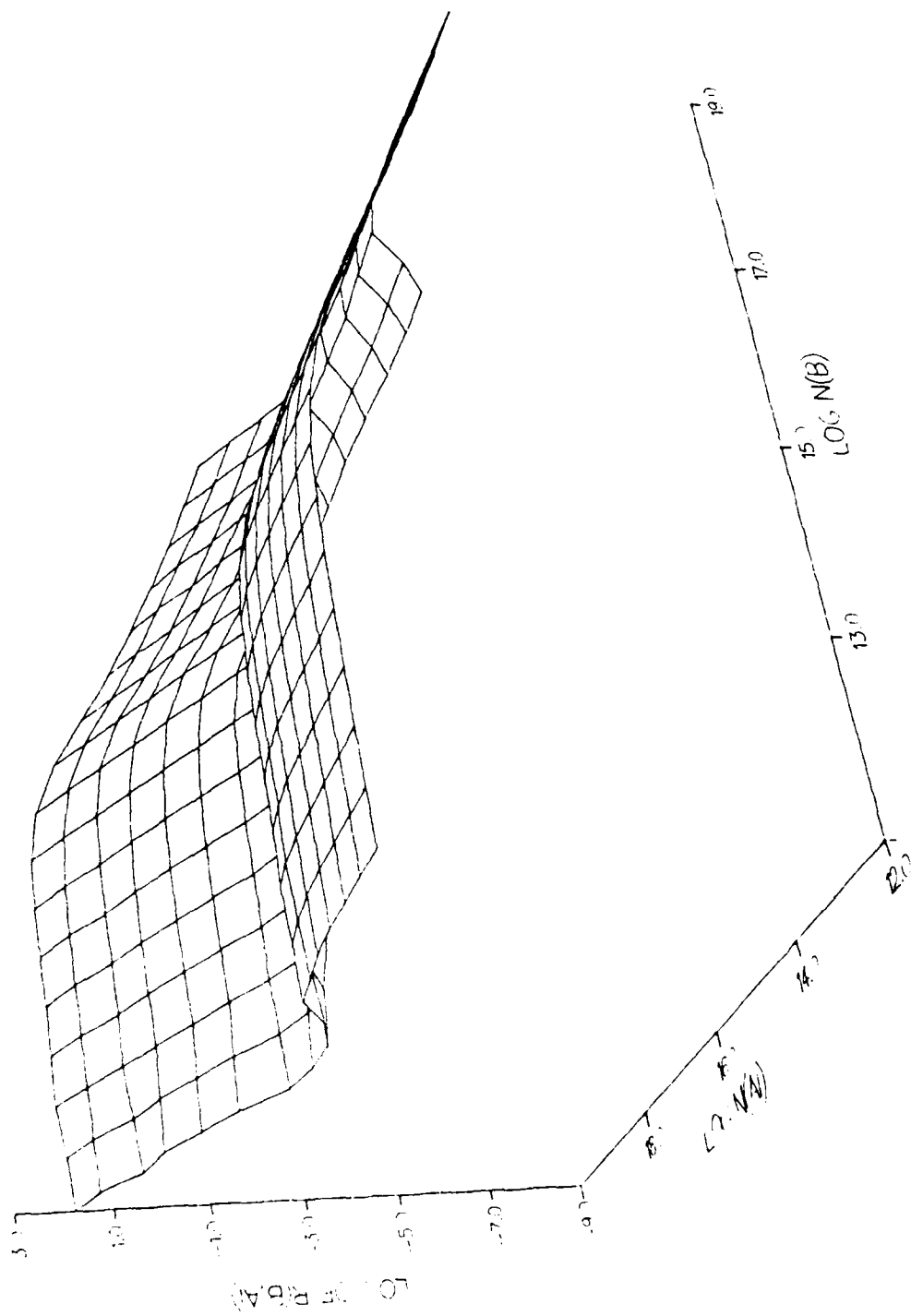


Figure 18c. Another view of $R(B, Al)$ for $N_B / N_{Al} = 0.5$ as a function of N_B and N_{Al} .

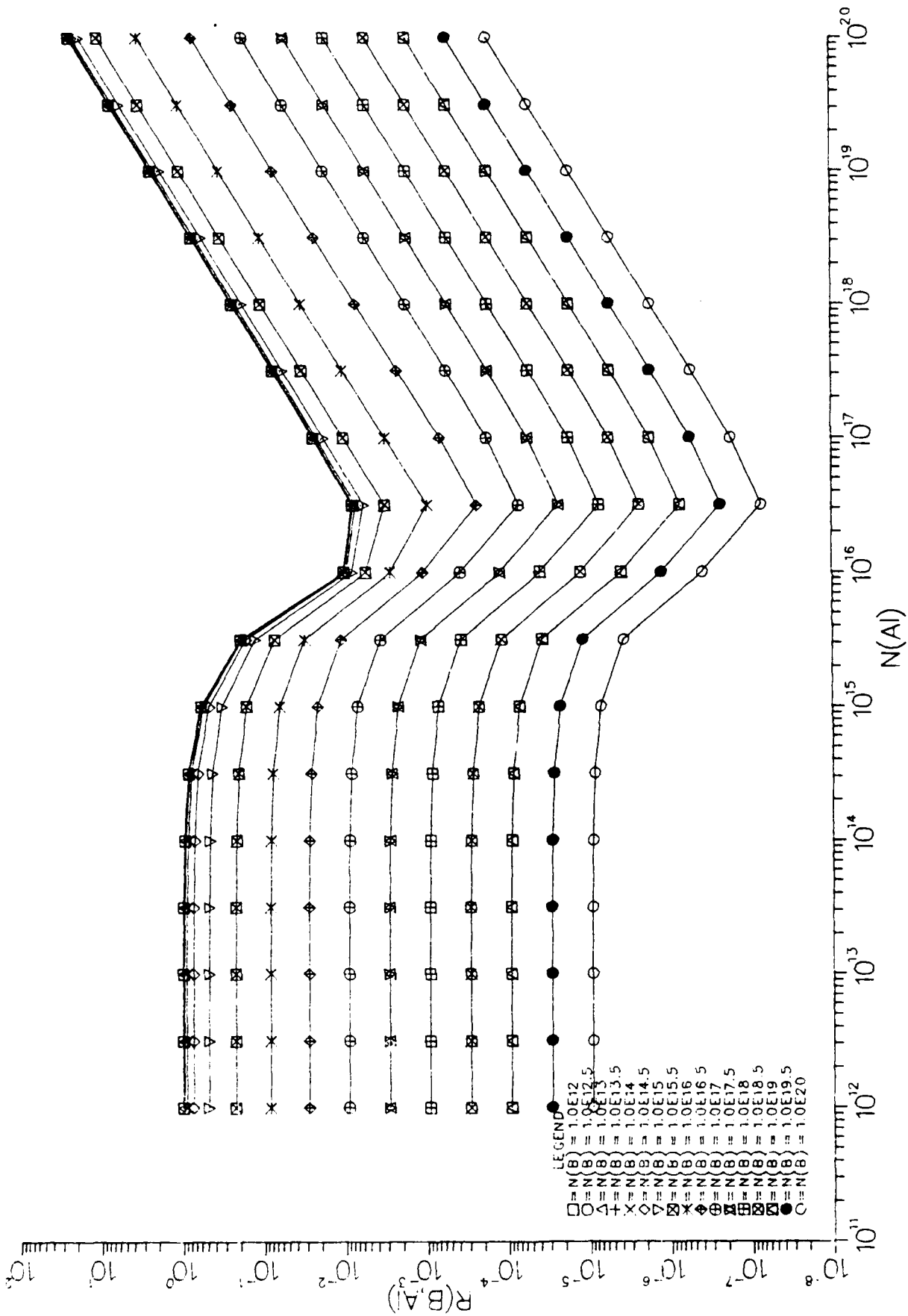


Figure 19a. $R(B,Al)$ for $\gamma_B/\gamma_{Al} = 2$ as functions of N_{Al} for given N_B .

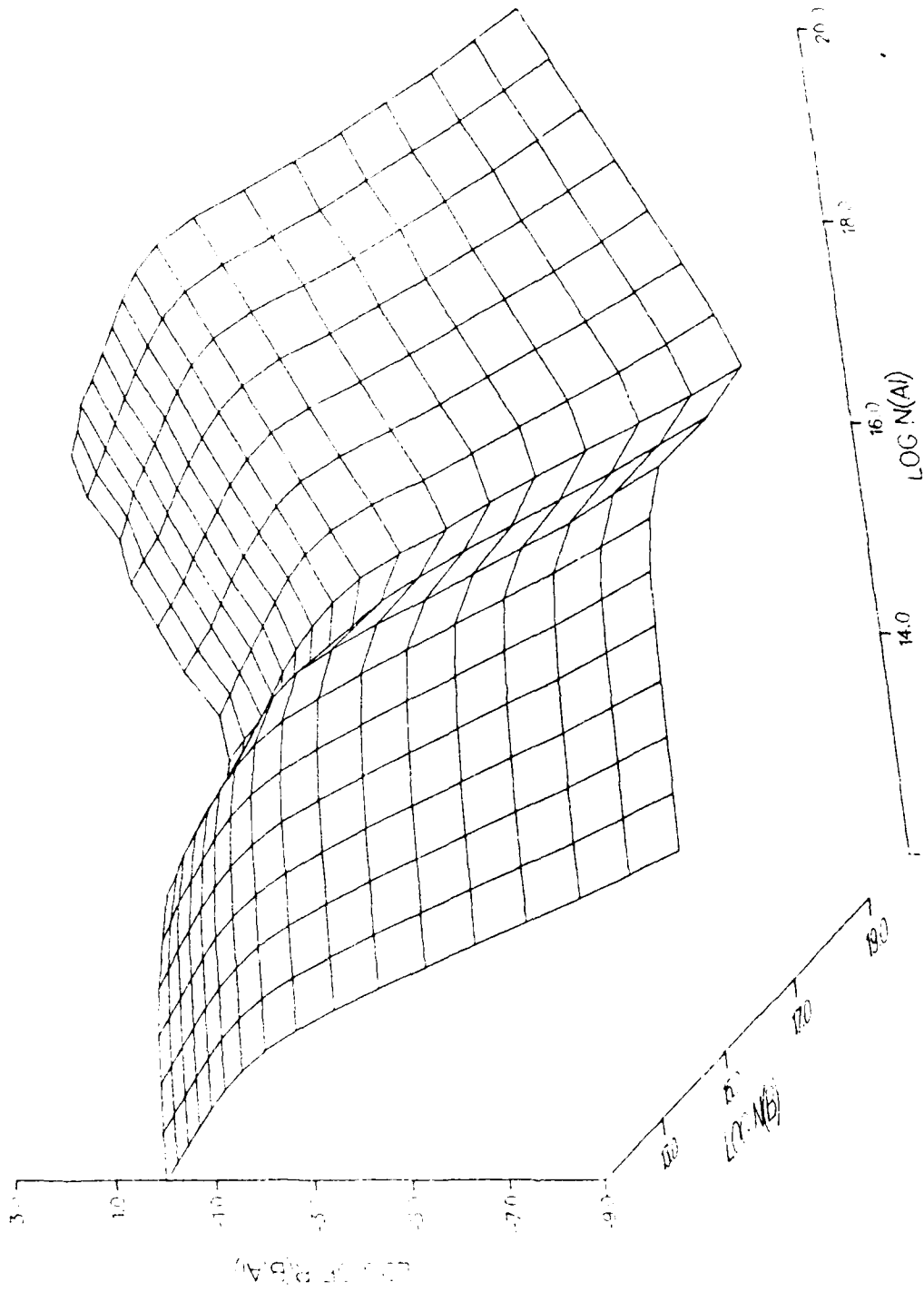


Figure 19b. One view of $R(B, A1)$ for $B/A1 = 2$ as a function of N_B and N_{A1} .

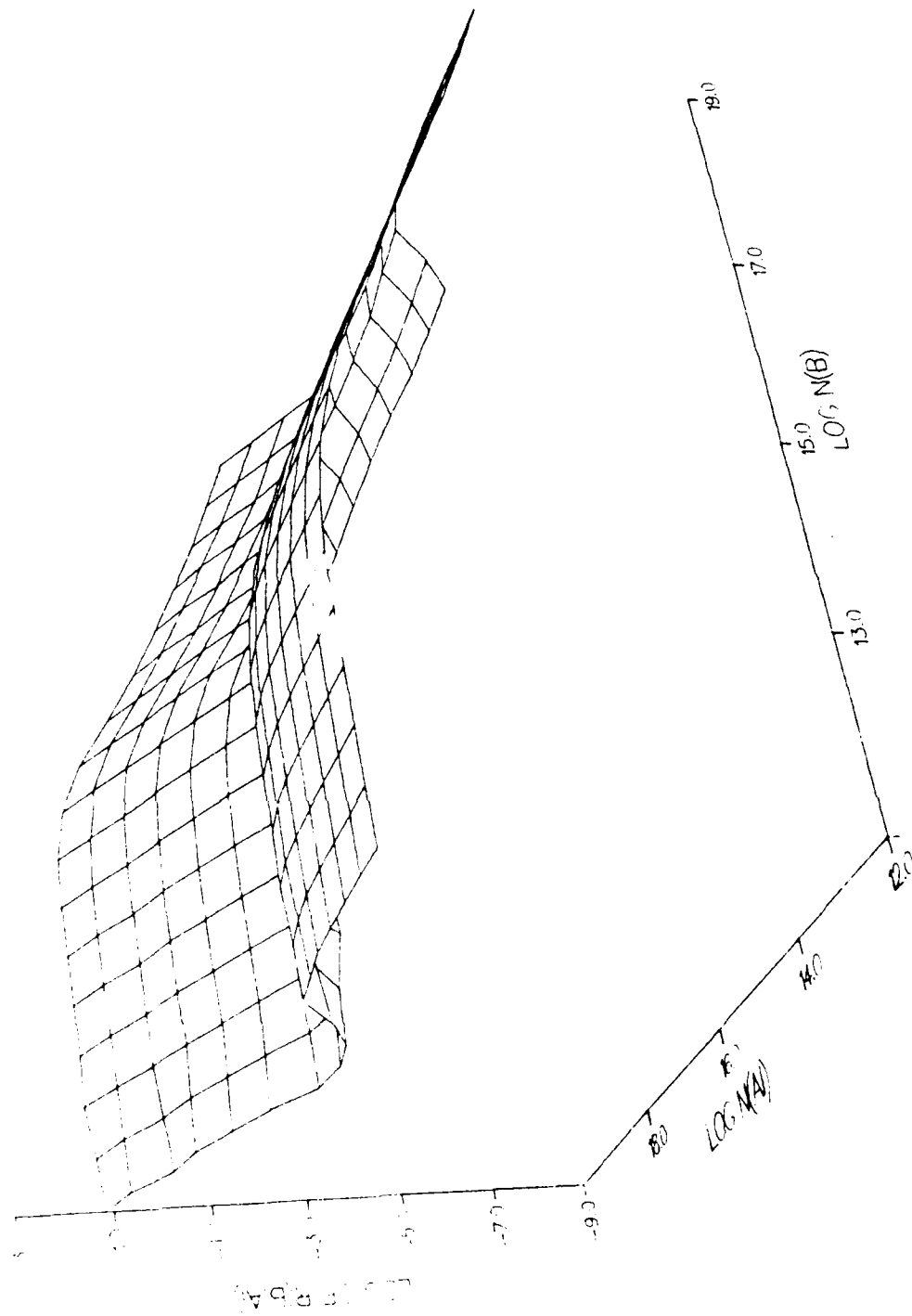


Figure 19c. Another view of $R(B, A)$ for $N_B / N_{Al} = 2$ as a function of N_B and N_{Al} .

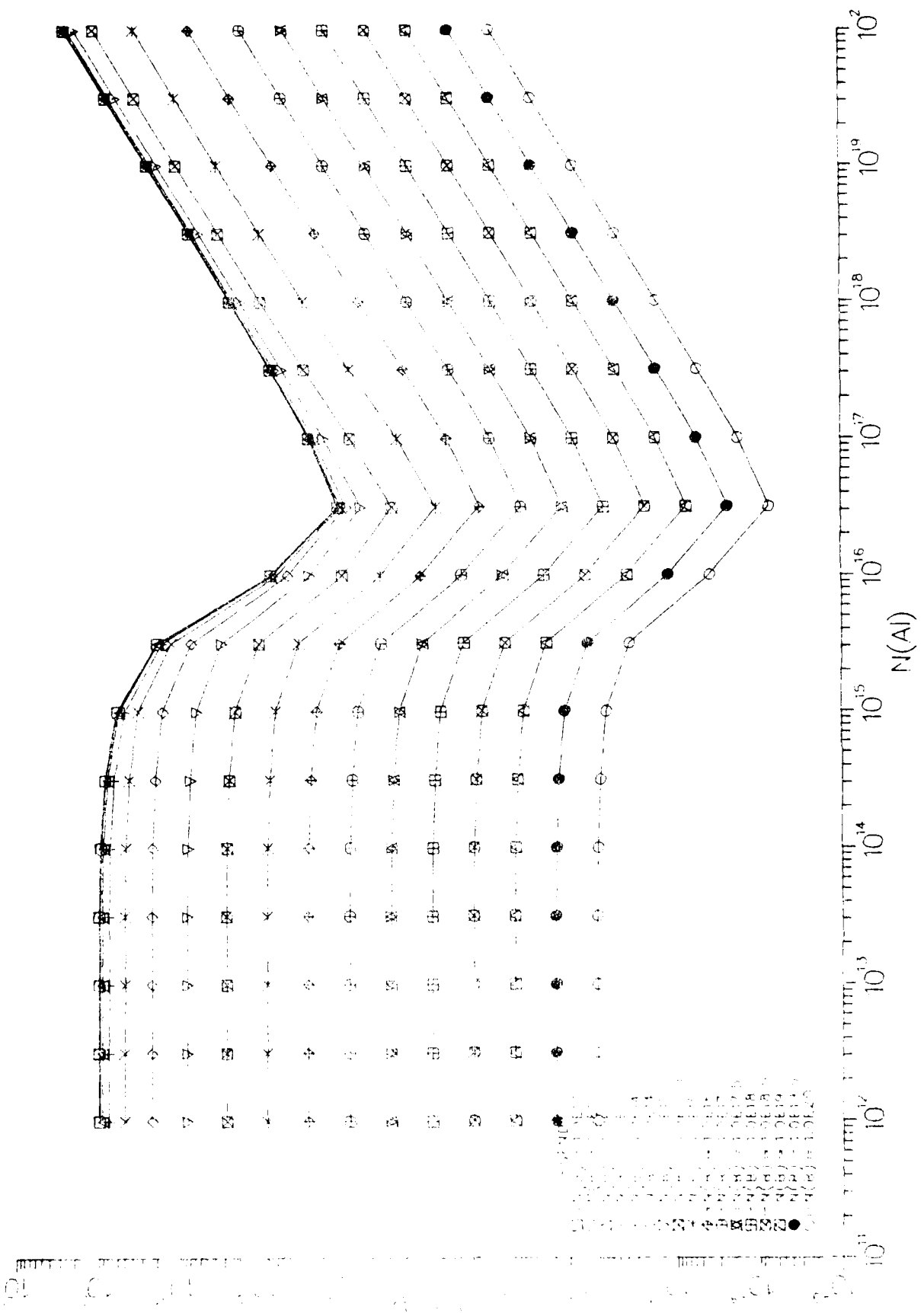


Figure 20a. $R(L, Al)$ for $B/Al = 20$ as functions of N_{Al} for given N .

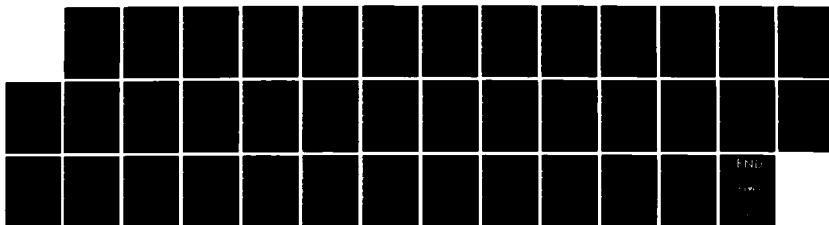
AD-A155 452

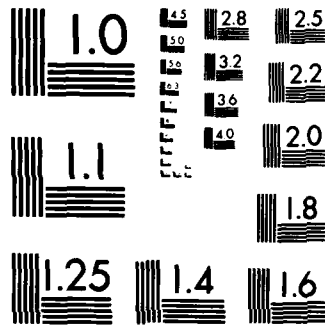
A THEORY OF EXCITON PHOTOLUMINESCENCE FOR TWO TYPES OF
NEUTRAL ACCEPTORS I. (U) DAYTON UNIV OH RESEARCH INST
D S MOROI ET AL FEB 85 UDR-TR-85-10 AFWAL-TR-85-4031
F33615-81-C-5095 F/G 20/12

2/2

UNCLASSIFIED

NL





MICROCOPY RESOLUTION TEST CHART
NATIONAL BUREAU OF STANDARDS-1963-A

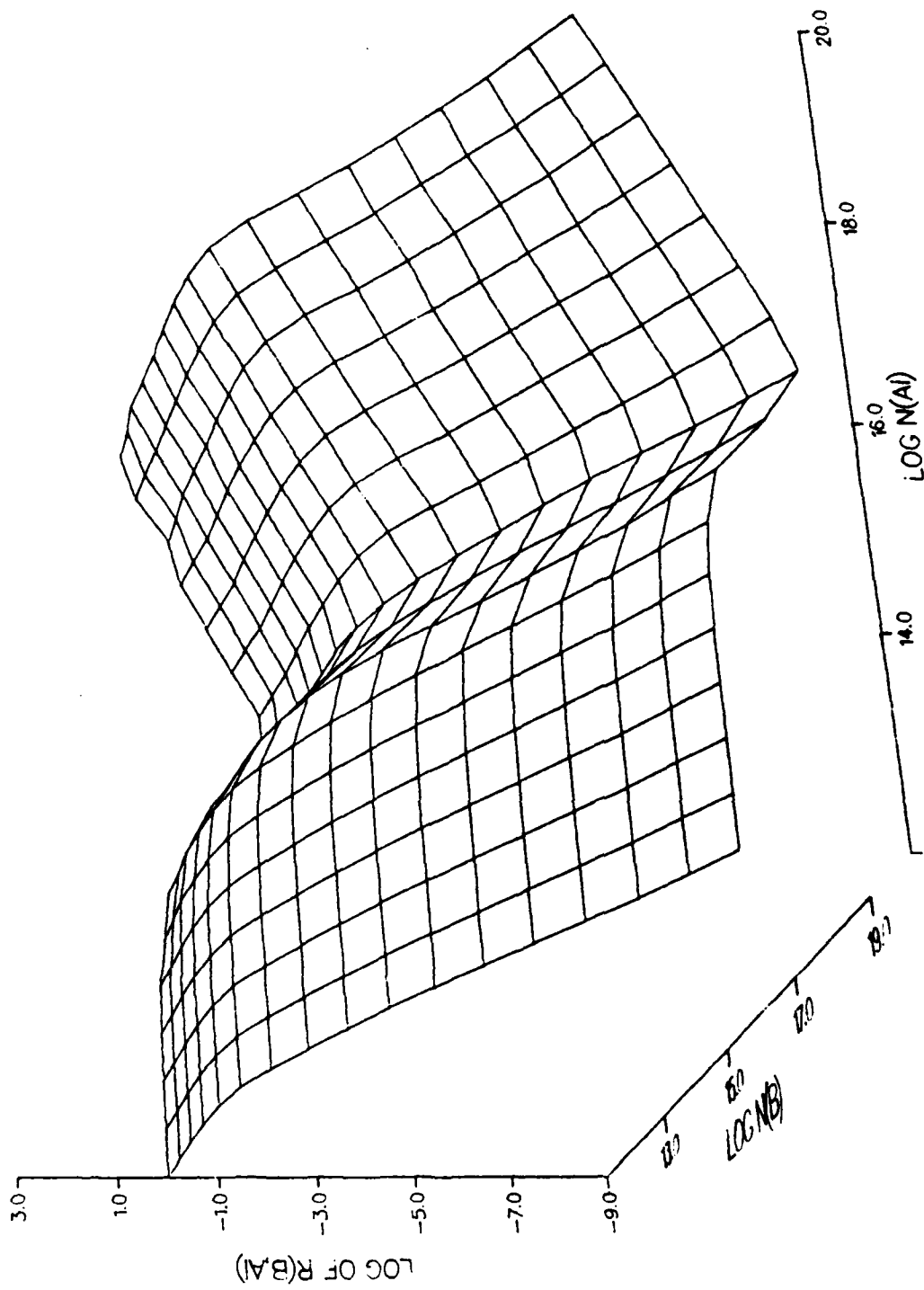


Figure 20b. One view of $R(B,A)$ for $\sigma_B/\sigma_{Al} = 20$ as a function of N_B and N_{Al} .

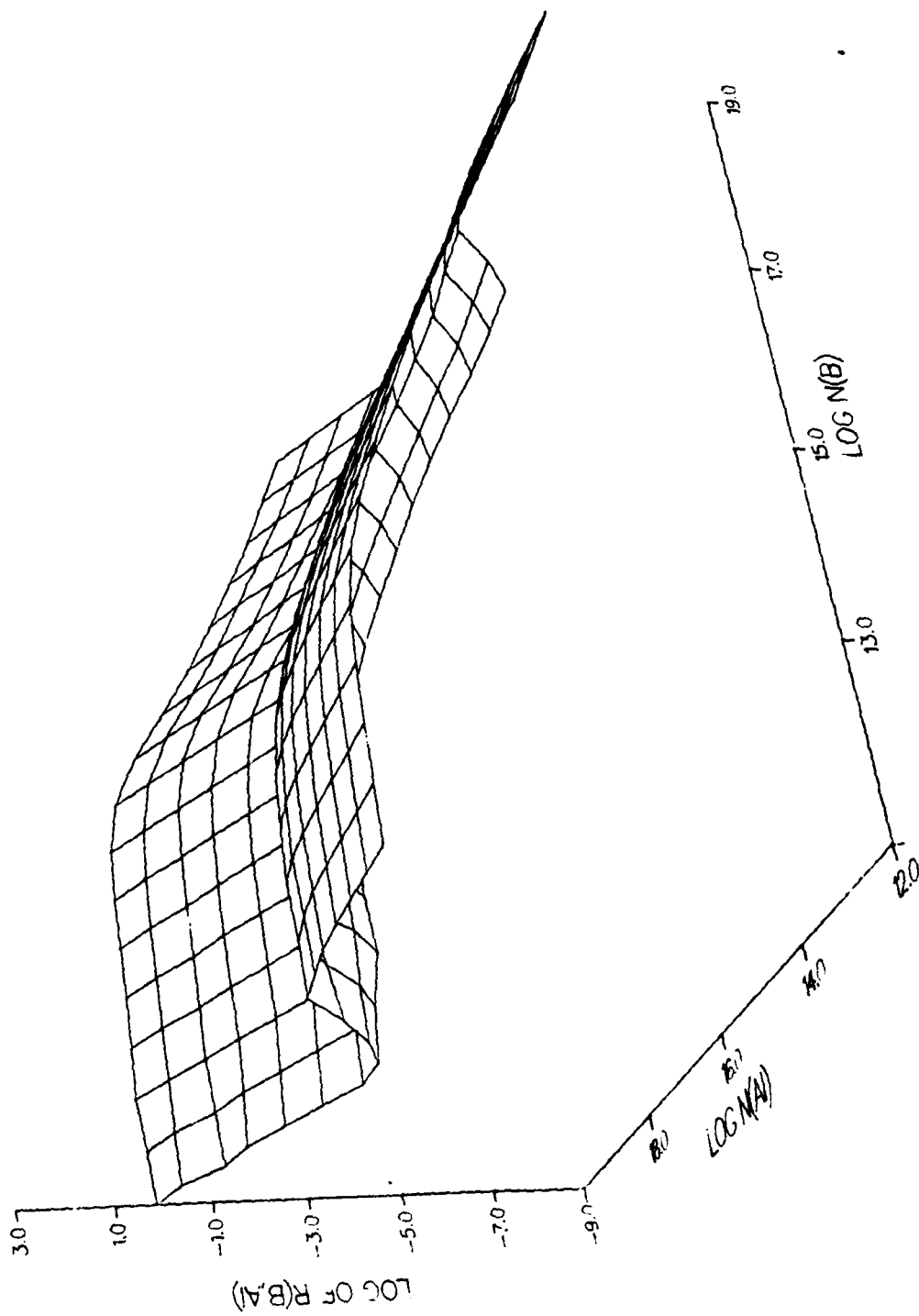


Figure 20c. Another view of $R(B,A)$ for $\sigma_{B/\sigma_{A1}} = 20$ as a function of N_B and N_{A1} .

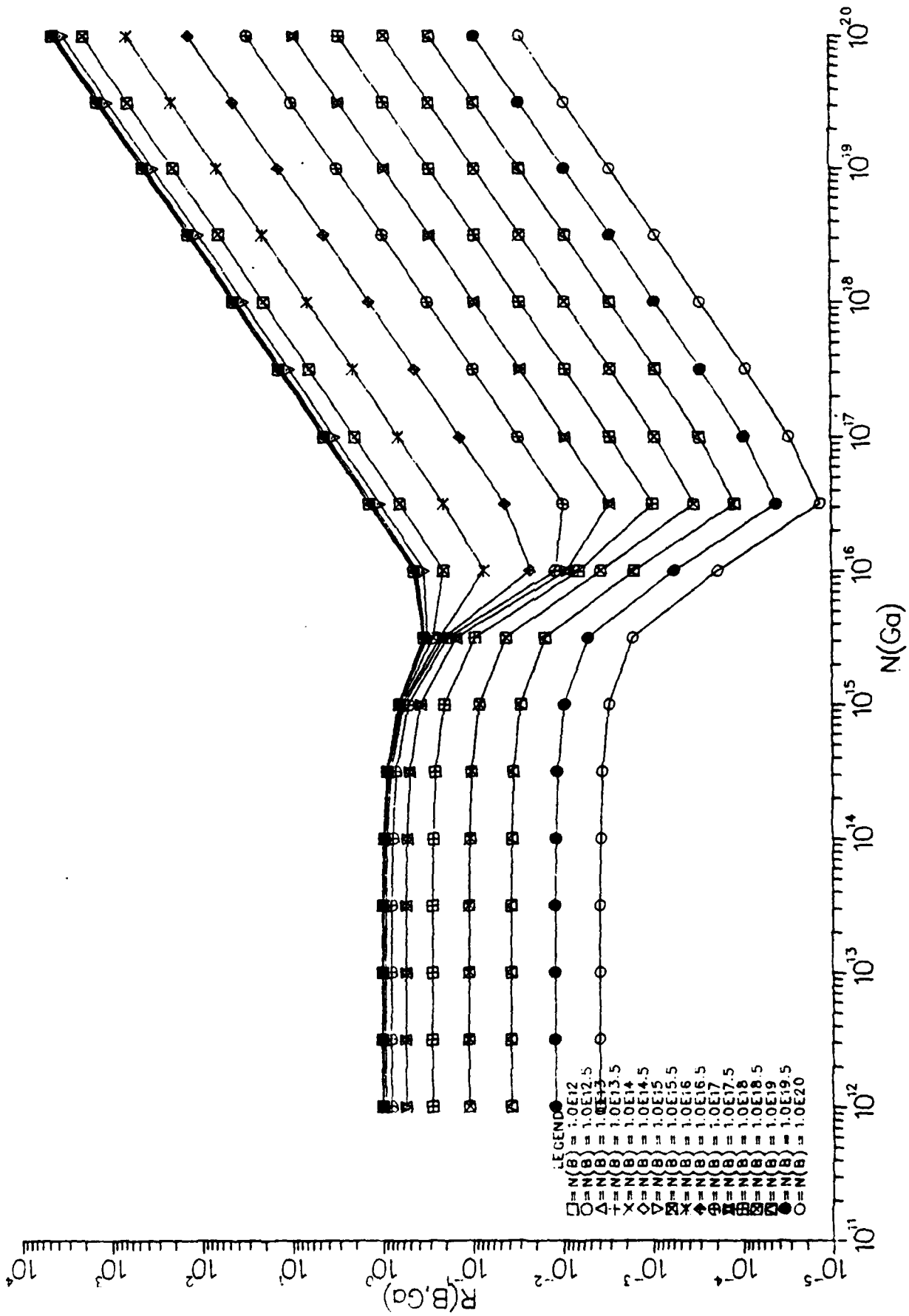


Figure 21a. $R(B, Ga)$ for $\sigma_B/\sigma_{Ga} = 0.005$ as functions of N_{Ga} for given N_B .

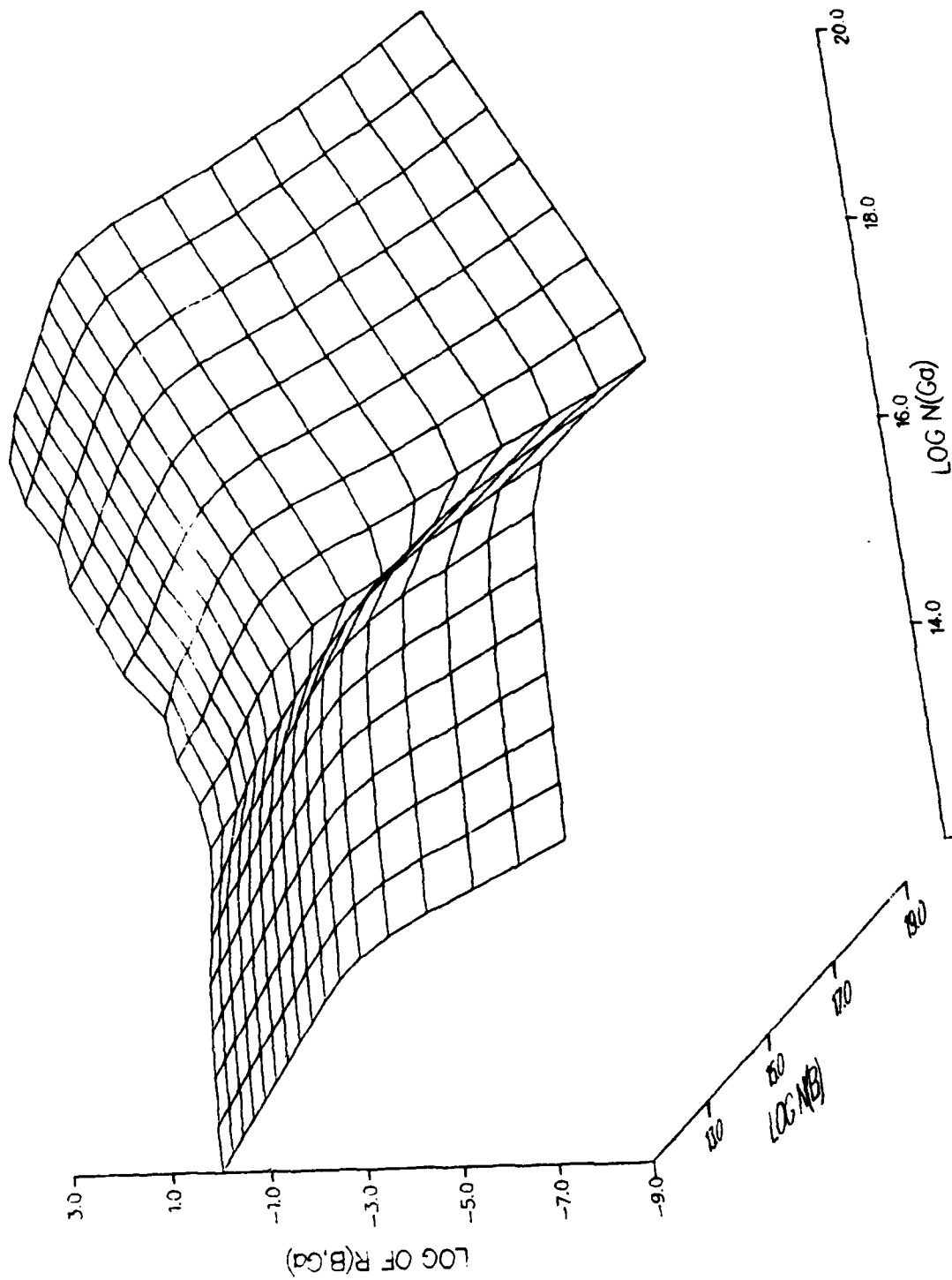


Figure 21b. One view of $R(B,Ga)$ for $\sigma_B/\sigma_{Ga} = 0.005$ as a function of N_B and N_{Ga} .

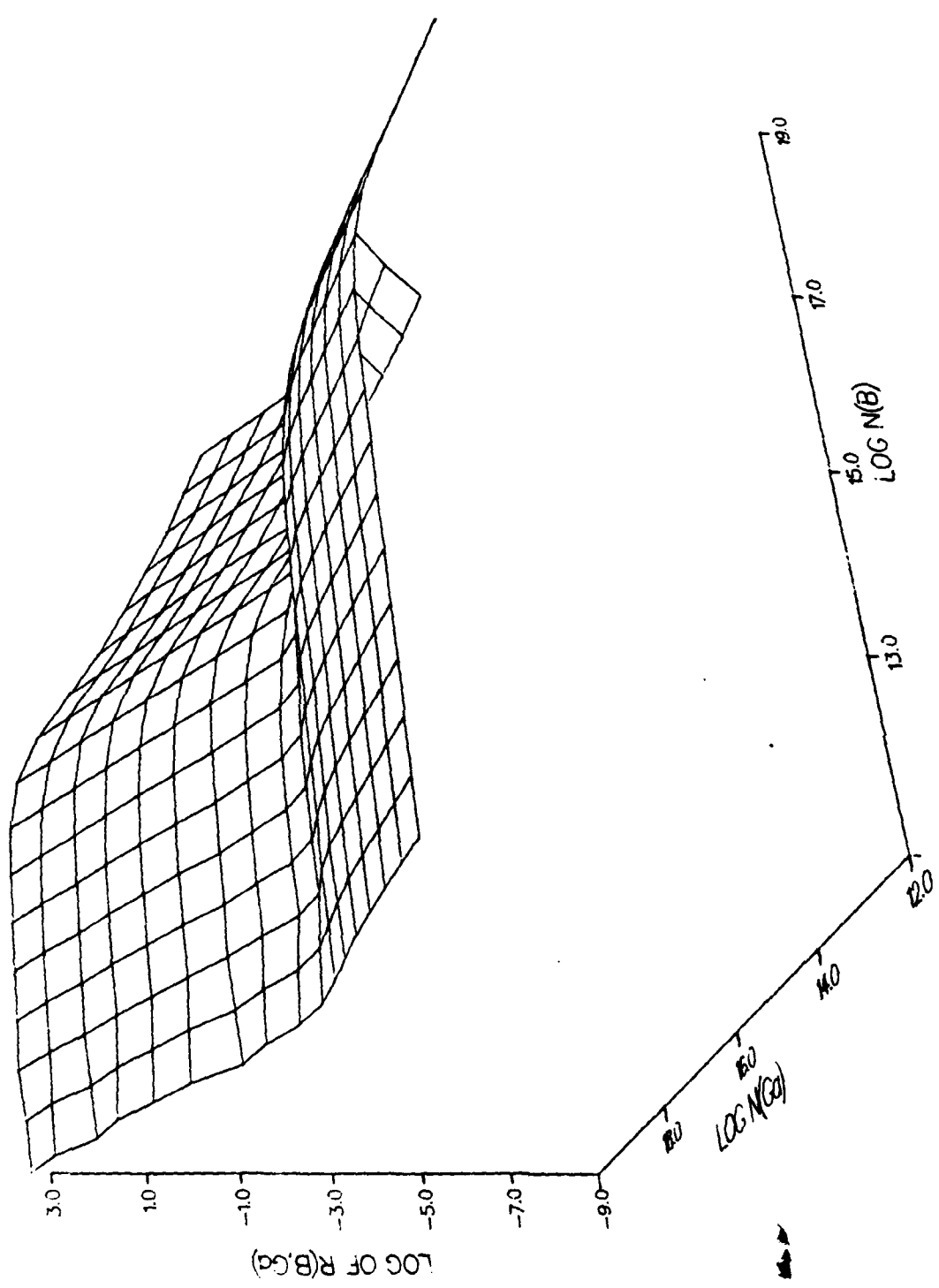


Figure 21c. Another view of $R(B, Ga)$ for $\sigma_B/\sigma_{Ga} = 0.005$ as a function of N_B and N_{Ga} .

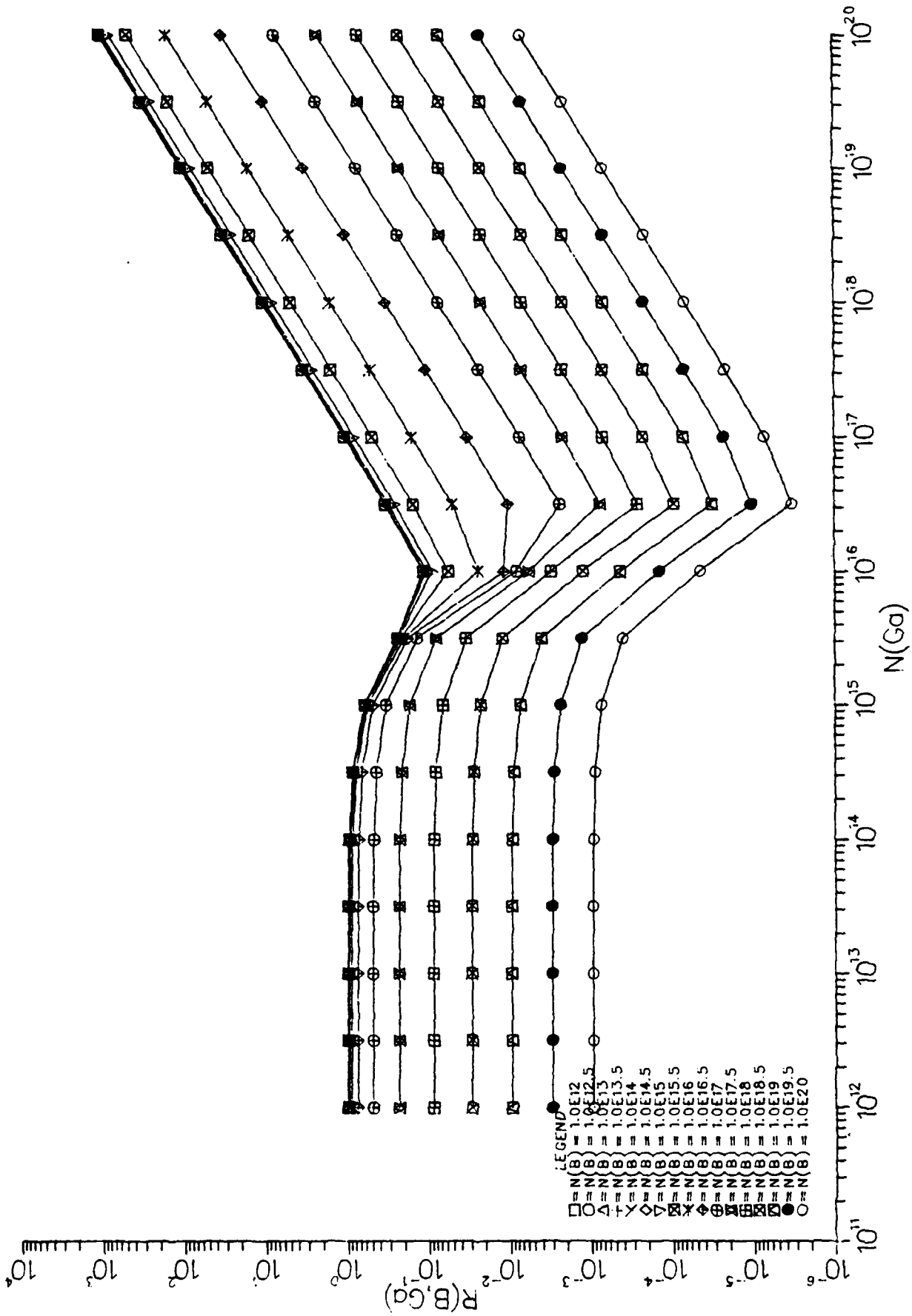


Figure 22a. $R(B, Ga)$ for $\sigma_B/\sigma_{Ga} = 0.02$ as functions of N_{Ga} for given N_B .

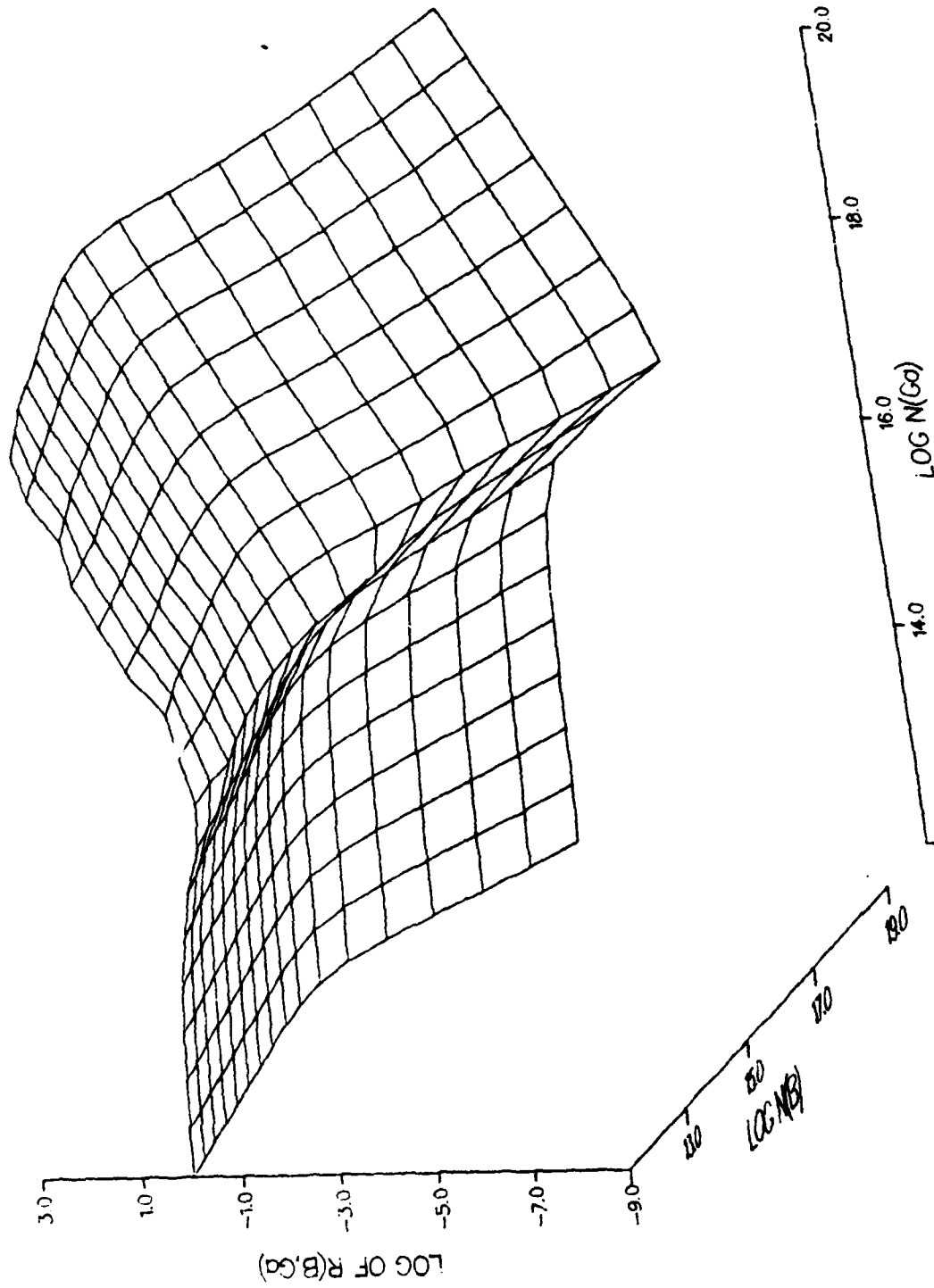


Figure 22b. One view of $R(B, Ga)$ for $\sigma_B/\sigma_{Ga} = 0.02$ as a function of N_B and N_{Ga} .

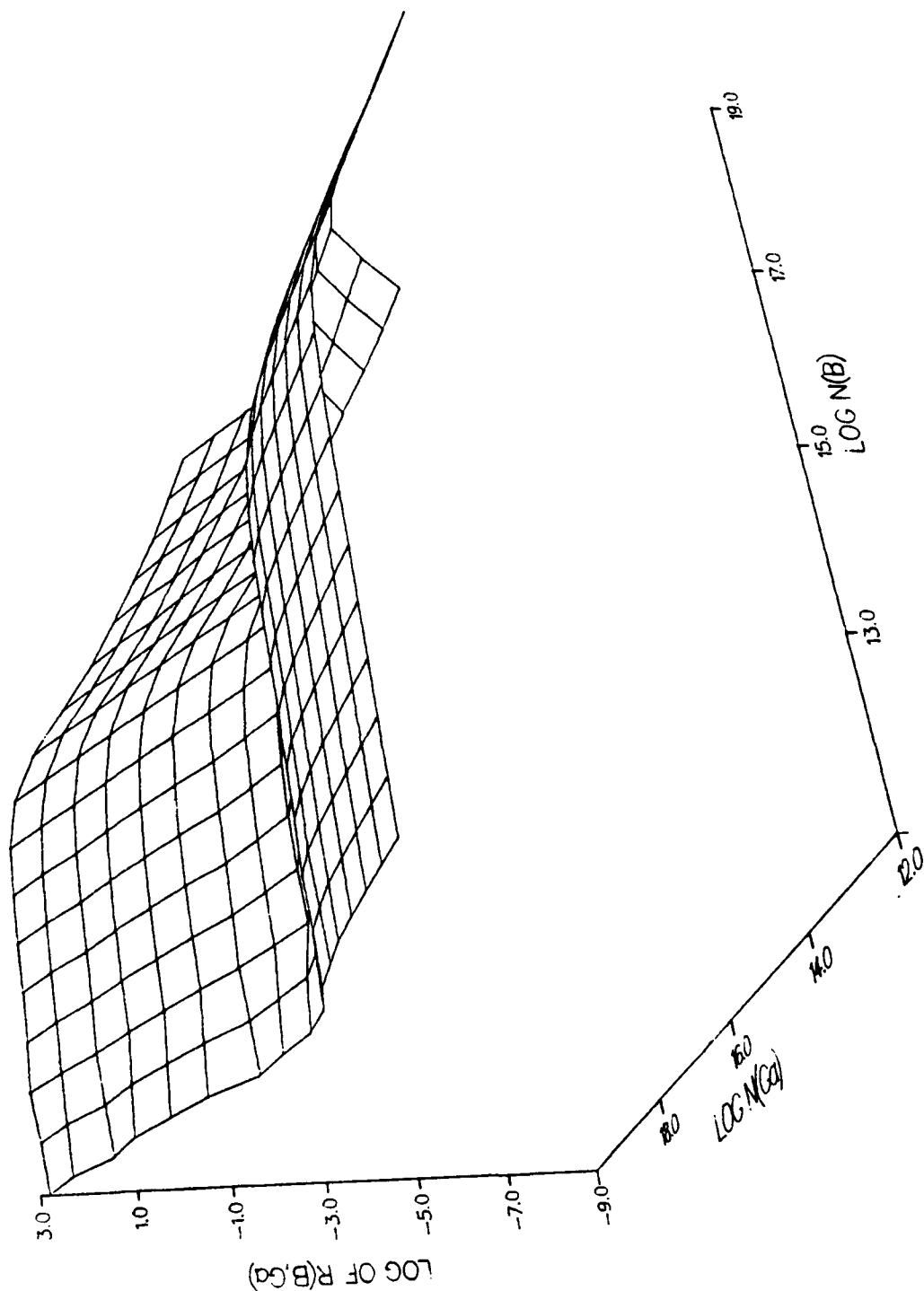


Figure 22c. Another view of $R(B, Ga)$ for $\sigma_{B/\sigma_{Ga}} = 0.02$ as a function of N_B and N_{Ga} .

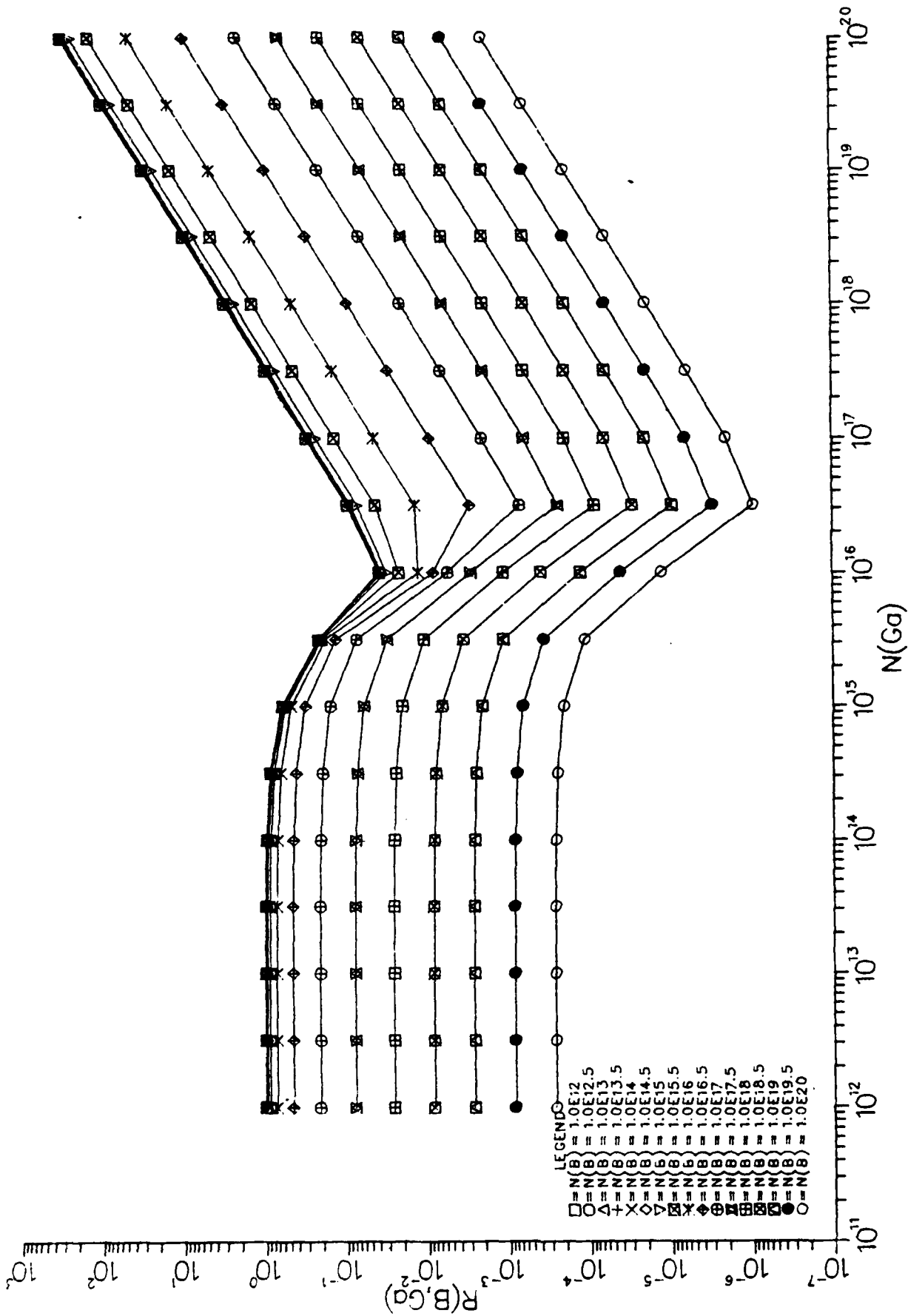


Figure 23a. $R(B, Ga)$ for $\sigma_B/\sigma_{Ga} = 1/14$ as functions of N_{Ga} for given N_B .

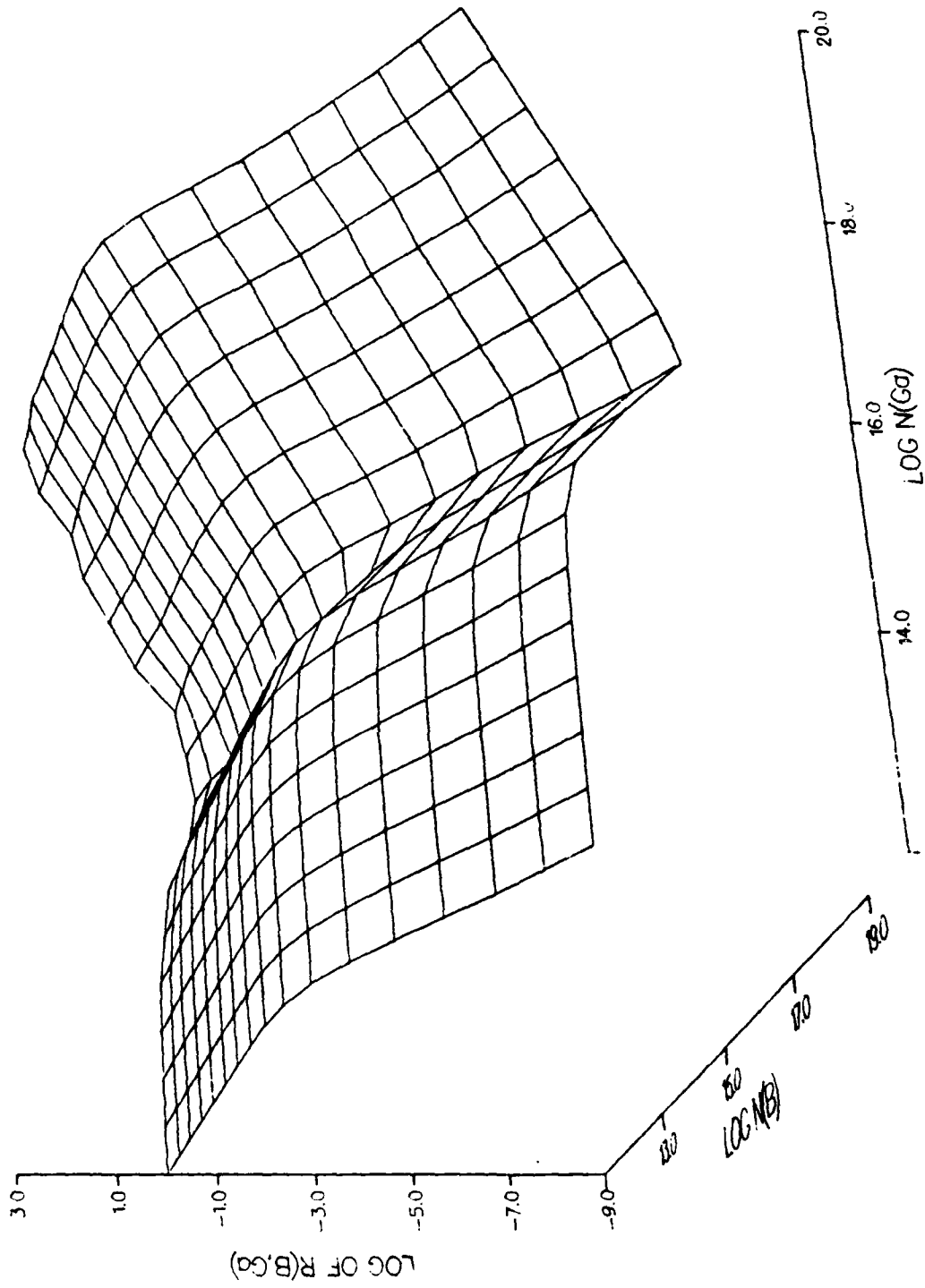


Figure 23b. One view of $R(B, Ga)$ for $\sigma_B/\sigma_{Ga} = 1/14$ as a function of N_B and N_{Ga} .

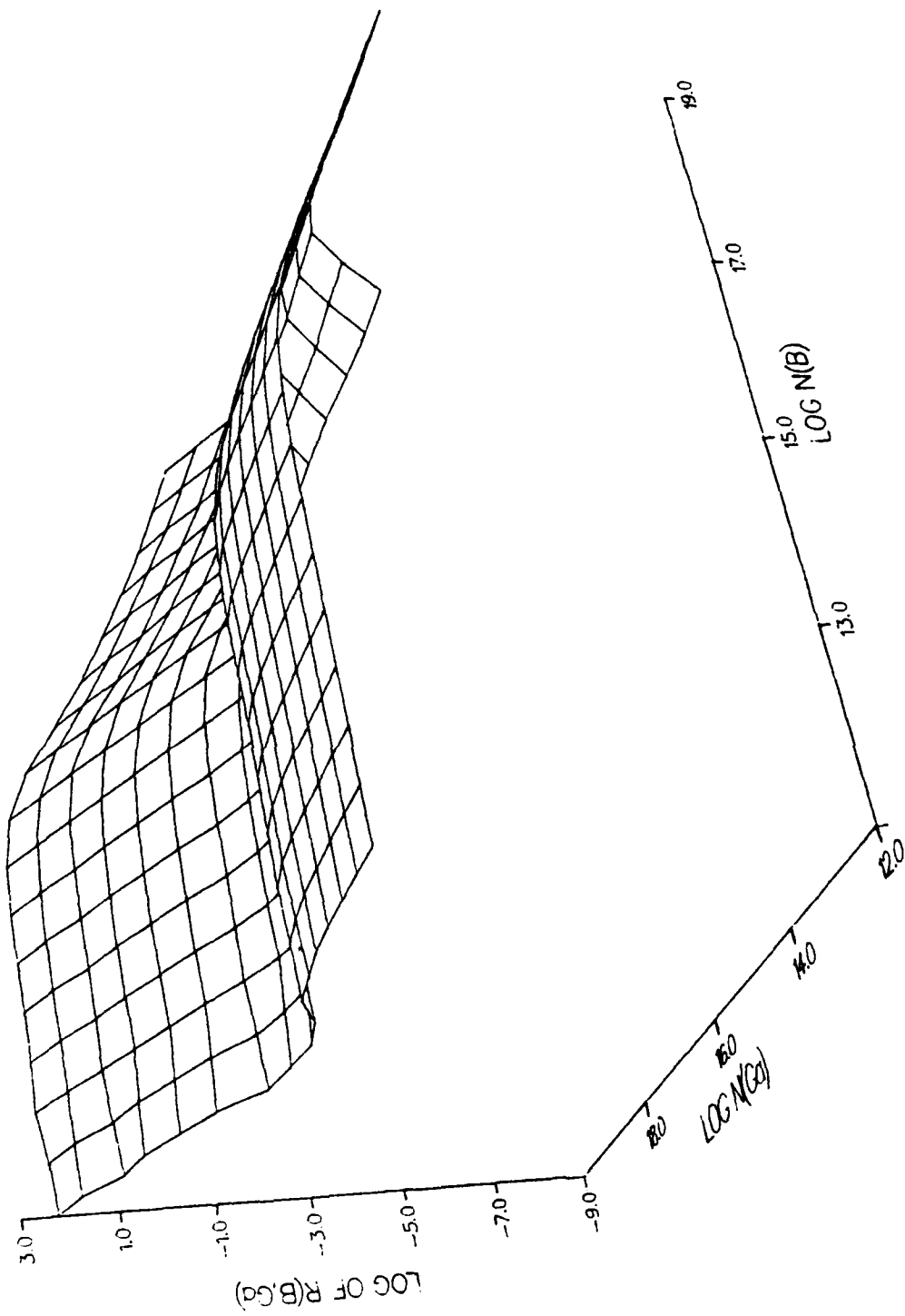


Figure 23c. Another view of $R(B,Ga)$ for $\sigma_B/\sigma_{Ga} = 1/14$ as a function of N_B and N_{Ga} .

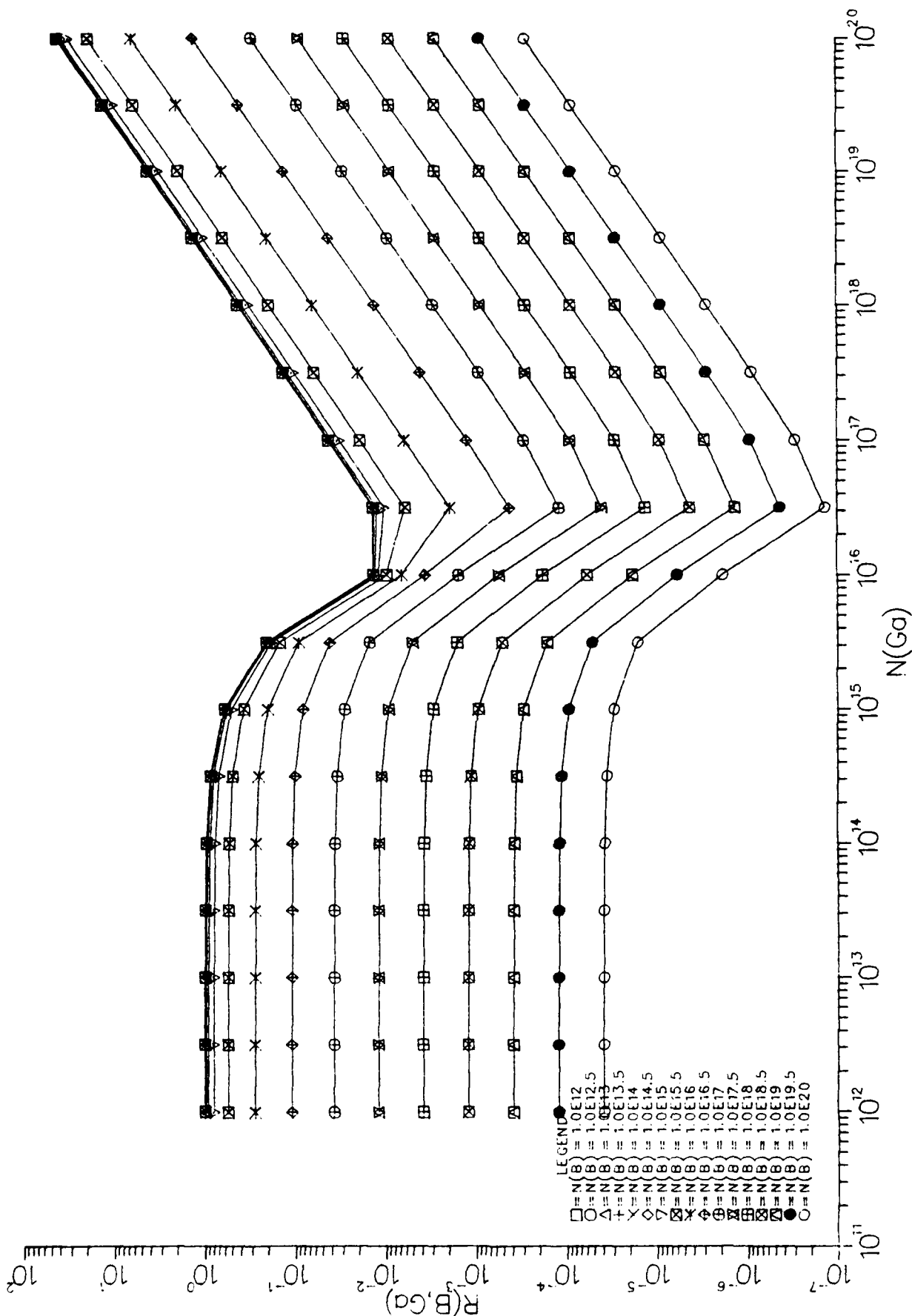


Figure 24a. $R(B, Ga)$ for $\sigma_B/\sigma_{Ga} = 0.5$ as functions of N_{Ga} for given N_B .

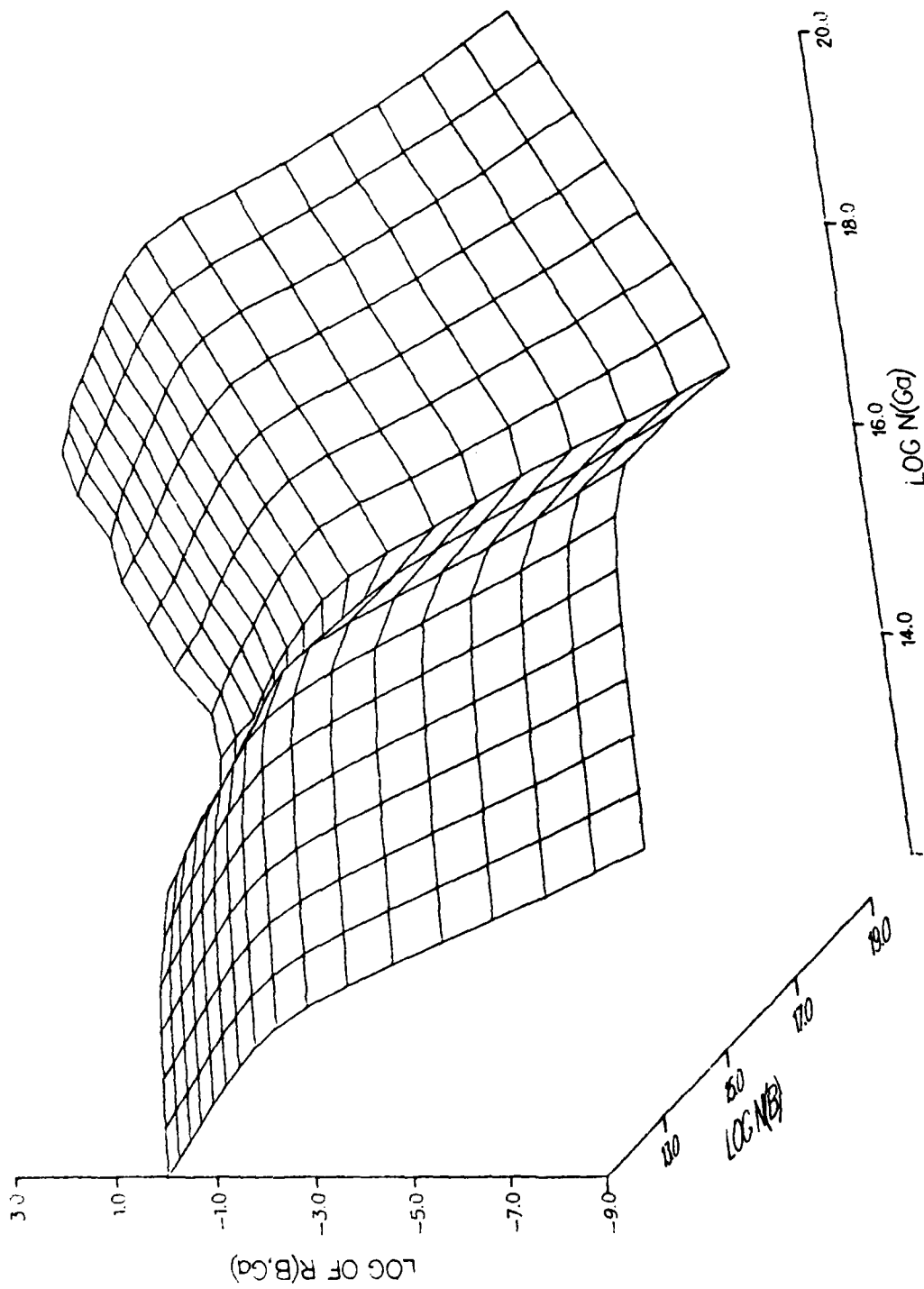


Figure 24b. One view of $R(B,Ga)$ for $\sigma_B/\sigma_{Ga} = 0.5$ as a function of N_B and N_{Ga} .

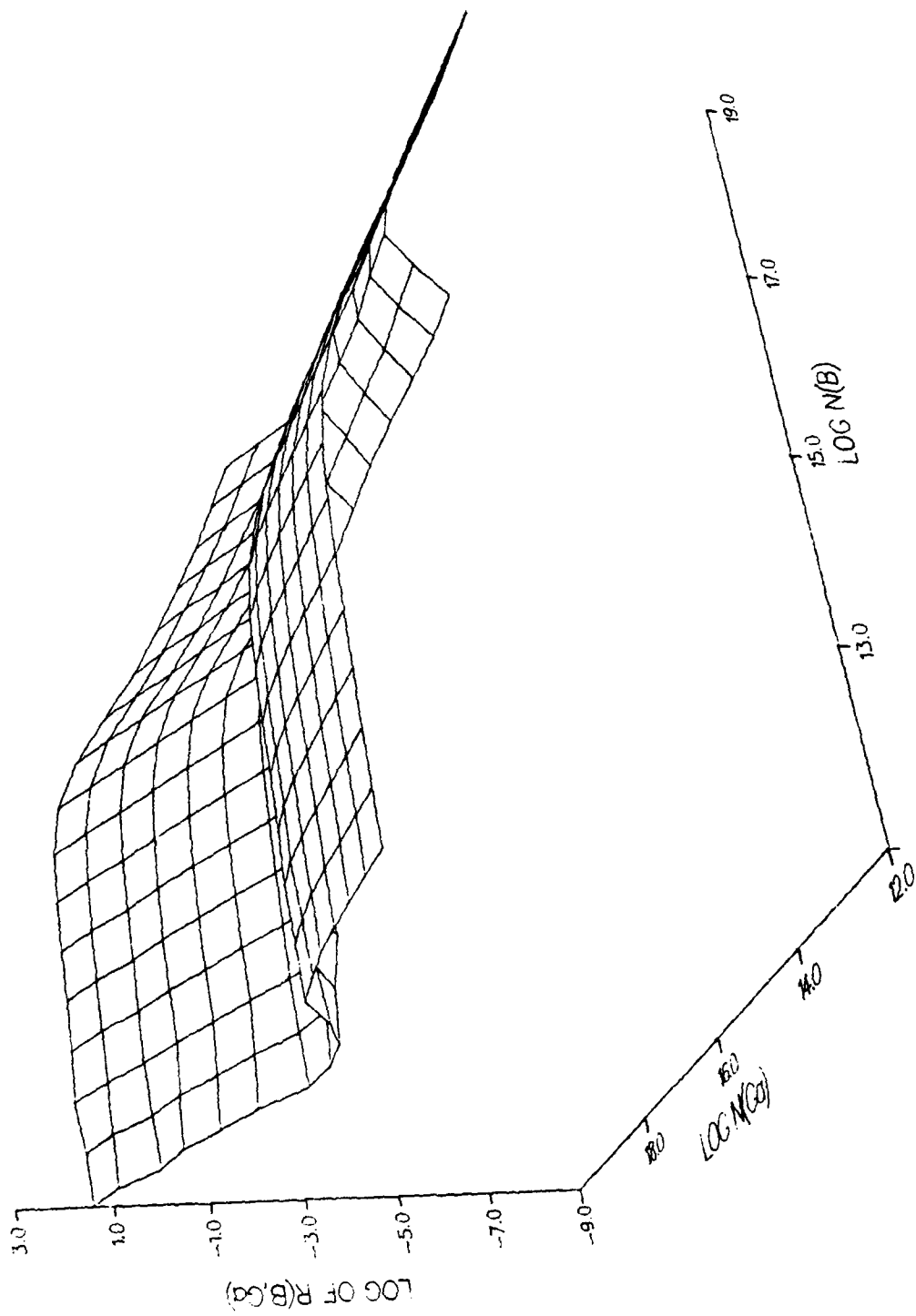


Figure 24c. Another view of $R(B, Ga)$ for $\sigma_B / \sigma_{Ga} = 0.5$ as a function of N_B and N_{Ga} .

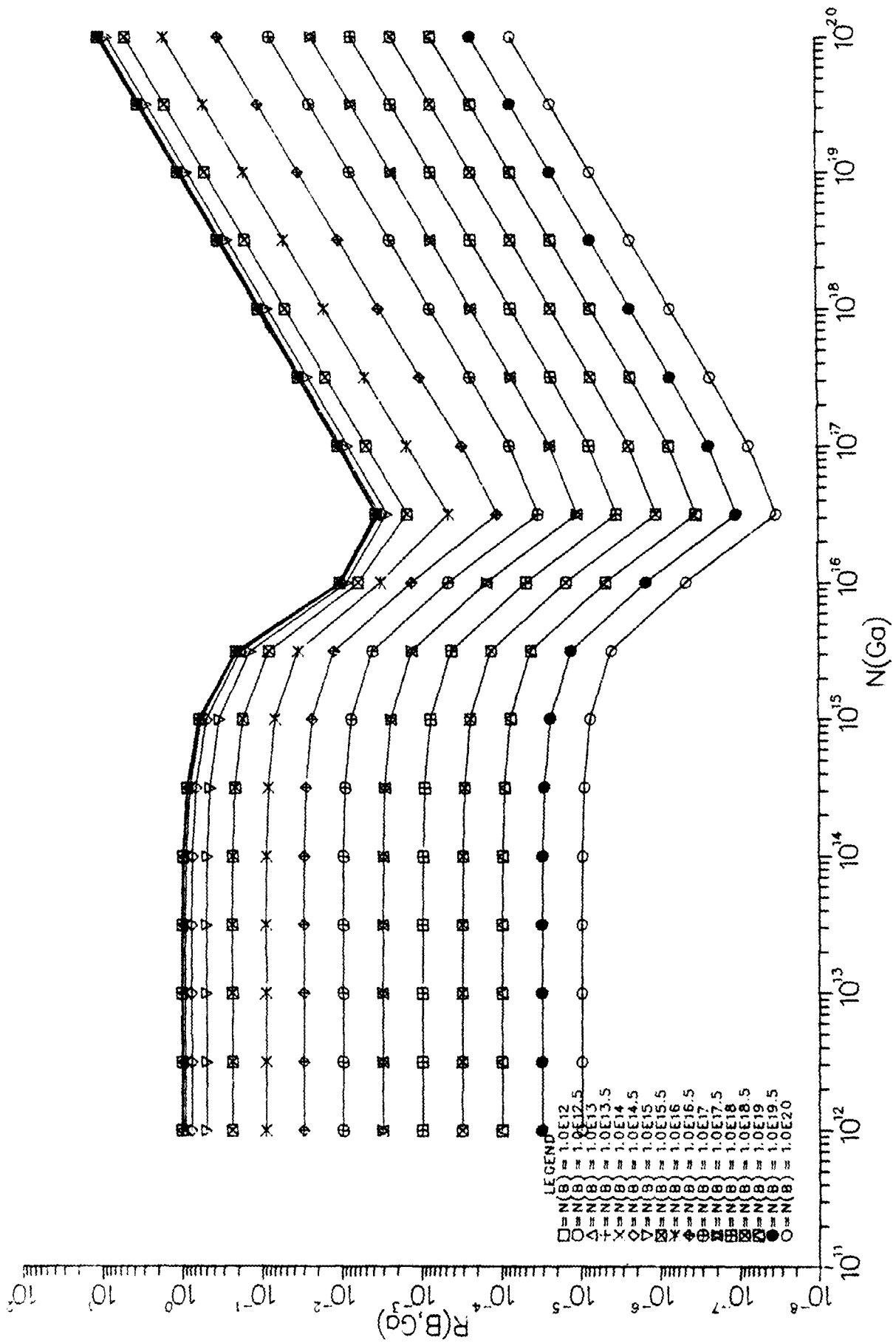


Figure 25a. $R(B, Ga)$ for $\sigma_B/\sigma_{Ga} = 2$ as functions of N_{Ga} for given N_B .

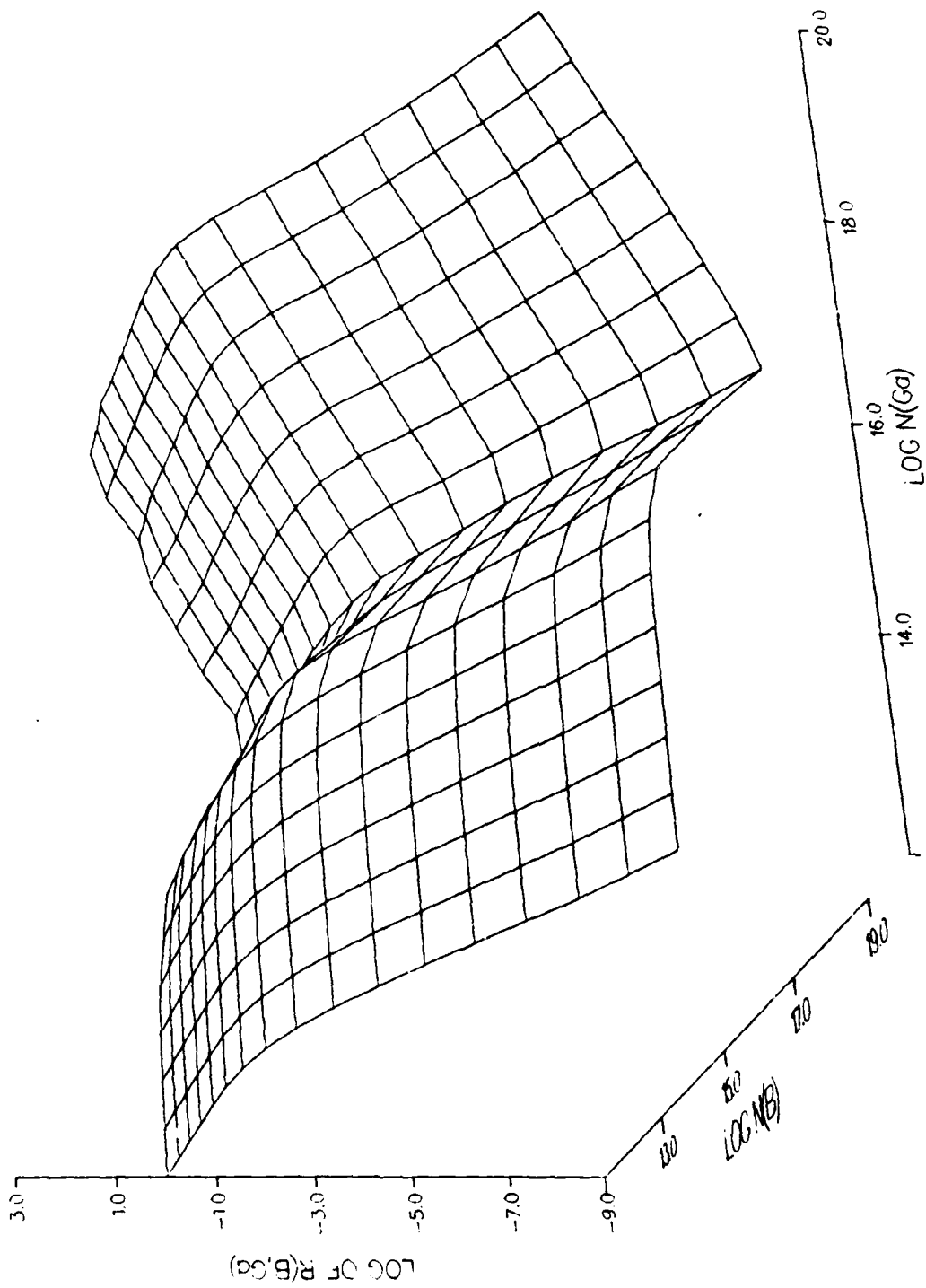


Figure 25b. One view of $R(B, Ga)$ for $\sigma_B/\sigma_{Ga} = 2$ as a function of N_B and N_{Ga} .

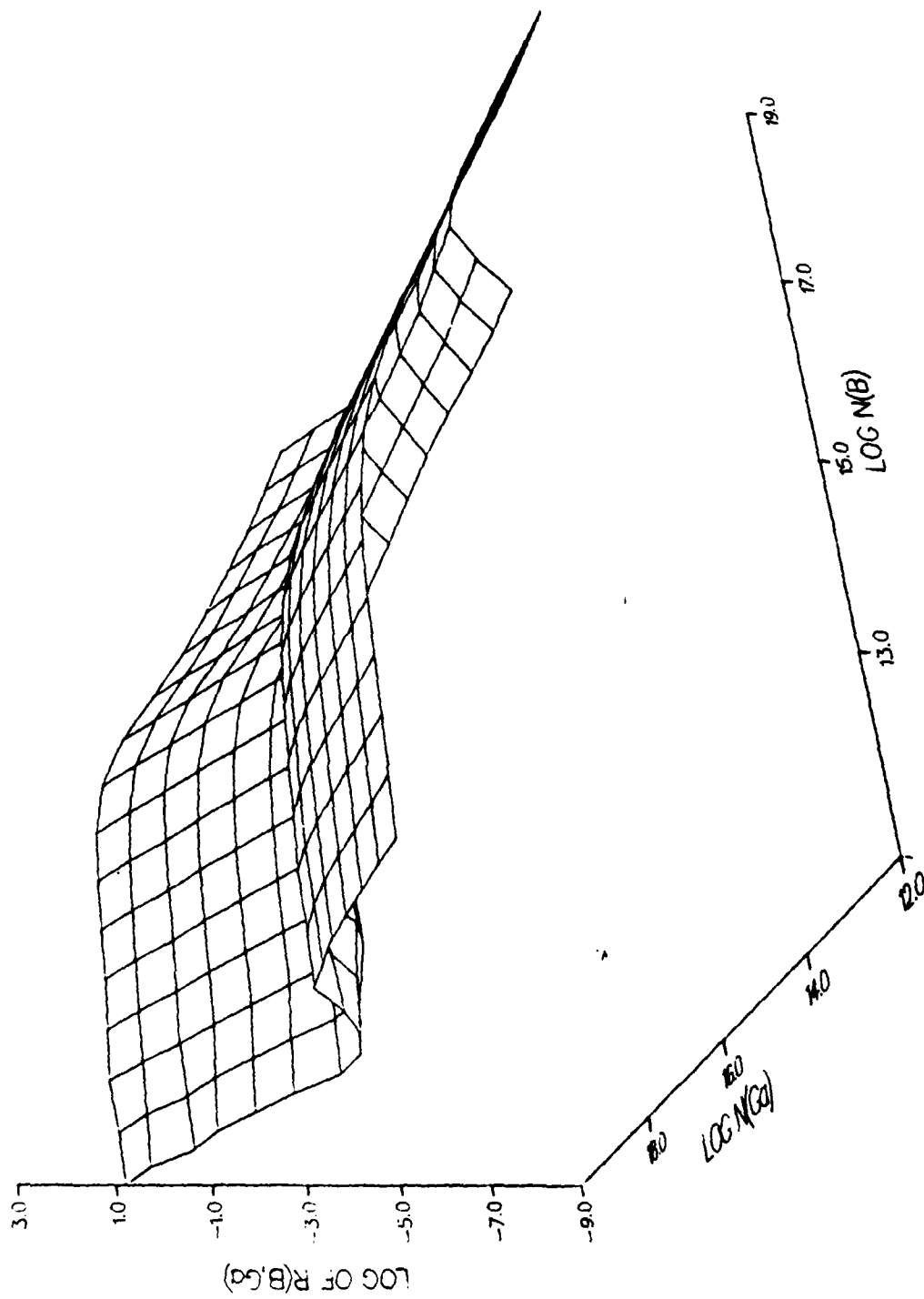


Figure 25c. Another view of $K(B, Ga)$ for $\sigma_{B/Ga} = 2$ as a function of N_B and N_{Ga} .

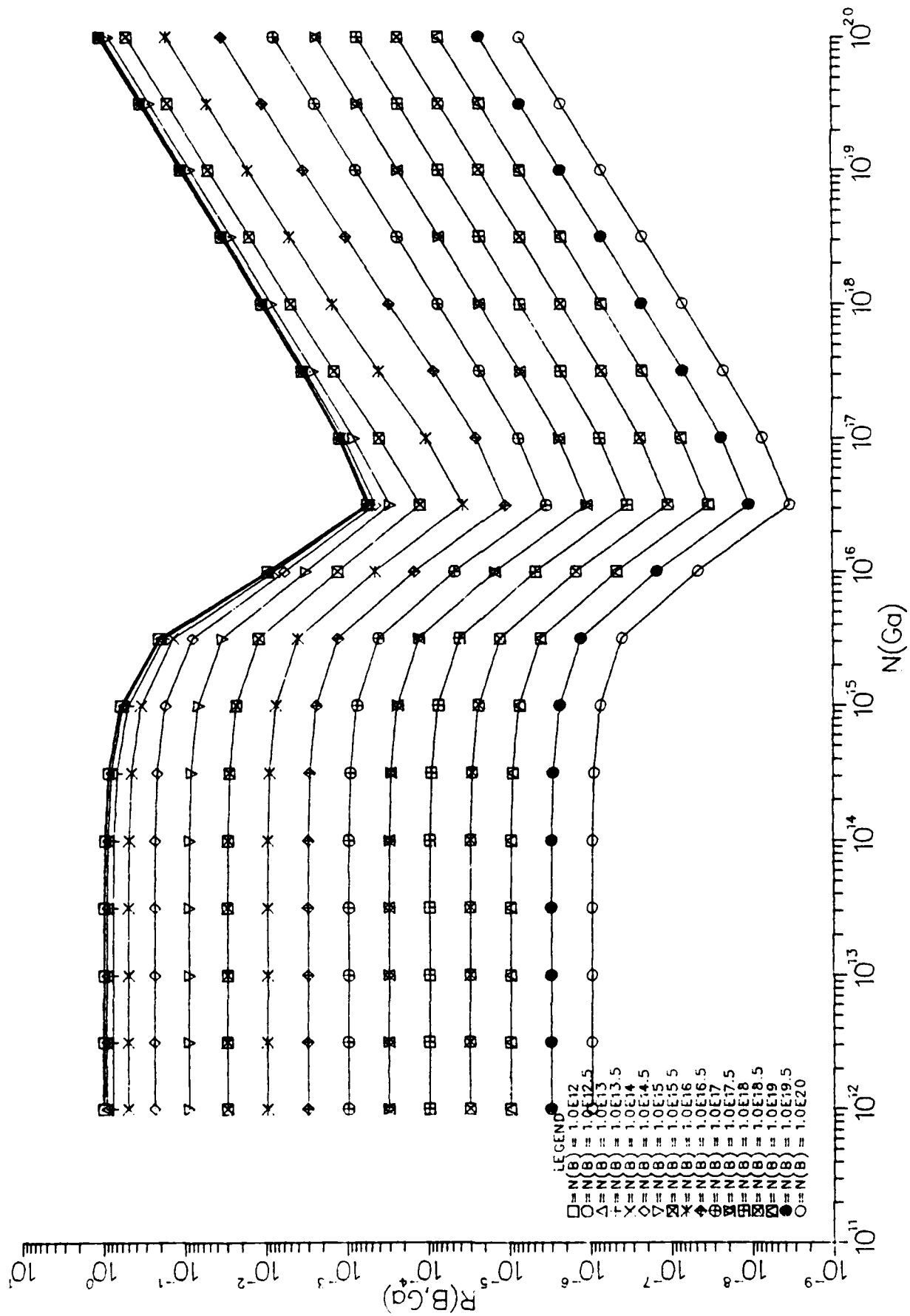


Figure 26a. $R(B, Ga)$ for $N_B / Ga = 20$ as functions of N_{Ga} for given N_B .

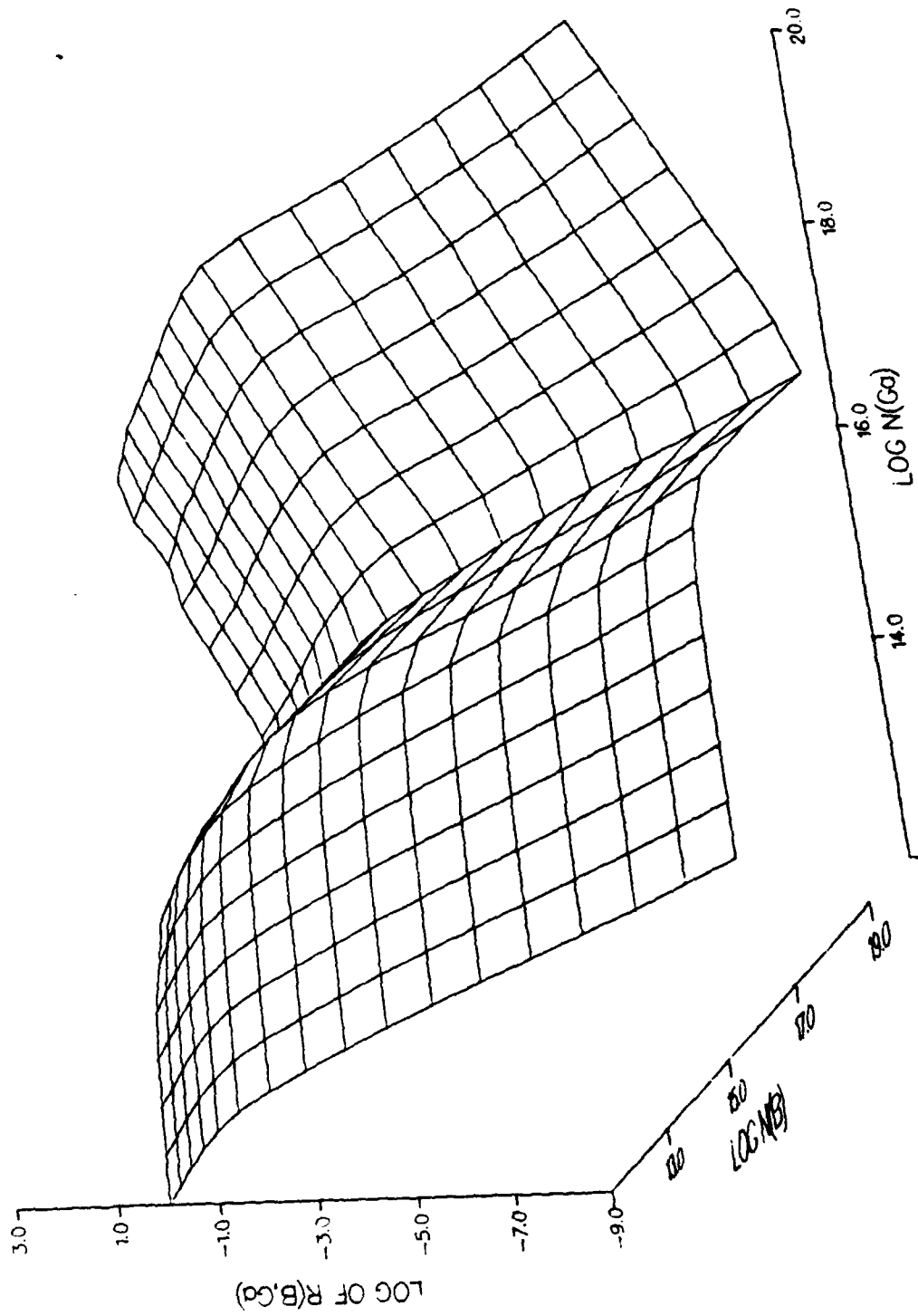


Figure 26b. One view of $R(B,Ga)$ for $\sigma_B/\sigma_{Ga} = 20$ as a function of N_B and N_{Ga} .

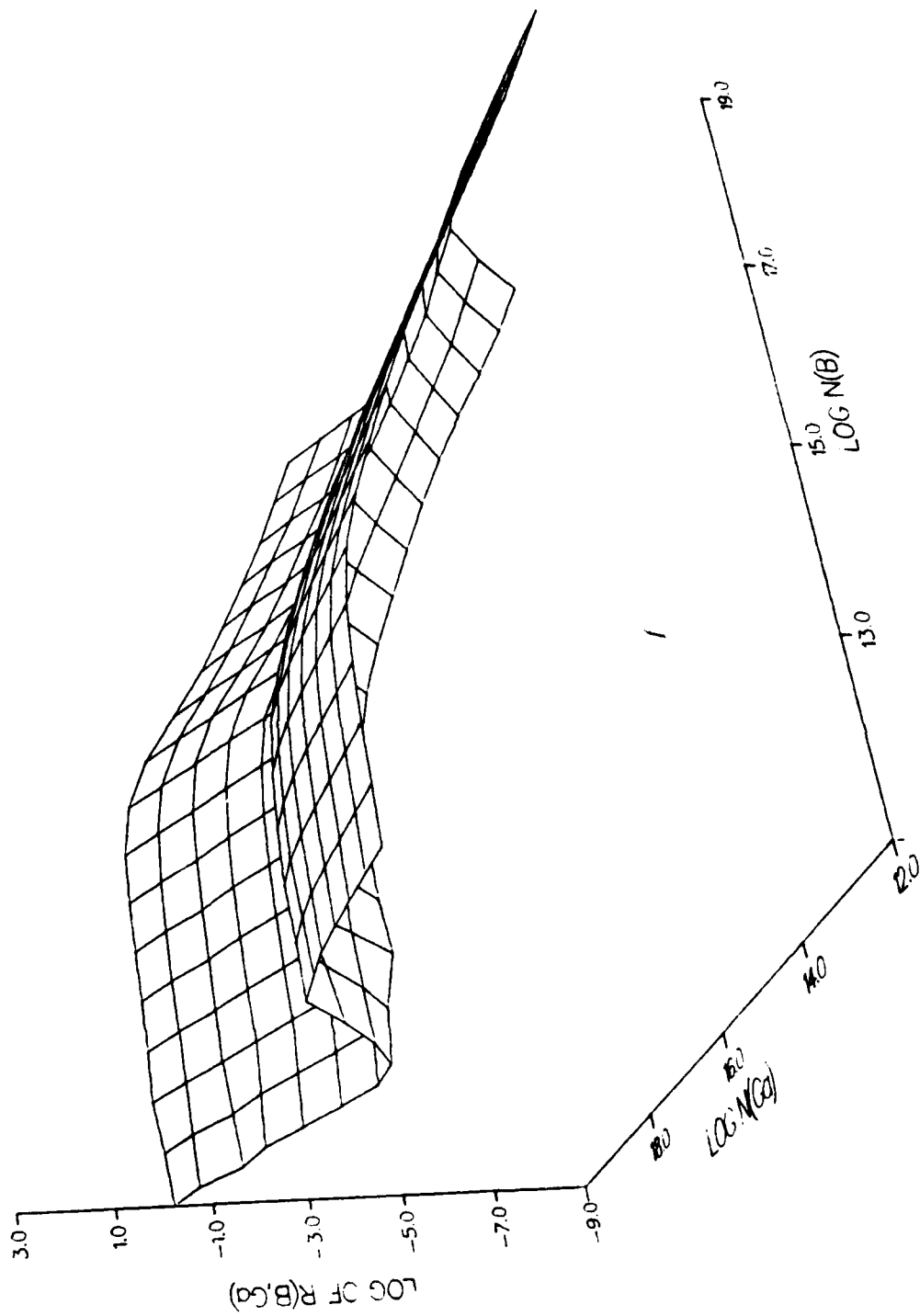


Figure 26c. Another view of $R(B,Ga)$ for $J_{B/Ga} = 20$ as a function of N_B and N_{Ga} .

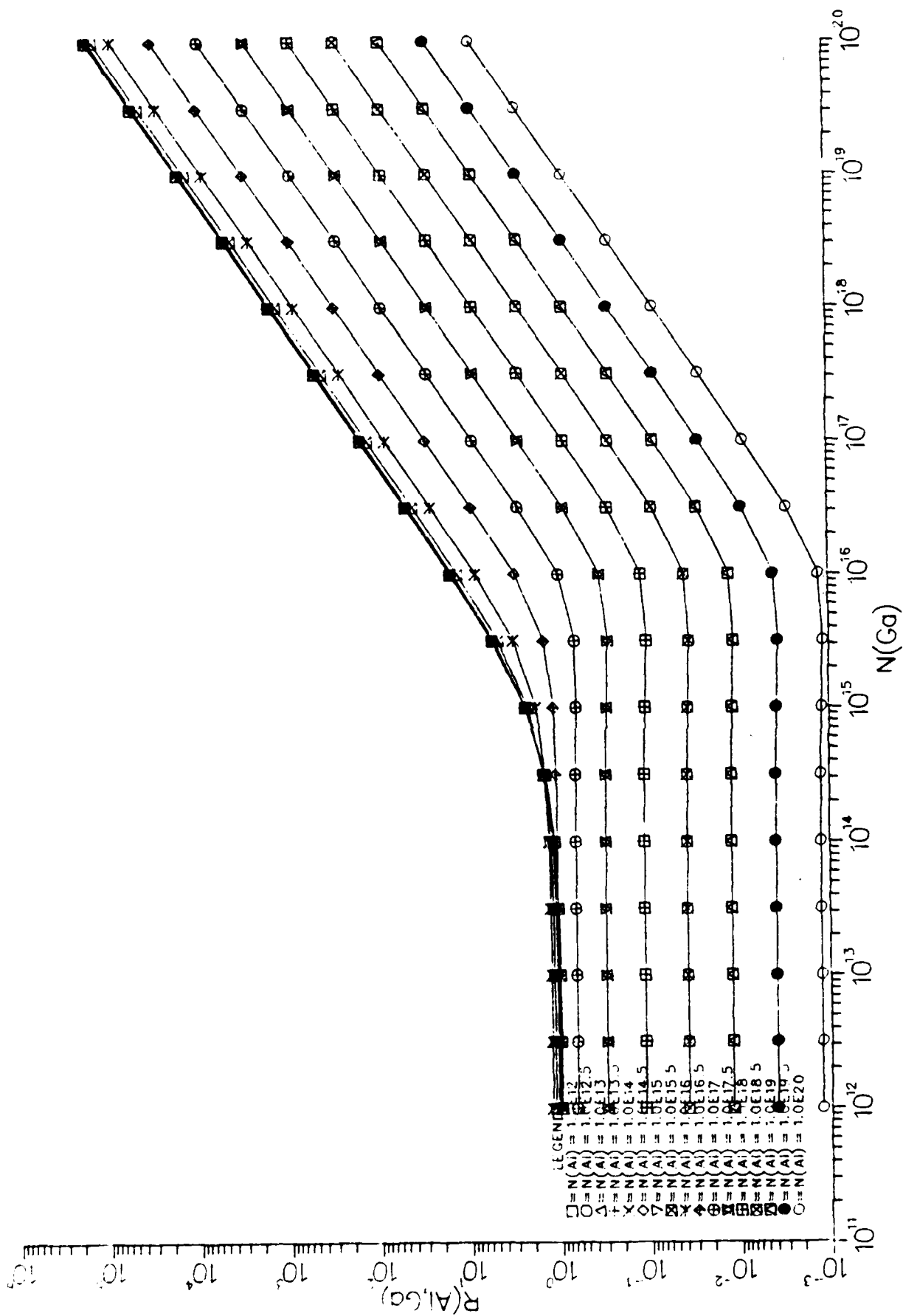


Figure 27a. $R(\text{Al}, \text{Ga})$ for $\sigma_{\text{Al}/\text{Ga}} = 0.05$ as functions of N_{Ga} for given N_{Al} .

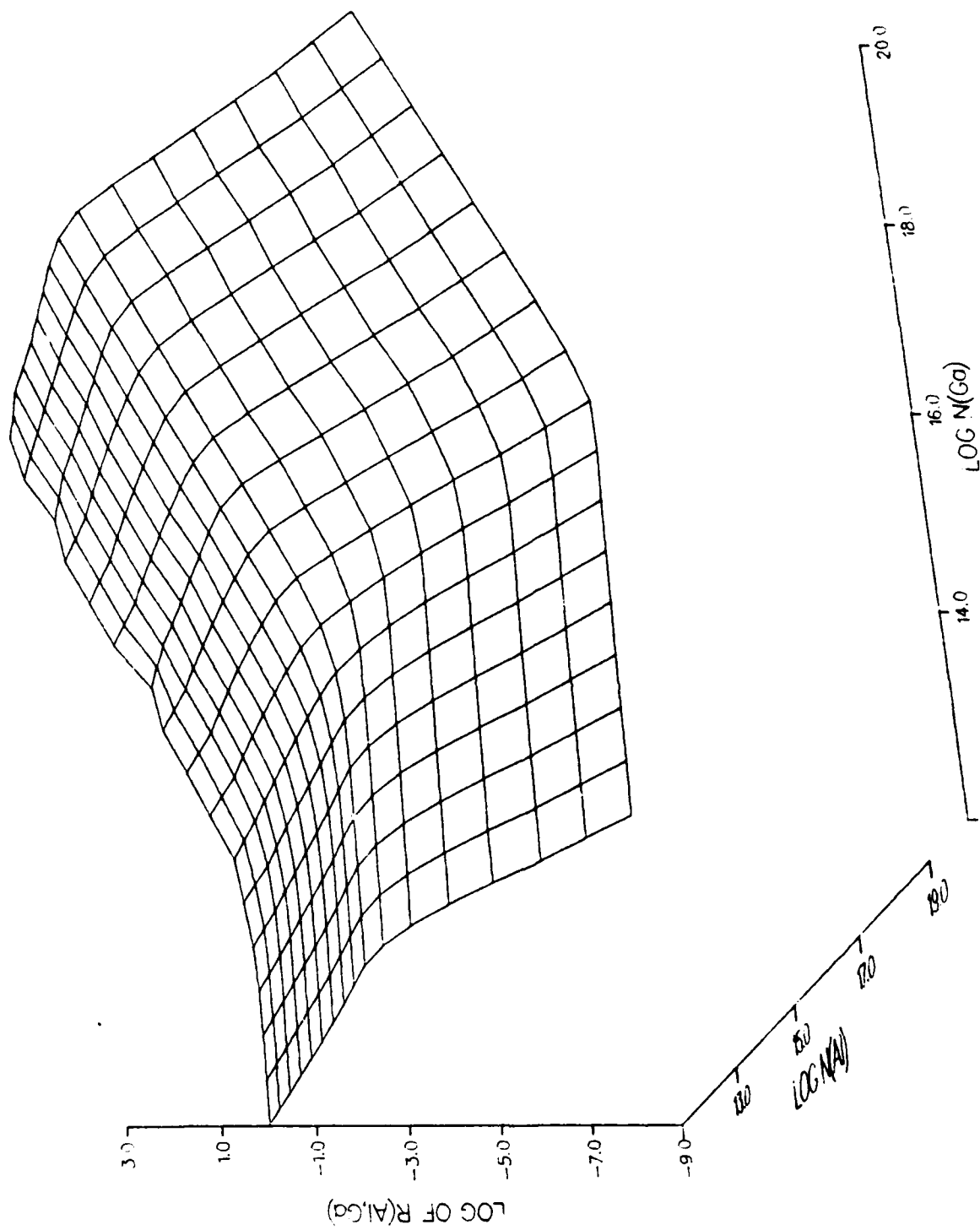


Figure 27b. One view of $R(\text{Al}, \text{Ga})$ for $\sigma_{\text{Al}/\text{Ga}} = 0.05$ as a function of N_{Al} and N_{Ga} .

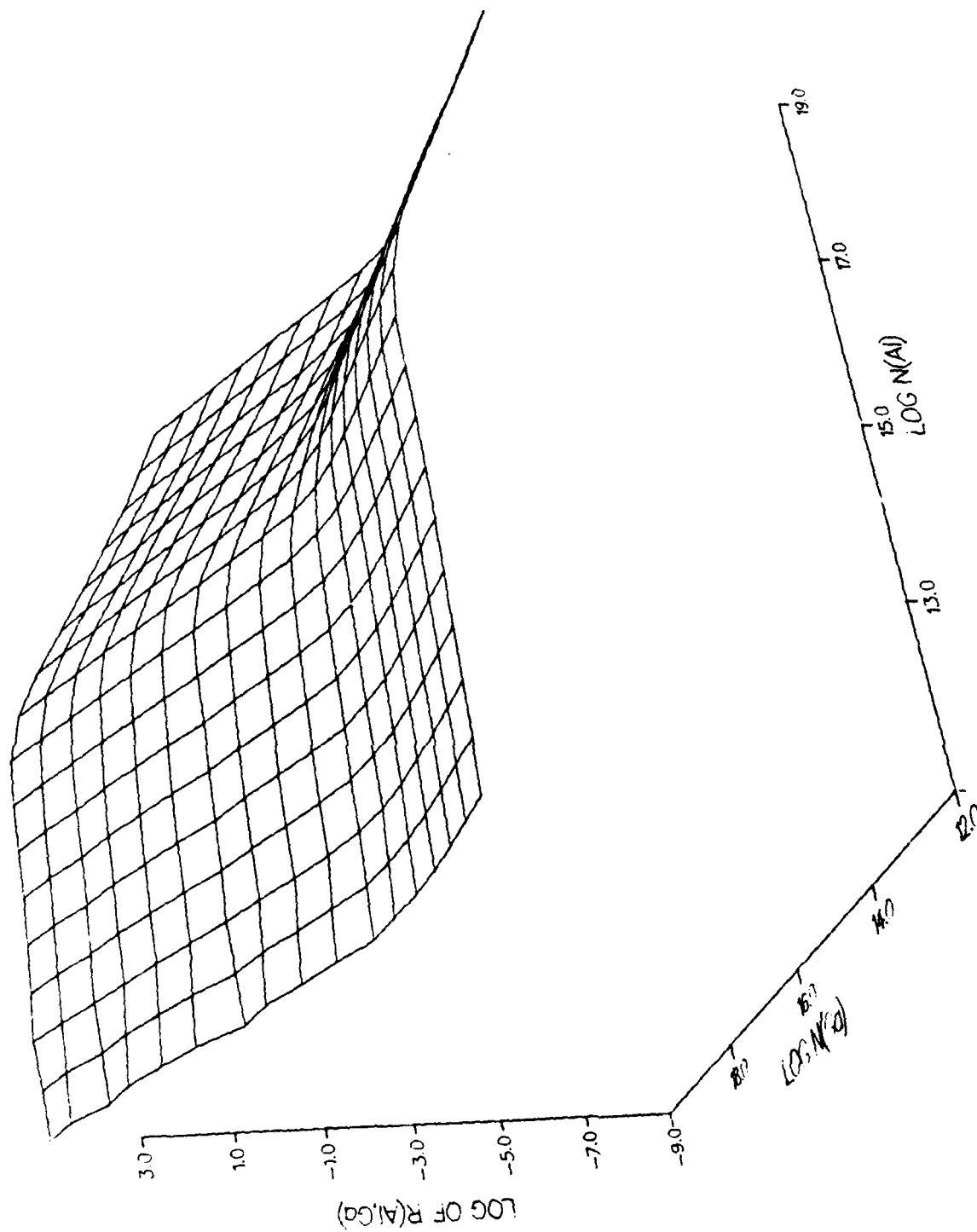


Figure 27c. Another view of $R(\text{Al}, \text{Ga})$ for $\sigma_{\text{Al}/\sigma_{\text{Ga}}} = 0.05$ as a function of N_{Al} and N_{Ga} .

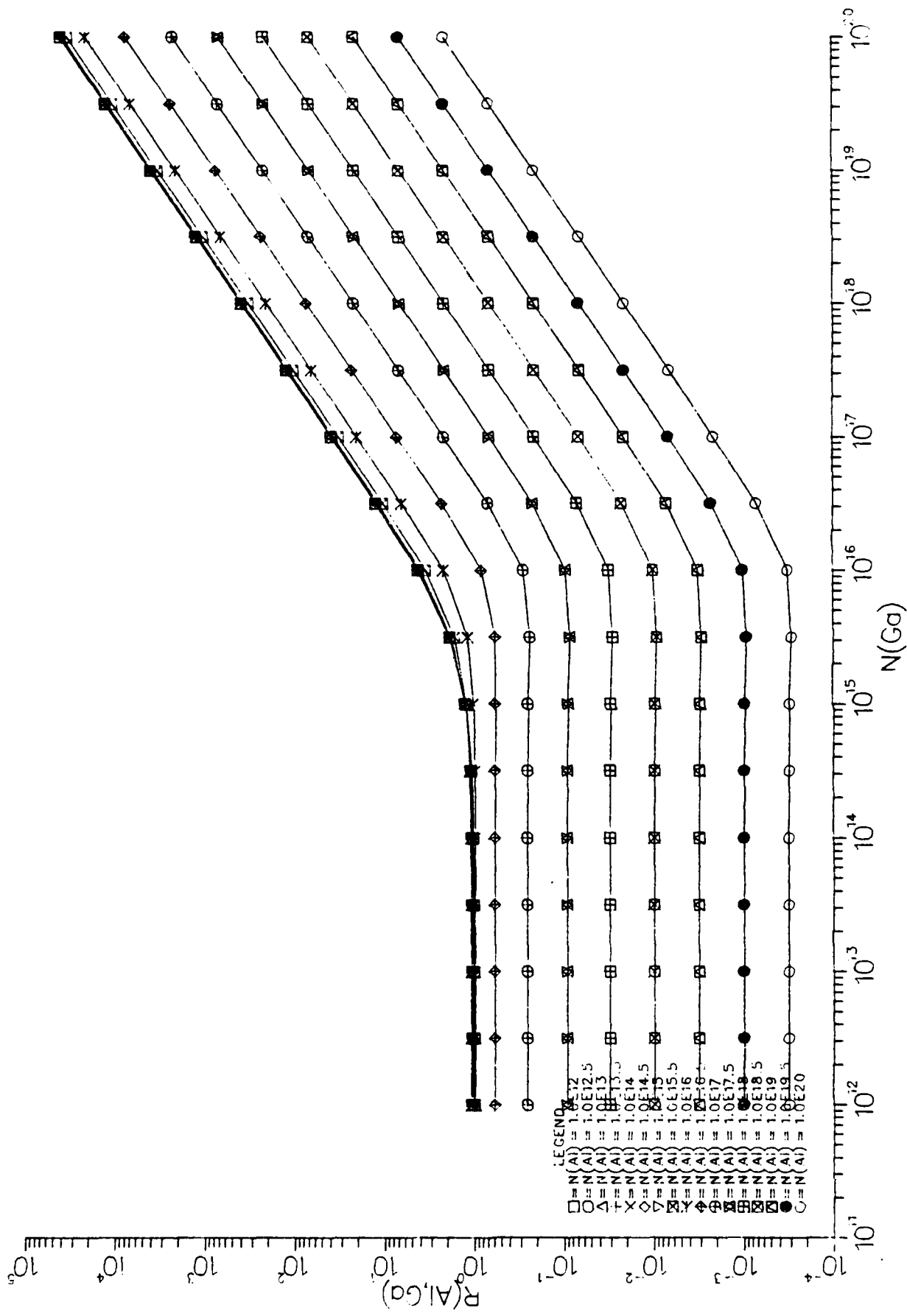


Figure 28a. $R(Al, Ga)$ for $N_{Al}/N_{Ga} = 0.2$ as functions of N_{Ga} for given N_{Al} .

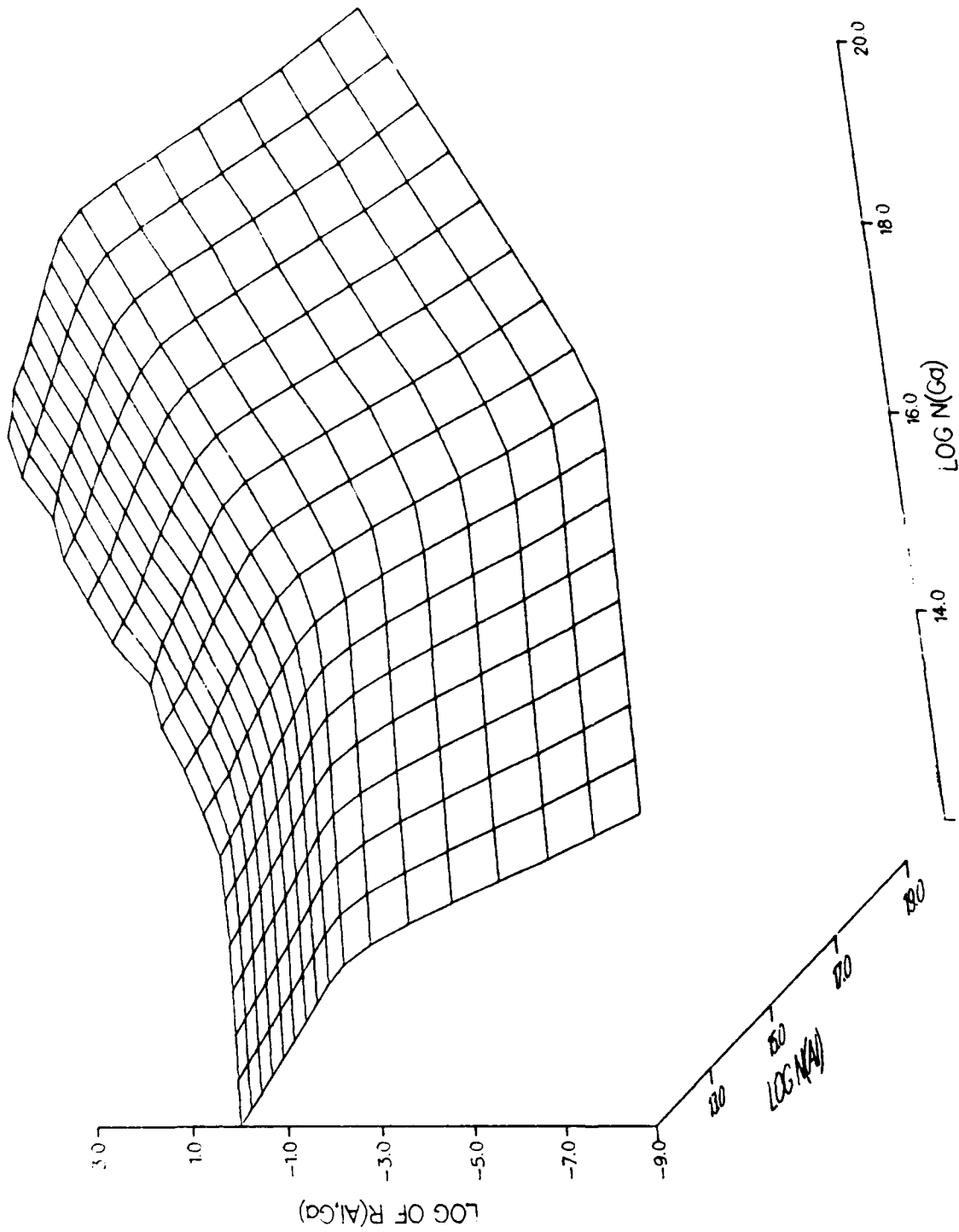


Figure 28b. One view of $R(\text{Al}, \text{Ga})$ for $c_{\text{Al}}/c_{\text{Ga}} = 0.2$ as a function of N_{Al} and N_{Ga} .

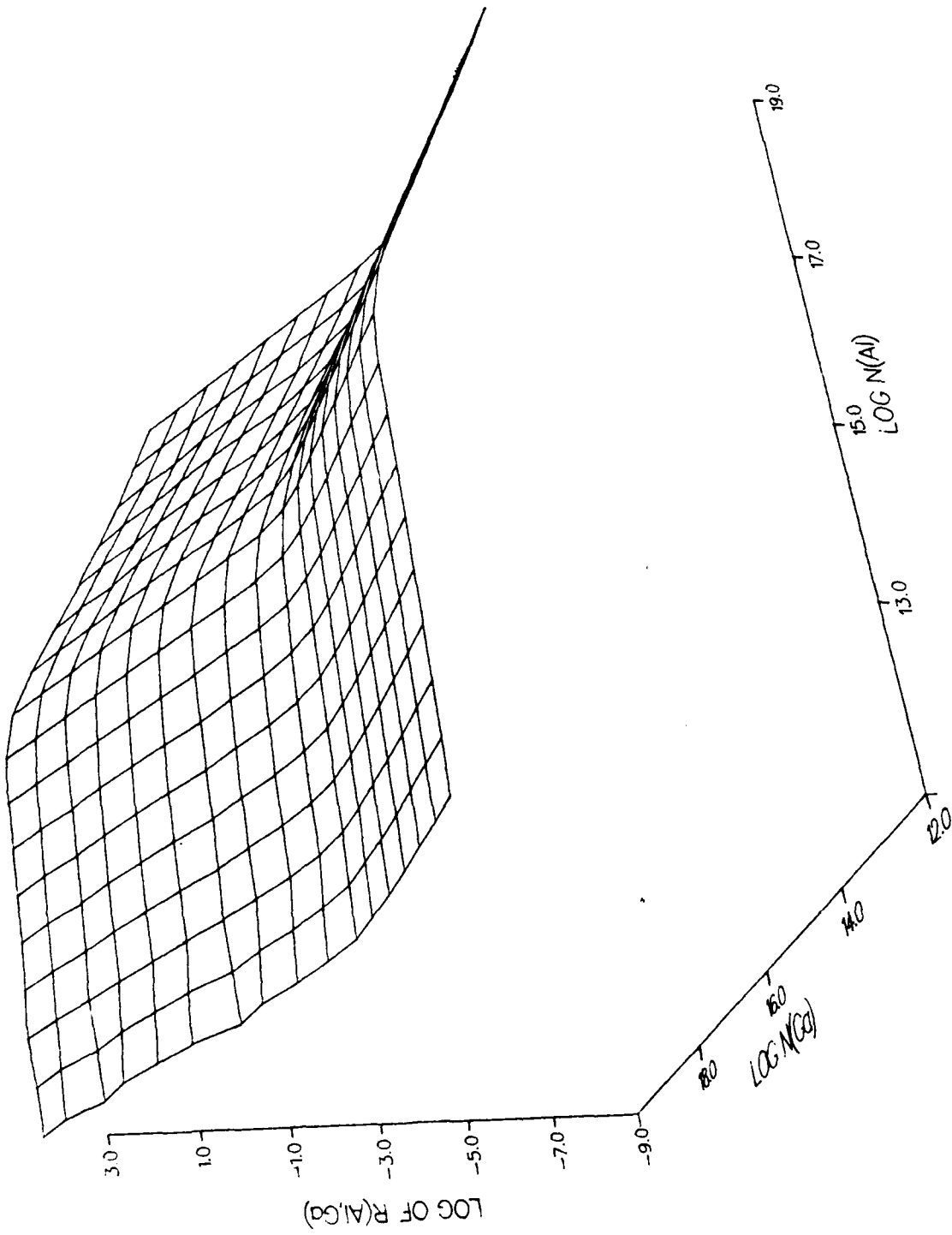


Figure 28c. Another view of $R(\text{Al}, \text{Ga})$ for $\sigma_{\text{Al}}/\sigma_{\text{Ga}} = 0.2$ as a function of N_{Al} and N_{Ga} .

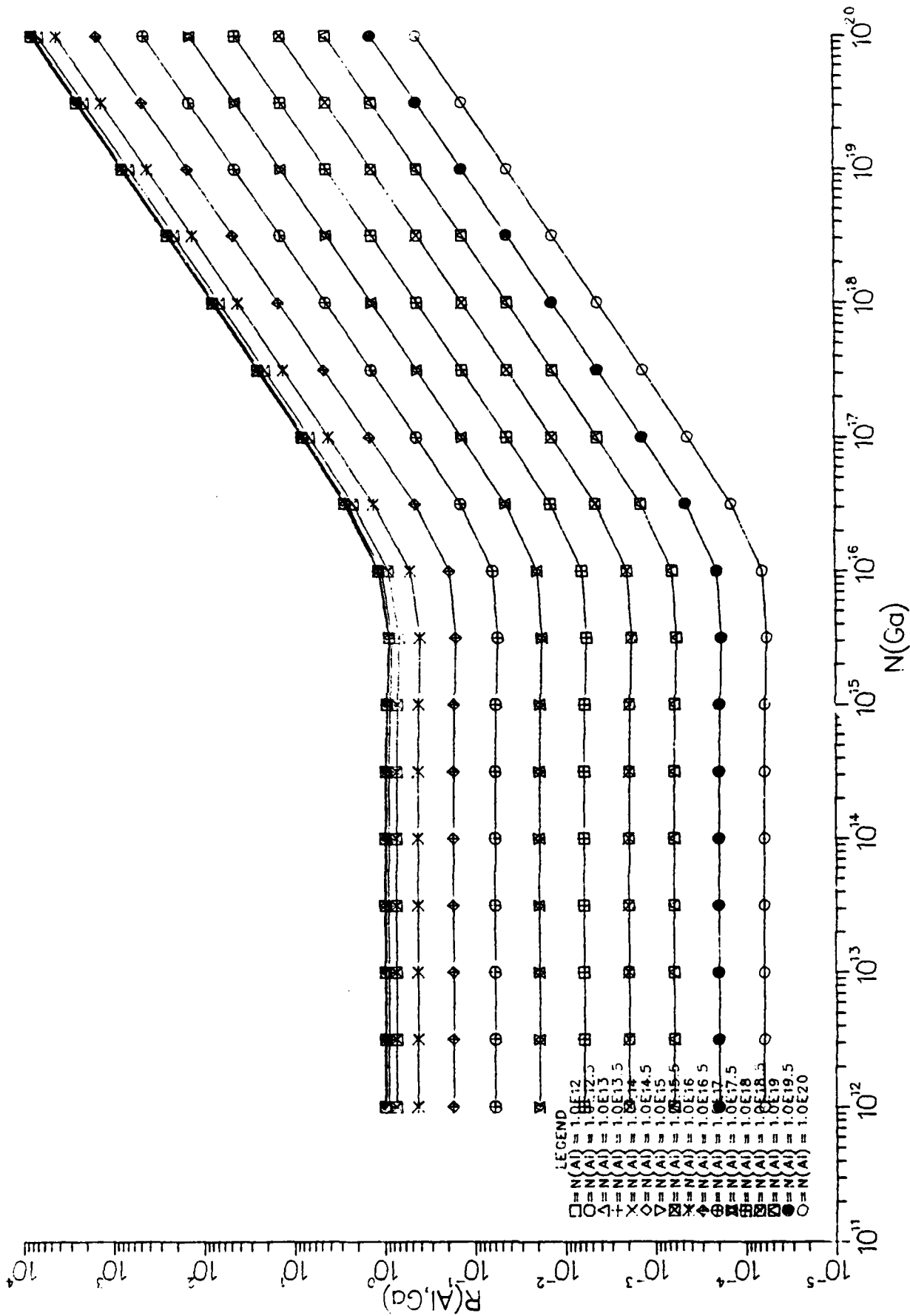


Figure 29a. $R(\text{Al}, \text{Ga})$ for $\sigma_{\text{Al}/\text{Ga}} = 1$ as functions of N_{Ga} for given N_{Al} .

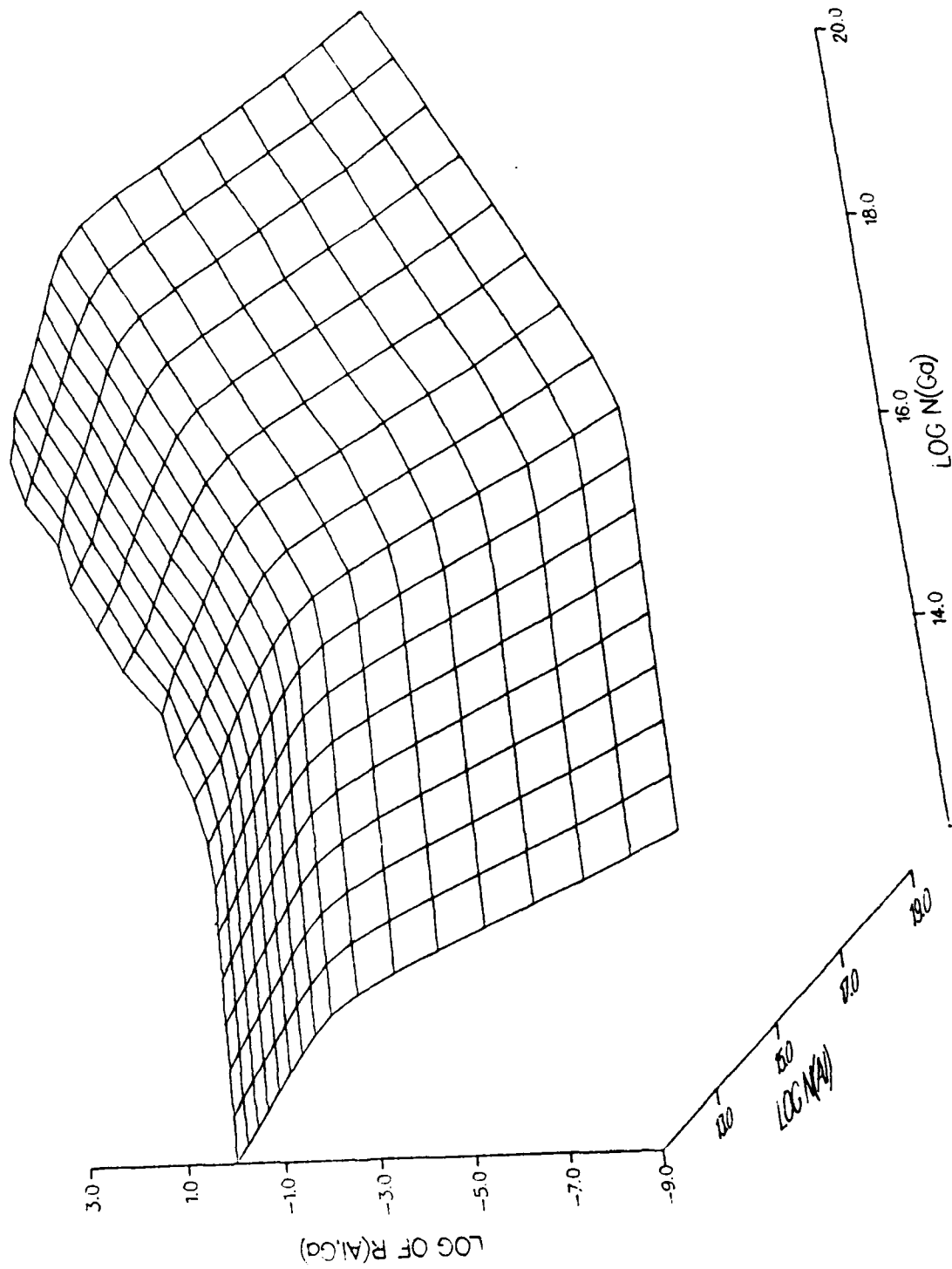


Figure 29b. One view of $R(\text{Al}, \text{Ga})$ for $\sigma_{\text{Al}/\sigma_{\text{Ga}}} = 1$ as a function of N_{Al} and N_{Ga} .

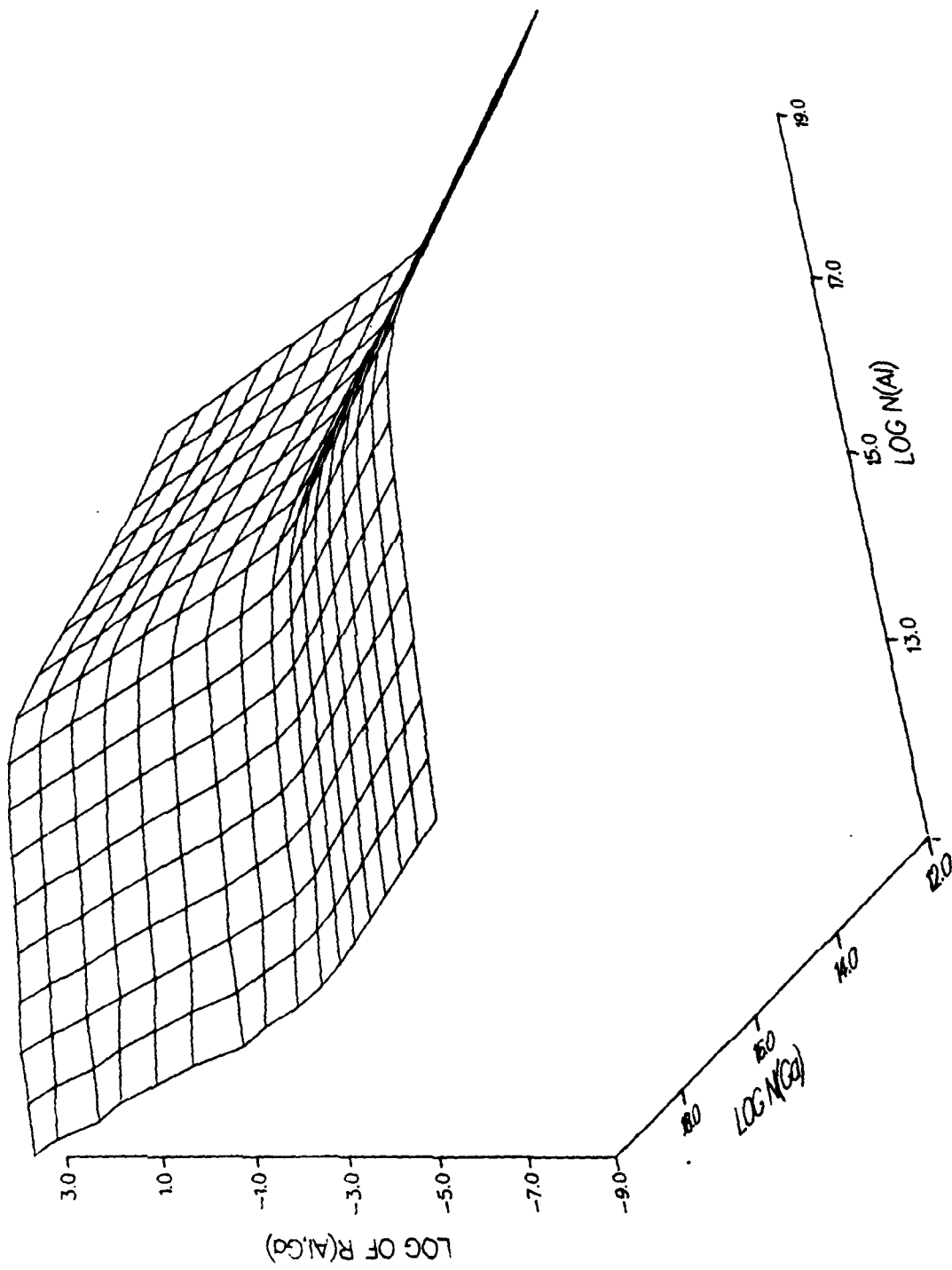


Figure 29c. Another view of $R(\text{Al}, \text{Ga})$ for $\sigma_{\text{Al}}/\sigma_{\text{Ga}} = 1$ as a function of N_{Al} and N_{Ga} .

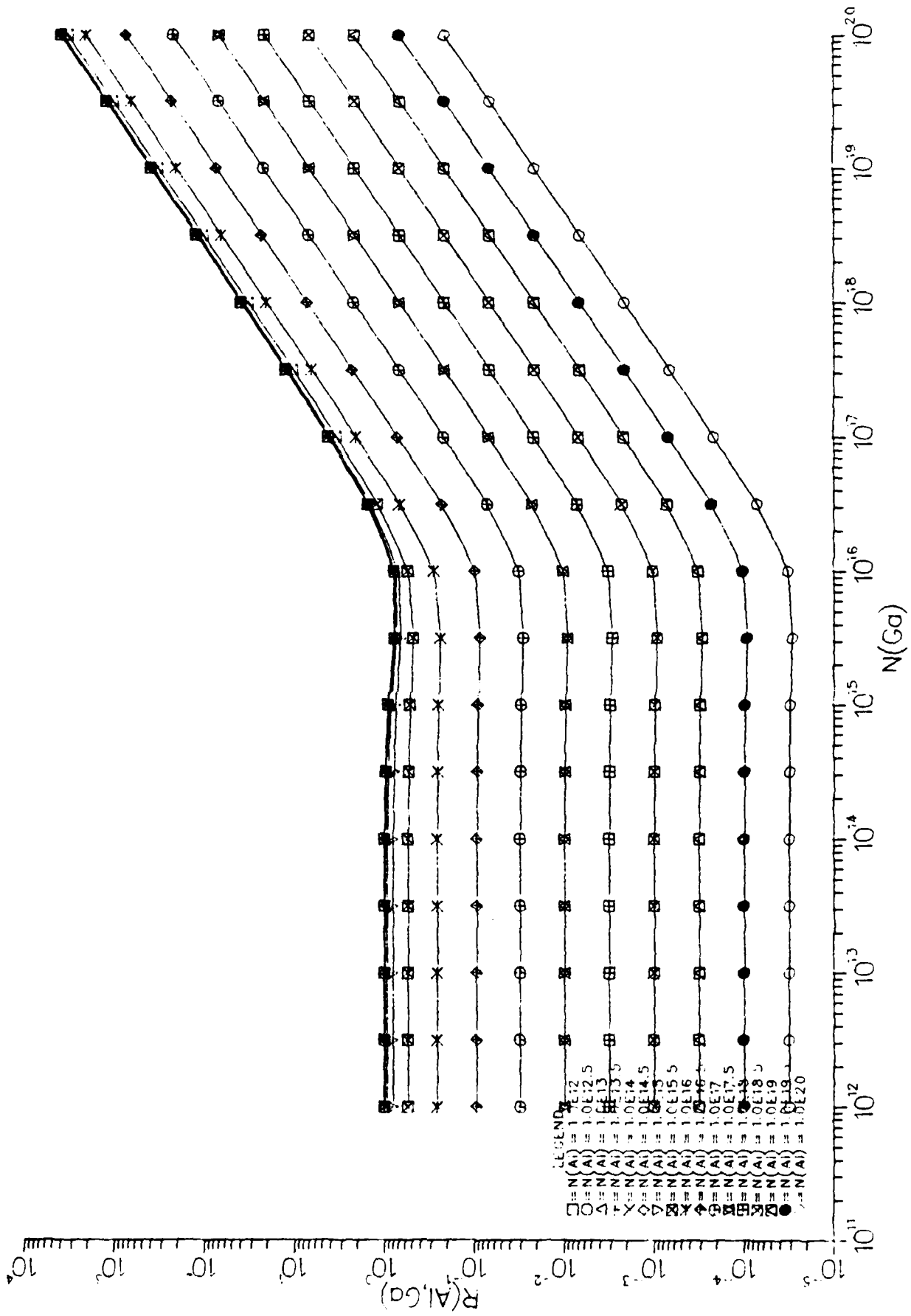


Figure 30a. $R(\text{Al}, \text{Ga})$ for $^{27}\text{Al}/^{70}\text{Ga} = 2$ as functions of N_{Ga} for given N_{Al} .

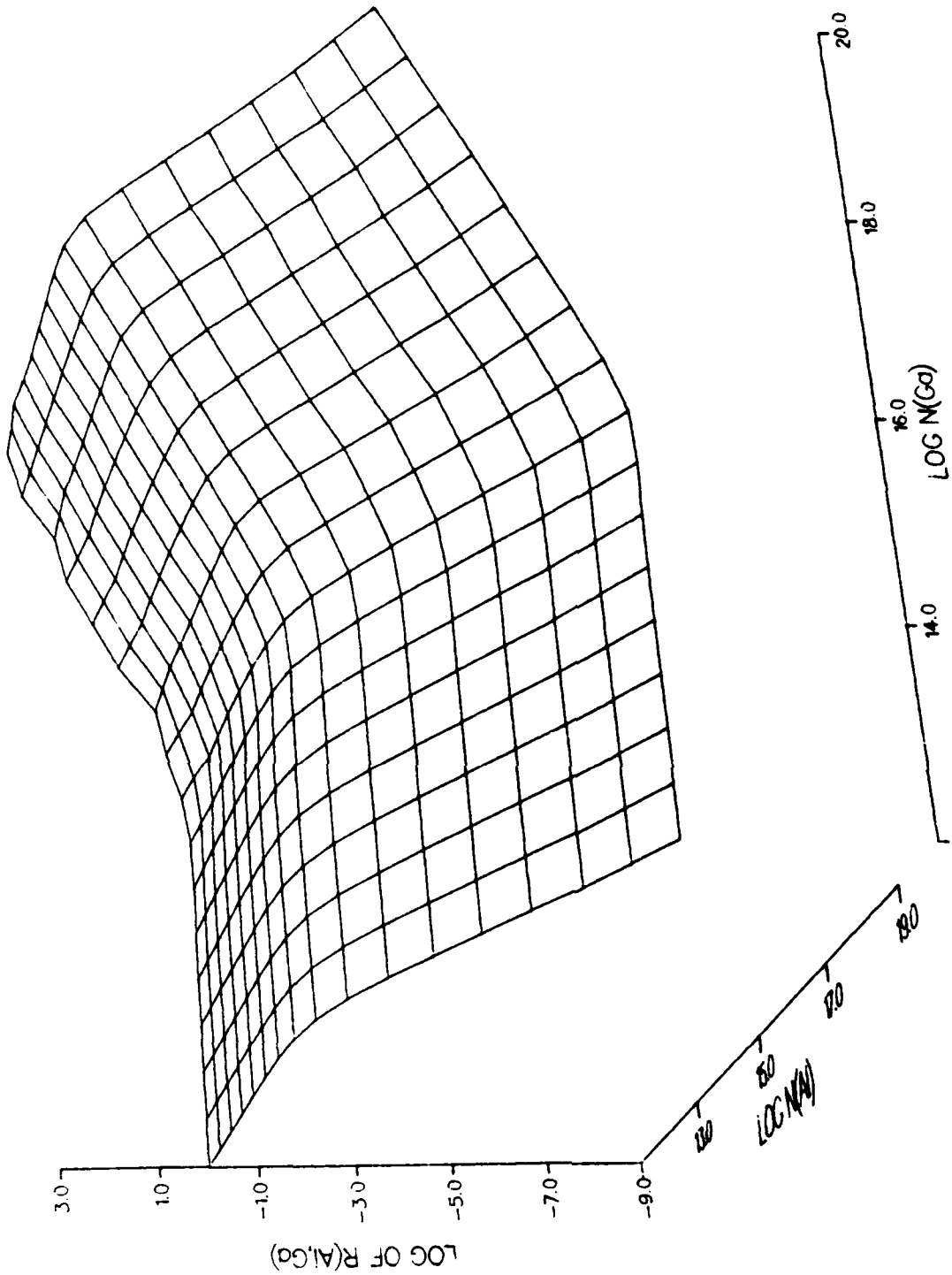


Figure 30b. One view of $R(\text{Al}, \text{Ga})$ for $\sigma_{\text{Al}/\sigma_{\text{Ga}}} = 2$ as a function of N_{Al} and N_{Ga} .

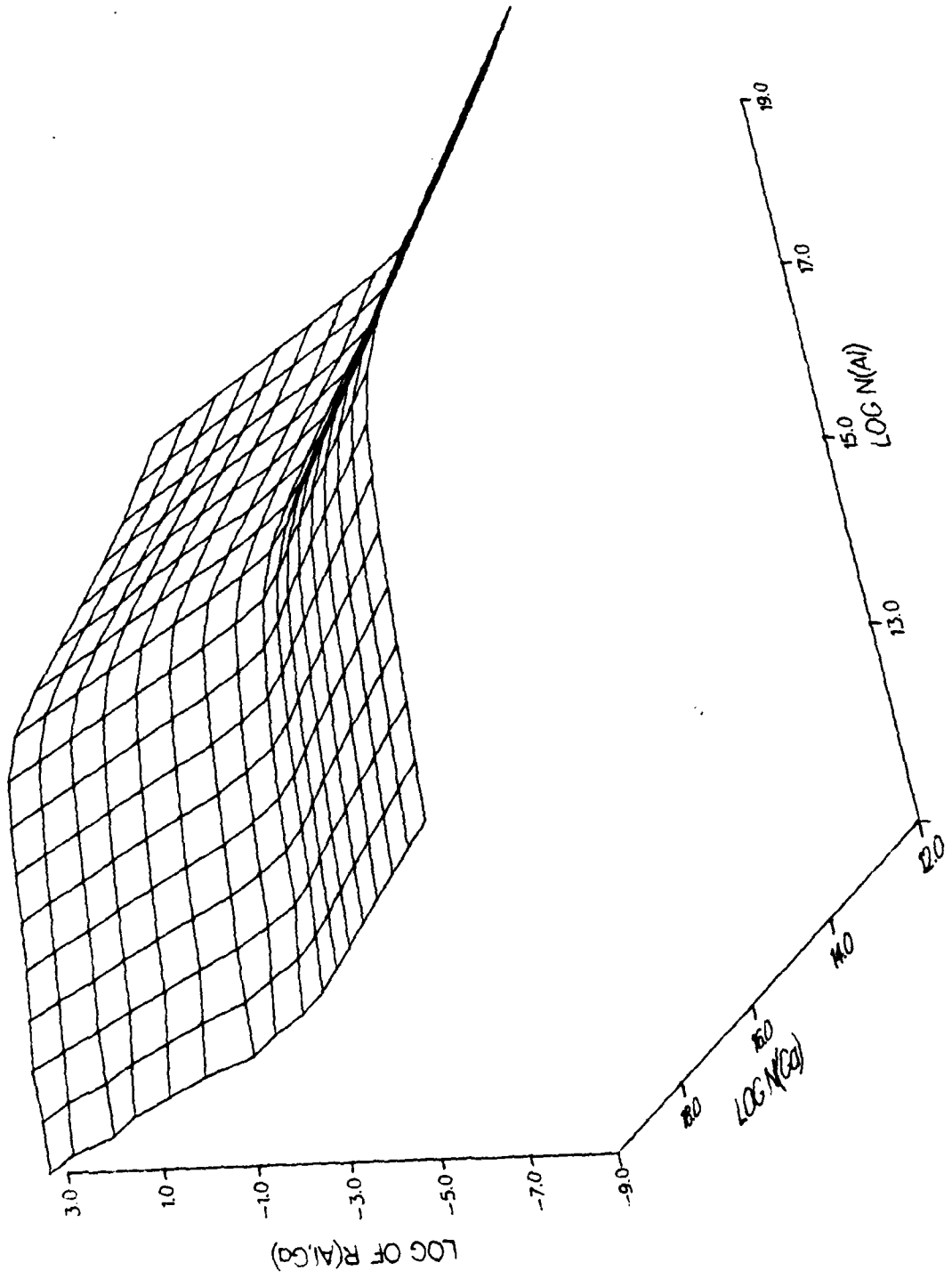


Figure 30c. Another view of $R(\text{Al}, \text{Ga})$ for $\sigma_{\text{Al}/\sigma_{\text{Ga}}} = 2$ as a function of N_{Al} and N_{Ga} .

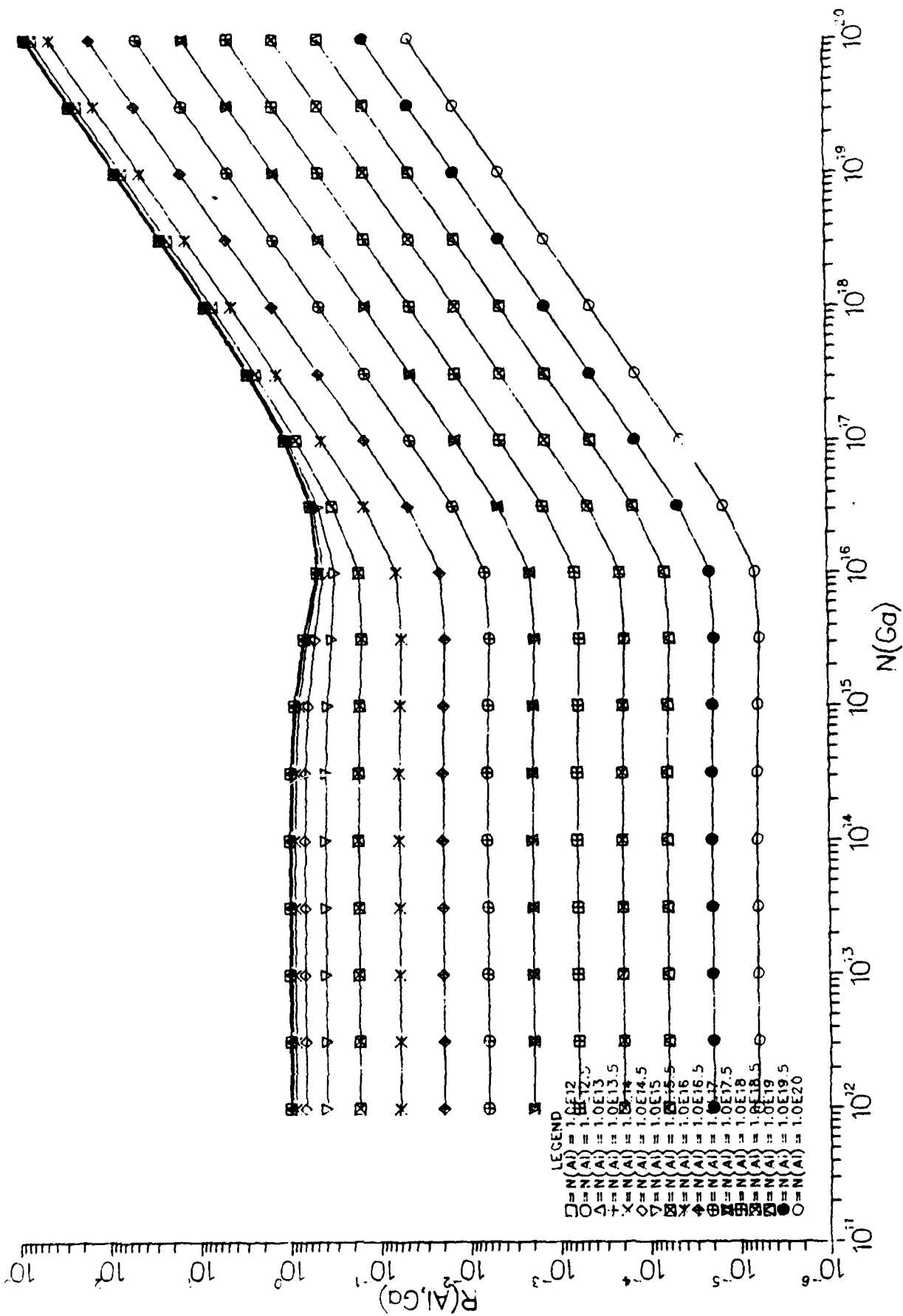


Figure 3la. $R(Al, Ga)$ for $\sigma_{Al/Ga} = 10$ as functions of N_{Ga} for given N_{Al} .

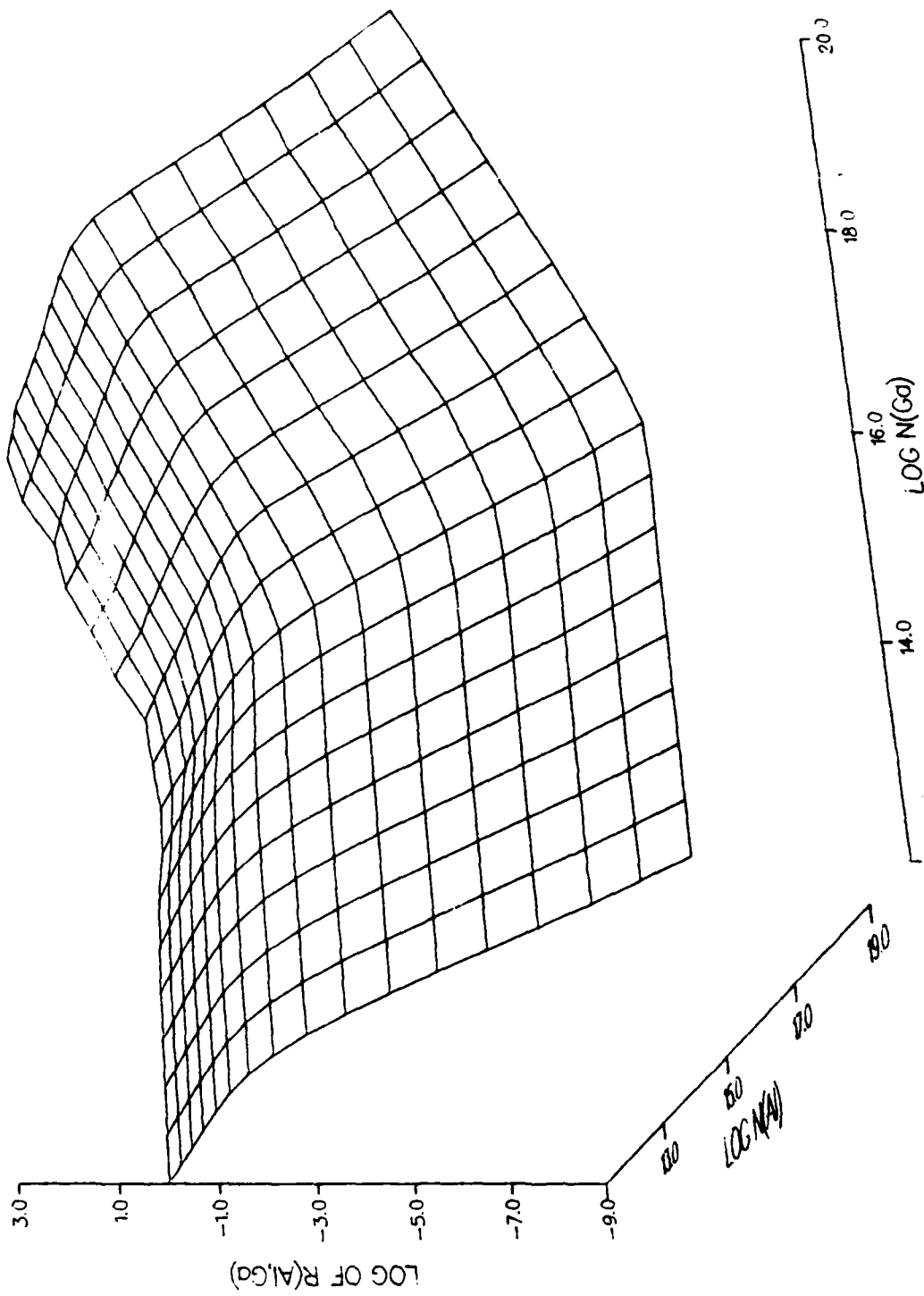


Figure 3lb. One view of $R(\text{Al}, \text{Ga})$ for $\sigma_{\text{Al}/\text{Ga}} = 20$ as a function of N_{Al} and N_{Ga} .

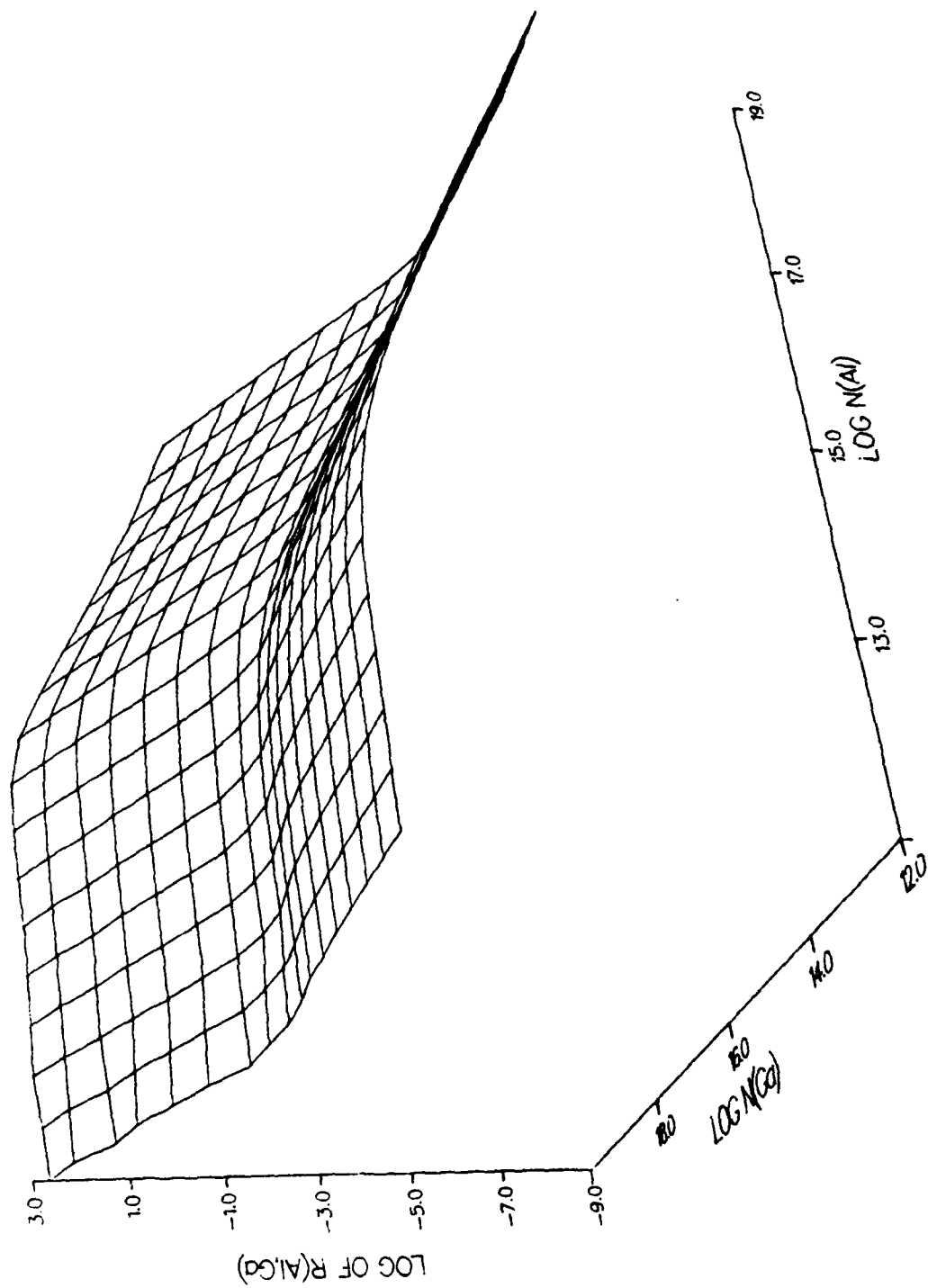


Figure 3lc. Another view of $R(\text{Al}, \text{Ga})$ for $\sigma_{\text{Al}}/\sigma_{\text{Ga}} = 20$ as a function of N_{Al} and N_{Ga} .

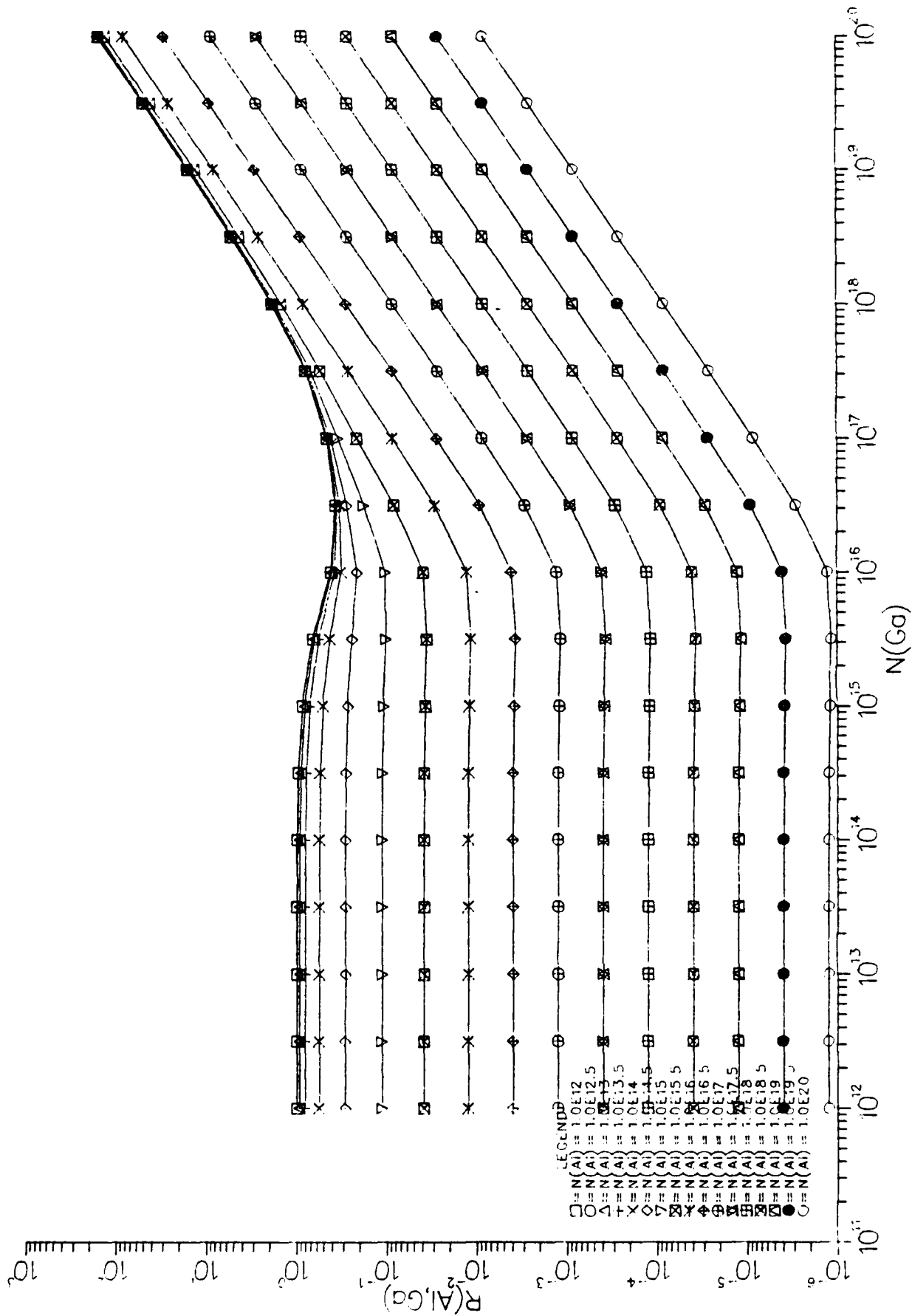


Figure 32a. $R(Al, Ga)$ for $N_{Al}/N_{Ga} = 50$ as functions of N_{Ga} for given N_{Al} .

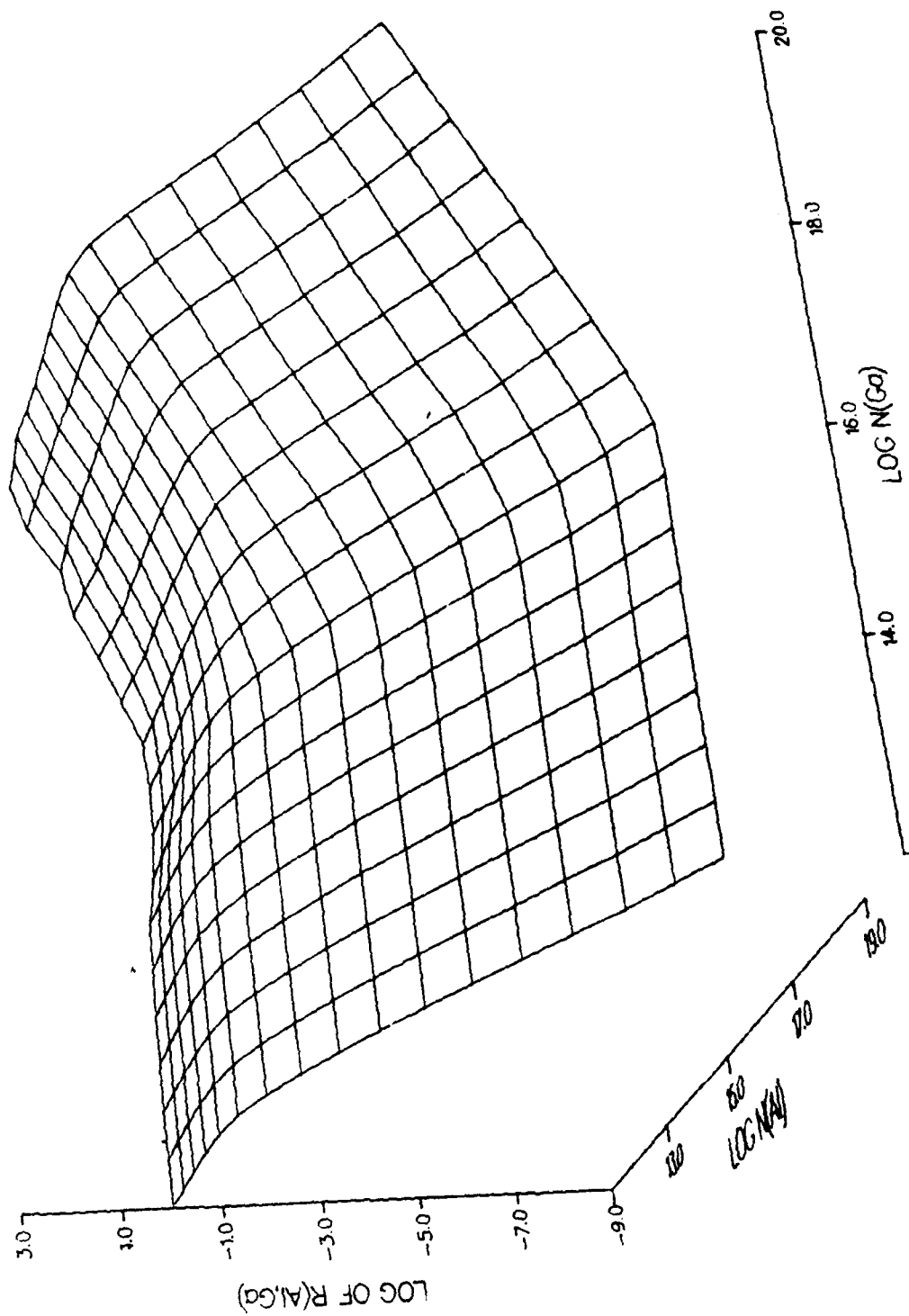


Figure 32b. One view of $R(\text{Al}, \text{Ga})$ for $\sigma_{\text{Al}}/\sigma_{\text{Ga}} = 50$ as a function of N_{Al} and N_{Ga} .

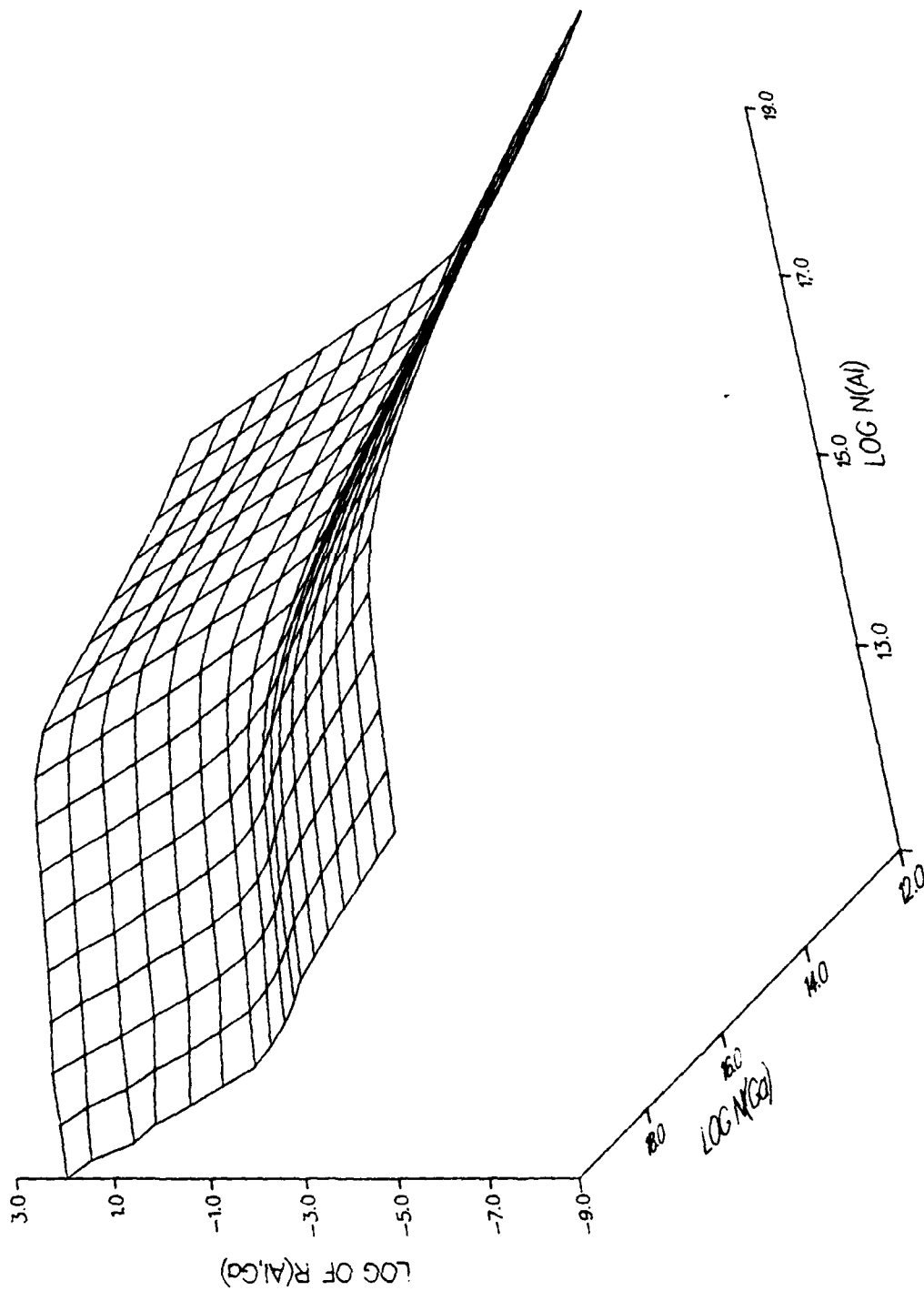


Figure 32c. Another view of $R(\text{Al,Ga})$ for $\sigma_{\text{Al}/\sigma_{\text{Ga}}} = 50$ as a function of N_{Al} and N_{Ga} .

END

FILMED

8-85

DTIC